2005-06-16

Myosin IX: A Single-Headed Processive Motor

Taketoshi Kambara
Worcester Polytechnic Institute

MYOSIN IX:
A SINGLE-HEADED PROCESSIVE MOTOR

BY

TAKETOSHI KAMBARA

A Dissertation
Submitted to the Faculty
of the
WORCESTER POLYTECHNIC INSTITUTE
in partial fulfillment of the requirements for the
Degree of Doctor of Philosophy
in
Biomedical Science
May 2005

APPROVED:

_____

Mitsuo Ikebe, Ph.D., Major Advisor
University of Massachusetts Medical School

_____

Joseph C. Bagshaw, Ph.D., Co-Advisor
Worcester Polytechnic Institute

_____

Daniel G. Gibson III, Ph.D.
Worcester Polytechnic Institute

_____

Thomas W. Honeyman, Ph.D.
University of Massachusetts

_____

George Witman, Ph.D.
University of Massachusetts

ABSTRACT

The class IX myosin is a member of the myosin superfamily and found in variety of tissues. Myosin IX is quite unique among the myosin superfamily in that the tail region contains a GTPase-activating protein (GAP) domain for the small GTP-binding protein, Rho. Recently it was reported that myosin IX shows processive movement that travels on an actin filament for a long distance. This was an intriguing discovery, because myosin IX is a "single-headed" myosin unlike other processive myosins which have "double-headed" structure. It has been thought that "processive" motors walk on their track with their two heads, thus traveling for a long distance. Therefore, it is reasonable to expect that the processive movement of single headed myosin IX is based on the unique feature of myosin IX motor function. In this study, I investigated the mechanism of processive movement of single-headed myosins by analyzing the mechanism of ATPase cycle of myosin IX that is closely correlated with the cross-bridge cycle (the mechanical cycle of actomyosin).

In the first part, I performed the transient enzyme kinetic analysis of myosin IX using the motor domain construct to avoid the complexity raised by the presence of the tail domain. It was revealed that the kinetical characteristics of myosin IX ATPase is quite different from other processive myosins. It was particularly notable that the affinity of the weak actin binding state of Myosin IX was extremely high comparing with known myosins. It is thought that the high affinity for actin throughout the ATPase cycle is a major component to explain the processive movement of myosin IX.

In the second part of this study, I cloned full-length human myosin IX construct to further investigate the regulation of motor activity of myosin IX. It was revealed that the basal ATPase activity but not the actin dependent ATPase activity of myosin IX is inhibited by its tail region. Furthermore full-

length myosin IX is regulated by calcium, presumably due to the calcium binding to the CaM light chain. These result suggest that the tail domain serves as a regulatory component of myosin IX.

ACKNOWLEDGEMENTS

First and foremost, I would like to express my greatest gratitude and thanks to my Major Advisor, Dr. Mitsuo Ikebe, for his outstanding advice and guidance throughout my thesis project. Without his immense help and support this thesis would have never been possible. I would like to thank him for taking me into his lab and giving me the greatest opportunity I have ever had in my academic life, which is to learn through his exceptional knowledge and experience. I have had the greatest honor of being trained by him in one-to-one sessions, and his time and patience were extremely valuable to me. My endless thanks go to him for making me appreciate science, and respect the profession once again, so that I can now have a better future.

I would like to extend my sincere thanks to my committee members, Dr. Joe Bagshaw, Dr. Daniel Gibson and Dr. Tom Honeyman, and Dr. George Witman for their valuable advice and optimism throughout my thesis program.

Additionally I would like to thank many member of Ikebe's Lab at the University of Massachusetts Medical School for support throughout this project.

And finally I especially thank my family for their relentless support.

TABLE OF CONTENTS

LIST OF FIGURES

LIST OF TABLES

CHAPTER ONE: INTRODUCTION

PART 1. BACKGROUND

I: Myosin overview

1. Myosin superfamily

1.1 Conventional myosin

Myosin is a molecular motor that moves on actin filament using chemical energy of ATP hydrolysis. The mechanism underlying this mechanochemical energy transduction remains unknown. Myosins are typically composed of three functional subdomains: (1) the motor domain that interacts with actin and binds ATP, (2) the neck domain which binds light chains or calmodulin, and (3) tail domain (**Fig. I-1**). Most well characterized myosin is Myosin II, which is referred to as 'conventional' myosin since this was the only class of myosin known for the decades. Class II myosins mainly play a role in muscle contraction. Members of this class have a two-headed structure, due to dimerization of the heavy chain in the tail by formation of coiled-coil (**Fig. I-2A**). The tails of myosin II self-associate to form filament that is characteristic for myosin II. Bipolar filaments are found in sarcomeric muscles (**Fig. I-2B**). These filaments have a central bare zone, which is not populated by motor domains and are designed to pull actin filaments toward the center. Smooth muscle myosins can form side polar filaments which have no central bare zone (Xu et al., 1996) (**Fig. I-2C**). These filaments may allow for the extreme shortening that is seen in smooth muscle tissues. Therefore, myosin IIs are able to generate force and move at high velocity by formation of filaments.

1.2. Unconventional myosin

Since the description of the first class of unconventional myosin, myosin I, 16 additional classes,

based on phylogenetic comparisons of motor domains and features of the tail, have been identified (Hodge and Cope, 2000; Sellers, 2000; Berg et al., 2001) (**Fig. I-3**). Thus, myosin superfamily is currently composed of 18 classes. These myosins are referred to as 'Unconventional' myosin compared to filament forming conventional myosin II. Members of myosin superfamily share common domains (**Fig. I-3**): (1) the motor domains are relatively conserved with exception of several surface loops and the amino-terminus. Surface loops are indicated to play an important role in diverse motor function that is determined by actin-binding rate and affinity, and rates of product release. (2) Light chains bind to a helical sequence termed IQ motif found in the neck region which has a consensus sequence of IqxxxRGxxxR (Cheney and Mooseker, 1992). The number of IQ motifs present in the necks of different myosins can vary between zero and seven. Conventional myosin-II has specific light chains, whereas most of characterized unconventional myosins use CaM as light chain. These light chains play an important role in the regulation of motor function of myosin. The smooth muscle myosin is activated by phosphorylation of regulatory light chain. CaM which binds to unconventional myosin is Ca binding protein, and some unconventional myosins are regulated by Ca. Therefore, the number of the IQ motif is directly related to the regulation for diverse motor function of myosin superfamily. (3) The tail domains are the most diverse domains among myosin superfamily. Functional domains, such as SH3 domain, FERM domain, and PH domain are found in the tail of some myosins. Tail of many myosin contains coiled-coil region that allows myosin to dimerize and form two-headed structure. It is likely that the tail domain plays an important role in determining functional properties of myosin by specifying where and with what myosin interacts within the cell. Critical issues underling the diverse biological function of the myosin superfamily are: 1) function of the class specific unique tail domain, and 2) motor function and its regulation.

1.3. Diverse cellular functions of myosin superfamily

The functions of each class of myosin have been shown to be distinct (**Fig. I-4**). Class I is implicated

in endocytic and exocytic membrane traffic (Novak et al., 1995; Geli and Riezman, 1996; Jung et al., 1996; Raposo et al., 1999), whereas class II, or conventional myosin, is known to be a component of the contractile ring in dividing cells and the sarcomere in muscle cells. Myosin III is localized to the photoreceptor cells in the retina and functions in signal transduction (Montell and Rubin, 1988). Myosin V and XI have been shown to be organelle motors in animals and plants, respectively. Myosin VI has been shown to move toward the minus end of actin filaments (Wells et al., 1999); therefore, it is a reverse motor (Wells et al., 1999), and one that is important for vesicular membrane traffic, cell migration and mitosis (Buss et al., 2004). Myosin VII is identified as deafness gene. The other classes of myosin superfamily all possess specific functional properties, although most have not been characterized biochemically.

1.4. Motor function of myosin - Directionality of myosin

It is generally believed that the tail domain of myosin provides the source of functional diversity. However, unique and specific properties of motor allow myosin to accomplish a specific physiological task. Members of the myosin superfamily of actin-based motor proteins were previously thought to move only towards the barbed end (plus end) of the actin filament. Myosin VI has been shown to move towards the pointed end (minus end) of the actin filament – the opposite direction of all other characterized myosins (Wells et al., 1999). The myosin VI motors differ from other myosins in that they have a 53-residue insertion in the 'converter' at the base of the rod-like lever arm (Wells et al., 1999). One predicted that this unique insertion might determine the reverse direction of myosin VI. However, Homma *et al*. showed that chimera having myosin V motor domain and myosin VI neck domain (including unique insert) moves plus end of actin filament, regardless of the presence of 53-amini acids insertion. Thus, this insertion is not responsible for the directionality. Remarkably, the myosin VI lever arm appears to rotate in the opposite direction to smooth muscle myosin II, a plus-end motor, when ADP is released from the motor or 'head', as analyzed by cryoelectron microscopy (Wells et al., 1999). This has been interpreted to mean

that movement of myosin VI towards actin minus ends is due to a molecular cog in the converter region that reverses the direction of movement of the lever arm. The converter domain could thus modulate interactions between the motor and the lever arm to determine motor directionality. However, the molecular mechanism of this oppose directionality is unknown.

1.5. Motor function of myosin - Processivity of myosin

Like directionality, processivity is a property that is intrinsic to motor function. Processivity refers to the ability of a motor to bind to a filament and take successive steps before detaching. Processive movement by a molecular motor was first demonstrated for a single molecule of conventional kinesin (Howard et al., 1989), which steps by 8 nm increments along the microtubule (Svoboda et al., 1993), corresponding to the spacing of tubulin dimers in a protofilament, reaching a maximum force of 7–8 pN. Myosin V has recently been shown to move processively (Mehta et al., 1999). A two-heads-bound state has recently been observed in negatively stained electron micrographs of dimeric myosin V bound to actin (Walker et al., 2000). Two-headed binding to actin was increased by adding ADP at low concentration, consistent with the idea that myosin V complexed to ADP binds tightly to actin. The average distance between the two heads bound to the actin filament was 36 nm, which corresponds to the helical repeat of the filament. Remarkably, a myosin V molecule can walk linearly along an actin filament, stepping over the helical turns by taking ‘strides’ or physical steps of 36 nm (Walker et al., 2000). The mechanism of processive movement is not understood. However, several models have been proposed. The most widely accepted model is hand-over-hand model that heads alternate between leading and trailing position on actin. (Details of hand-over-hand model are mentioned below.)

2. Myosin IX

Class IX myosins have been found in rat (Reinhard et al., 1995; Chieregatti et al., 1998), human (Wirth et al., 1996; Bahler et al., 1997), mouse (Grewal et al., 1999) and C. elegans. In mammals,

class IX myosins are expressed in variety of tissues and cell types (Reinhard et al., 1995; Wirth et al., 1996; Chieregatti et al., 1998). Class IX myosins contain a number of unique features in comparison to the other classes of myosins characterized thus far. The most extensively characterized class IX myosins include the two myosin IX isoforms in rat (Myr5 and Myr 7 (Reinhard et al., 1995; Muller et al., 1997; Chieregatti et al., 1998)) and human (myosin-IXb and myosin-IXa (Wirth et al., 1996; Post et al., 1998; Inoue et al., 2002; O'Connell and Mooseker, 2003). Both class IX myosins have similar overall domain structure (**Fig. I-5**), although they exhibit distinct tissue expression patterns (Reinhard et al., 1995; Wirth et al., 1996; Chieregatti et al., 1998).

2.1. Structure of myosin IXb

The motor domain of myosin IX contains distinctive features compared with other myosins (**Fig. I-3** and **Fig. I-5**). First, there is an N-terminal extension of about 150 amino acids that is structurally homologous to a Ras binding domain, although expressed fusion protein containing this domain from Myr 5 lacks Ras binding activity (Kalhammer et al., 1997). The function of this domain is not yet identified. There is a large insertion (about 140 amino acid) in the head domain at the position of loop2. It has been shown that the change in size and charge of loop2 sequence in myosin II significantly affects the actin-activated ATPase activity, and mechanochemical coupling and actin binding (Uyeda et al., 1994; Rovner et al., 1997). Since the location of this large insertion is near the proposed actin binding interface (Schroder et al., 1993), it is plausible that the large insertion of myosin IX has a critical function in dictating the characteristic of myosin IX motor function. Between the motor and tail domain is a neck domain consisting of IQ light chain-binding motifs. Myosin IXb has four IQs, while myosin IXa has six. At least a subset of human myosin IXb light chains is calmodulin (CaM) (Post et al., 1998).

There are two potential functional domains in the tail domain of myosin IX. First, there is a zinc-binding domain that is similar to phospholipid binding domain of protein kinase C, also known

as C1 domain. Recent analysis of various C1 containing proteins revealed that C1 domains are classified into two types, “typical” and “atypical” (Hurley et al., 1997), which the former binds phorbol ester but the latter does not. The C1 domain in myosin IX is classified in to “atypical” and consistently the expressed domain failed to bind phorbol ester (Reinhard et al., 1995).

Second, there is a GTPase-activating protein (GAP) domain structurally homologous to GAPs for the Rho family of G proteins. Small G-protein Rho subfamily includes Rho, Rac and cdc42, and they are thought to regulate cytoskeletal organization in cells (Bar-Sagi and Hall, 2000). They function as a molecular switches being active in GTP form and inactive in GDP form. The stability of GTP form and GDP form is controlled by several small G-protein modulators such as GAP, GEF and GDI. GAP activates the GTP hydrolysis to produce the GDP bound form thus inactivating Rho family G-proteins. GEF promotes the transition of Rho subfamily proteins from the GDP bound form to GTP bound form, thus activating them, while GDI binds to Rho to stabilize the GDP bound inactive form. Biochemical characterizations of both bacterially expressed Myr 5 and Myr 7 tail domains and tissue-purified human myosin IXb demonstrate that these myosins are active GAPs for Rho but not Rac or Cdc42 (Reinhard et al., 1995; Chieregatti et al., 1998; Post et al., 1998). Moreover, overexpression of both Myr 5 and Myr 7 in cultured cells results in inactivation of Rho in these cells (Muller et al., 1997; Chieregatti et al., 1998). Thus, unlike proposed cargo-carrying functions for most other myosins, class IX myosins may be their own cargo, with the motor domain carrying its Rho-GAP tail to sites that require down-regulation of Rho-dependent signaling.

2.2. Motor function of myosin IXb

Despite the unusual structure of the motor domain, tissue isolated human myosin IXb exhibits robust gliding actin filament movements *in vitro* (Post et al., 1998). Velocities are reduced in the presence of Ca^{2+}, as has been observed for a number of CaM-containing myosins. Myosin

IXb does exhibit unusual actin-binding properties, in that myosin IXb co-sediments with actin in presence of ATP (Post et al., 1998), a property it shares with myosin-Va (Nascimento et al., 1996; Tauhata et al., 2001). Interestingly, high affinity binding to actin at steady state in the presence of ATP is thought to contribute to the unique motile properties of myosin-Va where biophysical studies have shown that this motor is capable of undergoing numerous interactions with an actin filament before diffusing away. Thus, myosin-Va is classified as a highly processive motor (Mehta et al., 1999). However, unlike myosin-Va, which is thought to generate processive motion through a coordinated interaction of two motor domains (Mehta et al., 1999; Rief et al., 2000; Walker et al., 2000), the heavy chain of class IX myosins lacks coiled-coil forming α-helical segments and thus is predicted to be single-headed. Two independent lines of evidence, hydrodynamic determination of native molecular weight and chemical cross-linking studies showed that tissue-isolated myosin IXb is a single-headed structure.

Although Myosin IXb is single-headed, tissue isolated myosin IXb and truncated myosin IXb construct that contains motor domain and IQ motifs show processive movement. This is consistent with the finding that myosin IX co-sediments with actin in the presence and absence of ATP. The key question is how myosin IXb, a single headed myosin, can move processively along actin filaments. It has been shown that myosin V, a two-headed myosin with an expanded neck, moves processively along actin filaments with large steps. Electron microscopic observations demonstrated that myosin V spans the long pitch 36-nm helical repeat of the actin filaments. The two heads of myosin V on an actin filament assume a polar conformation, in which one head is curved and the other is straighter. This has raised the hypothesis that the processive large steps of myosin V are produced by a tilting of the long neck domain of one head, which leads the partner head to the neighboring helical pitch of the actin filament. However, it is obviously impossible for myosin IXb to move processively by this mechanism, as it only has one head. For microtubule-based motors, KIF1A, a single headed kinesin family motor, functions through processive movements

along microtubules (Okada and Hirokawa, 1999). It was proposed for KIF1A, that an electrostatic interaction between a Lysine-rich loop of KIF1A and the Glu-rich carboxy-terminal end of tubulin (E-hook) occurs to prevent the diffusion of KIF1A away from microtubules (Okada and Hirokawa, 2000; Kikkawa et al., 2001). It is plausible that a similar mechanism is operating for the processive movement of myosin IXb on actin filaments.

Another interesting finding is that tissue isolated myosin IX moves plus-end of actin filament, while truncated myosin IXb is a minus-end-directed motor (O'Connell and Mooseker, 2003). The mechanism underlying this bi-directional movement of myosin IX is largely unknown. However, it was proposed that tail domain functions as a conformational switch to regulate the polarity of movement of the myosin IXb motor domain. Two candidates for regulating this polarity switch include Rho and zinc, as myosin IXb tail domain contains a Rho-GAP and a zinc-binding domain. However, motility in the presence of RhoA pre-loaded with the non-hydrolysable GTP analogue GTP-γS or 0.1 mM zinc chloride was plus-end-directed. These results suggest that myosin IXb is bi-directional and that the directionality of movement can be regulated in some way through head–tail interactions.

II: Overview of the myosin ATPase cycle

The actomyosin ATPase cycle appears to be conserved for all myosins. The reaction scheme is shown in **Fig. I-6**. The ATPase pathway is coupled to a mechanical model. The key steps are: 1) rapid binding of ATP to actin-bound myosin (actomyosin) ($K'_1k'_{+2}$), 2) dissociation of myosin from actin (k_{+8}), 3) the hydrolysis of ATP (k_{+3}), 4) rebinding of myosin to actin (k_{+9}), 5) the release of phosphate (k_{+4}), 6) the release of ADP (k_{+5}), 7) the rebinding of ATP. Intermediates are defined according to their affinity for actin. The M•ATP and M•ADP•Pi states are weak-binding

intermediates that attach and detach from actin filament with a low affinity (Kd > 1 μM). The AM and AM•ADP states are strong-binding intermediates that attach to actin filaments with higher affinity (Kd << 1 μM). The strong-binding states are force-bearing intermediates. It is widely believed that the force-generating power-stroke coincides with phosphate release at the transition from the weakly to strongly bound states.

1. Structural mechanism of ATPase cycle

The myosin cross-bridge is a molecular machine with communicating functional units: the actin-binding site, the ATP binding site, and the lever arm, which amplifies the small change at the active site into the large changes. A series of X-ray crystallography revealed the conformation of myosin during ATPase cycle (Rayment et al., 1993b; Fisher et al., 1995; Dominguez et al., 1998; Houdusse et al., 1999; Gerner et al., 2000; Houdusse et al., 2000) (**Fig. 7**). X-ray crystallography shows the myosin cross-bridge to exist in two conformations, the beginning and the end of the "power stroke." A long lever-arm undergoes a 60° to 70° rotation between the two states (**Fig. 7C**). This rotation is coupled with changes in the active site (OPEN to CLOSED) and phosphate release. Actin binding mediates the transition from CLOSED to OPEN.

ATP hydrolysis is coupled with the mechanical motor activity of myosin, which is thought to be universal among all myosin family members. Although the structural changes associated with each step of the ATP hydrolysis cycle of myosin are not completely understood, recent three-dimensional structural analysis of the myosin motor domain/nucleotide complex has provided important information for understanding of the molecular mechanism of myosin motor function (Rayment et al., 1993b; Fisher et al., 1995; Smith and Rayment, 1996). The myosin head contains several clefts, which divide the motor domain into distinct subdomains (**Fig. I-7A**). The cleft that splits the 50-kDa central segment of myosin S1 extends from the nucleotide binding pocket to the actin binding interface, and it is proposed that this cleft closes after ATP hydrolysis (Rayment et

al., 1993b; Rayment and Holden, 1994). This opening and closing process is thought to be coupled with weak and strong binding states, respectively. Furthermore, it is suggested that the closure of the nucleotide-binding pocket triggers a conformational change to generate a bent configuration (Wakabayashi et al., 1992), which is coupled with cross-bridge movement. ATP is bound in a narrow tunnel formed by three regions (P-loop, Switch I, and Switch II) composed of amino acid residues, which are highly conserved in the myosin superfamily (**Fig. 7B**). There are a number of interactions between the triphosphate moiety and the amino acid residues of myosin, which are thought to be important for tight ATP binding, rapid ATP hydrolysis, and the stabilization of the myosin·ADP·Pi metastable ternary complex.

2. Kinetic analysis of myosin superfamily

All characterized myosins share a common ATPase mechanism. However, detailed kinetic analyses suggest that modulation of the rate and equilibrium constants that define the ATPase cycle determines specific properties to these myosins. Understanding the kinetic mechanisms allows potential cellular functions of the different myosin classes to be better defined. The important parameters that influence the mechanical and motile properties of myosin are lifetime of predominant intermediate and the duty ratio. The duty ratio is defined as the fraction of the ATPase cycle that the myosin spends in strong-binding states. Low duty-ratio myosins spend a large proportion of time in the M•ATP and M•ADP•P states. On the other hand, high duty-ratio myosins spend a large proportion of time in the AM and AM•ADP states. The duty ratio of characterized myosins depends on the rates into and out of the strongly bound states, thus depends on the actin and nucleotide concentration.

Kinetic analysis of some members of myosin superfamily revealed that difference in biochemical rate constants provide myosins tuned for diverse biological functions as follows:

Myosin I --- Myosin-I isoforms are the single-headed, membrane-associated members of the myosin superfamily found in most eukaryotic cells. They play essential roles in membrane dynamics (Novak et al., 1995; Tang and Ostap, 2001), cytoskeletal structure (Dai et al., 1999), mechanical signal-transduction (Gillespie et al., 1993) and endosome processing (Novak et al., 1995; Geli and Riezman, 1996; Jung et al., 1996; Raposo et al., 1999). Myosin-Is are the most diverse of the unconventional myosins and are represented by at least two phylogenetically distinct subclasses based on sequence comparison of motor domains (Sokac and Bement, 2000). Subclass-1 myosin-I isoforms have long tails that contain lipid binding (TH1), proline-rich (TH2), and Src homology-3 (TH3) domains. Subclass-2 myosin-I isoforms have short tails that contain only TH1 domains and are also widely expressed.

The kinetic mechanisms of all characterized myosin-Is follow the same pathway with the same biochemical intermediates (Ostap and Pollard, 1996; Jontes et al., 1997; Coluccio and Geeves, 1999; Geeves et al., 2000). However, considerable kinetic variability exists within the myosin-I family. Key rate constants of subclass-1 isoforms are significantly faster (3–10-fold) than those of subclass-2 isoforms. The rates of ADP release from all subclass-1 isoforms are 10-fold faster than subclass-2 isoforms (Ostap and Pollard, 1996; Jontes et al., 1997; Coluccio and Geeves, 1999; Geeves et al., 2000). The rate of ADP release limits sliding velocity (Siemankowski et al., 1985), thus it is proposed that subclass-1 isoforms are better tuned for fast motility, whereas subclass-2 isoforms are better tuned for maintenance of force. All myosin-I isoforms are a low duty ratio motors, so under unloaded conditions it is predominantly weakly bound or detached from actin filaments. Therefore, for myosin I to support motility, a high effective duty ratio must be created by bringing together locally high concentrations of myosin and actin.

Myosin II --- Myosin-II isoforms are the major contractile proteins in muscle and also play several crucial roles in non-muscle contractility. Myosin-II molecules contain two motor domains

and assemble into filaments. The myosin-II family can be divided into non-muscle cytoplasmic, cardiac muscle, smooth muscle, and skeletal muscle subclasses, each with multiple isoforms.

All characterized muscle myosin-II isoforms have comparable unitary forces and displacements — a single skeletal muscle myosin-II molecule generates the same force and displacement as a single smooth muscle myosin-II molecule. However, the kinetic intermediate lifetimes and duty ratios of muscle isoforms show a great deal of variation that results in important mechanical differences, accounting for their functional diversity. For example, the duty ratio and the lifetime of the strong-binding states of smooth muscle myosin are significantly longer than those of skeletal muscle isoforms. In muscle tissue, these kinetic differences are likely to be responsible for smooth muscle having slower rates of contraction and producing higher forces than skeletal muscle. Recent investigations of non-muscle myosin-IIb demonstrate that it is a relatively high-duty-ratio motor under physiological actin and nucleotide concentrations (myosin is attached to actin for 20–50% of its ATPase cycle time). In this way it differs significantly from nonmuscle myosin-IIa and muscle myosin isoforms, which possess low duty ratios (myosin is attached to actin for 10% of its ATPase cycle time). Thus, non-muscle myosin-IIb appears to be adapted for cellular roles requiring tension maintenance, whereas non-muscle myosin-IIa is better suited to more rapid sliding.

Myosin V --- Myosin-V transports vesicles along actin filament tracks over long distances as a single, two-headed molecule. Detailed kinetic analysis of single-headed myosin V demonstrate that ATP binding, dissociation from actin, hydrolysis off actin and Pi release on actin are rapid (200-800 s^{-1}) and essentially irreversible, whereas ADP release is slow (16 s^{-1}) and rate-limiting (De La Cruz et al., 1999; Trybus et al., 1999). As a result, the predominant steady-state intermediate in the presence of physiological ATP concentrations is the strongly bound AM•ADP state, making myosin-V a high-duty-ratio motor.

Myosin VI --- Myosin-VI is apparently a two-headed molecule due to the presence of the putative coiled-coil sequence, does not associate into filaments, and may play a role in endocytosis and membrane trafficking. It was the first myosin discovered to move toward the pointed end of actin filaments (Wells et al., 1999). Myosin VI can walk in vitro as a processive motor when it is dimerized (Rock et al., 2001; Nishikawa et al., 2002; Rock et al., 2005), while myosin VI does not support processive movement when it is monomeric (Lister et al., 2004). Like myosin-V, myosin-VI is a high-duty-ratio motor as a result of its slow rate-limiting ADP release. Additionally, ATP binding is slow and weak (De La Cruz et al., 2001), resulting in a population of nucleotide-free AM (rigor) state intermediates under physiological conditions, which further increases the duty ratio. Thus myosin VI can achieve processive movement by formation of double-headed structure.

Duty ratio and processivity --- A high duty ratio is necessary for continuous movement of myosins. Myosin I and Myosin II are low-duty-ratio motors and must work in ensembles of many motors to sustain continuous sliding. This requirement has been demonstrated in vitro by examining sliding as a function of myosin density. Locally high concentrations of myosin II are created in cells by the assembly of myosin into filaments. Myosin V and Myosin VI are highly processive motor that individual molecule can take multiple steps along an actin filament track before dissociating. Each head of a processive two-headed myosin must have a high duty ratio (>0.5) to increase the probability that at least one motor domain is always attached to actin. Otherwise, the myosin and its transported cargo will diffuse away from actin track.

3. Model for processive movement

Many models have been proposed to account for the processive movement of myosin. Most widely accepted model is 'hand-over-hand' model (Forkey et al., 2003; Yildiz et al., 2003; Warshaw et al., 2005). This model predicts that myosin dwells predominantly in a state with the trailing head strongly bound to actin in the AM•ADP state, and the leading head in equilibrium between a

detached and an engaged-ADP•P state. The engaged-head is bound to actin but has not undergone its power-stroke. The trailing head impedes the leading head from binding actin strongly and slows the rate of Pi release. ADP release from the trailing head results in a conformational change that optimally positions the leading head for actin attachment, allowing the leading head to bind actin strongly, begin its power stroke, and eventually release Pi. The conformational change can be a rotation of the lever arm or, with myosin VI, a more complex, larger-scale rearrangement that has yet to be determined. At low ATP concentrations (at which some structural experiments have been performed), it has been proposed that the leading head may release its products before the trailing head dissociates. ATP binding to the trailing head dissociates it from actin, whereupon the leading-head power stroke swings the trailing head forward and the previous leading head now becomes the trailing head. A defining feature of this model is that the trailing head restricts the lead head from progressing through the cycle.

PART 2. MOTOR FUNCTION OF MYOSIN IXB: GOALS OF THE THESIS PROJECT

I: Kinetic analysis of truncated myosin IXb.

While the actin tranlocating activities of myosin IXb have been studied, there is no report for the ATPase activity of myosin IX. Two independent groups including our group showed that myosin IXb is a single-headed myosin and moves processively on actin filaments. Furthermore, myosin IXb does not dissociate from actin in the presence of ATP. These data imply that the mechanism of motility activity of myosin IX is different from other myosins. Kinetic analysis of myosin ATPase cycle allowed us to understand the mechanism of processive movement, when myosin V and myosin VI are found as processive motors. These myosins populate significant time at AM•ADP state that is strongly bound state with actin, resulting in high duty ratio. Therefore, my goals are

first to elucidate the ATPase activity of myosin IXb and its activation by actin, and second to understand kinetic mechanism of myosin IX to address the question how a single-headed myosin IXb moves processively on actin filaments.

II: Cloning of full-length myosin IXb and initial biochemical characterization of the ATPase activity of full-length myosin IXb.

It has been shown that the motor function of unconventional myosins is regulated by various regulatory mechanisms, such as phosphorylation, Ca-binding to light chains, and association with binding partners. In the case of myosin V and myosin VI, a degree of regulation by calcium is different between truncated constructs and full-length myosin. It has been shown that the global conformational change of the molecule causes a change in activity. Therefore, it is critical to better understand physiological motor function of myosin IX using full-length myosin IXb construct. The goal in this stage is to clone full-length myosin IXb, and examine the ATPase activity of full-length myosin IXb as a first step of biochemical characterization.

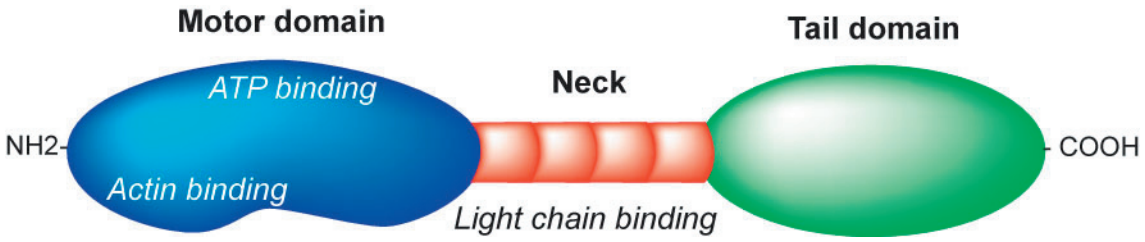

Fig. I-1. **Domain organization of myosin.** Motor domain contains ATP binding site and actin binding site, and shows ATP hydrolysis coupled with actin translocating activity. Neck region contains from zero to seven IQ motifs, and plays a role in regulation of motor function of myosin. C-terminal tail region is highly variable, and determines the cellular function of myosins.

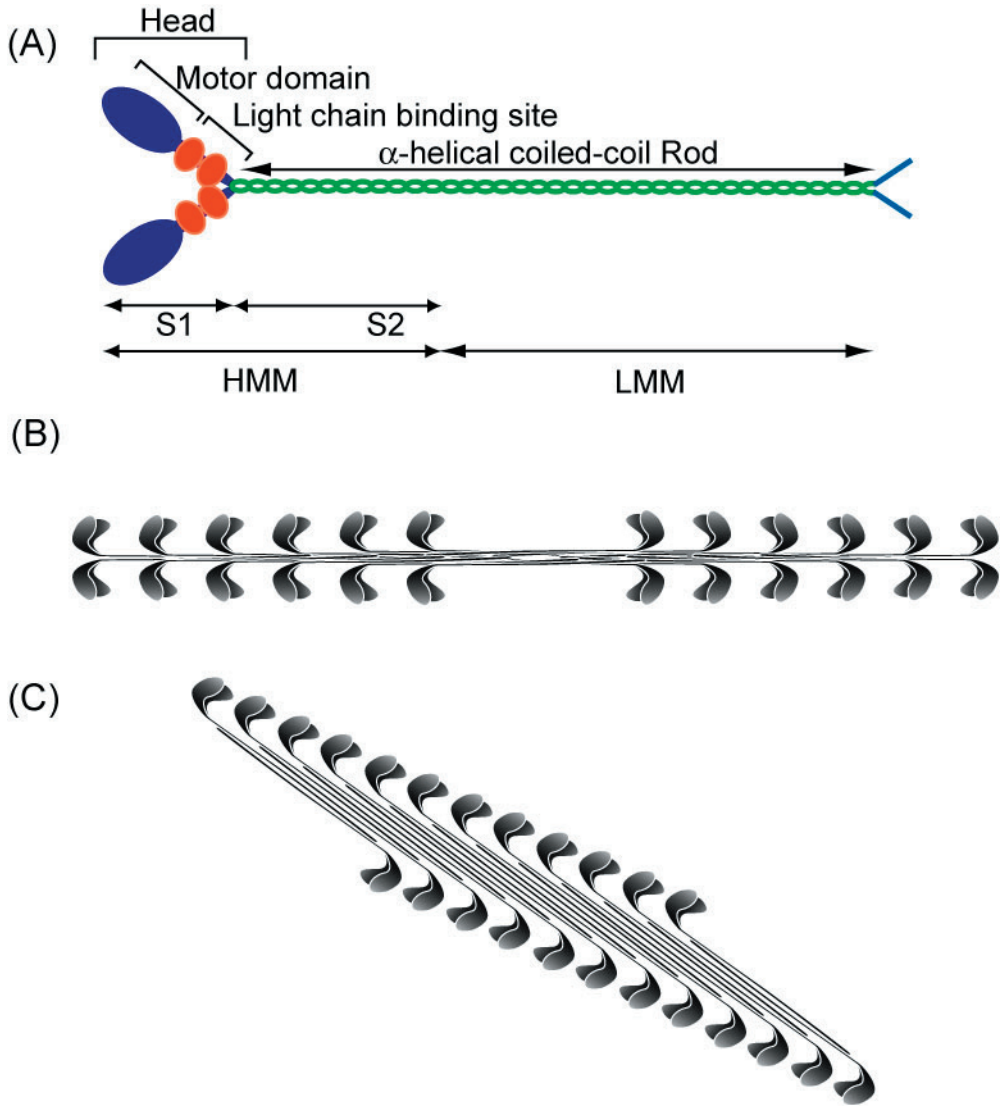

Fig. I-2. **Myosin II.** A, Myosin II forms double-headed structure. Long α-helix of tail region of myosin II forms coiled-coil. B, Bipolar filament. Under physiological conditions, myosins form aggregates that resemble thick filament. A thick filament of striated muscle typically contains several hundred molecules organized staggered array such that the myosin molecules are oriented with their globular heads pointing away from the filament's center. C, Side-polar filament. Side-polar filament does not have a central bare zone found in a bipolar filament. The side polar arrangement permits more myosin head attachment to actin than would be possible in bipolar thick filaments of the same length and a higher force per thick filament for the same amount of myosin. It allows also for greater muscle shortening, as actin filaments are less likely to encounter oppositely polarized actin molecules coming from the other direction.

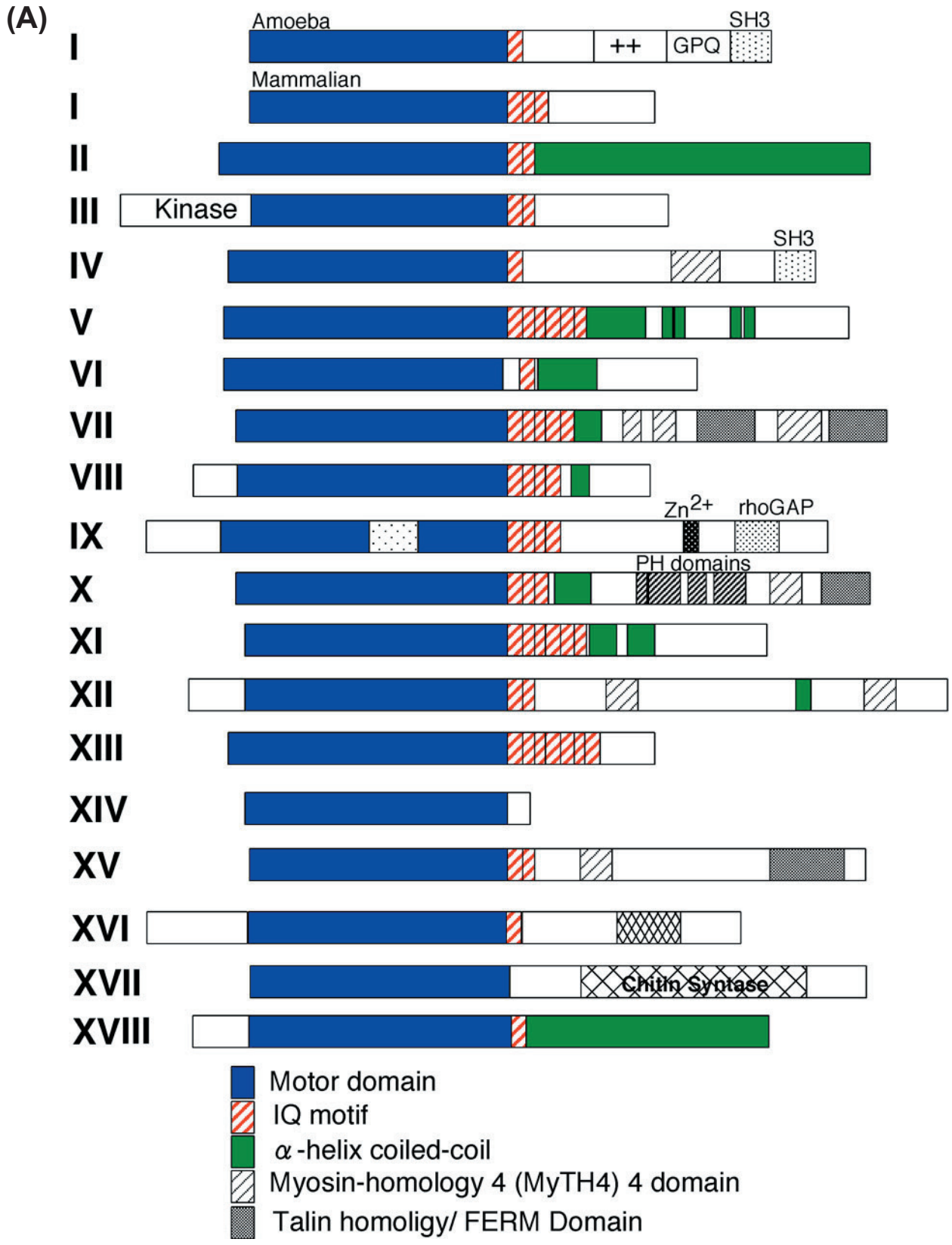
(A)
Amoeba
SH3
I
++
GPQ
Mammalian
I
II
III
Kinase
SH3
IV
V
VI
VII
VIII
Zn2+
rhoGAP
IX
PH domains
X
XI
XII
XIII
XIV
XV
XVI
XVII
Chitin Syntase
XVIII
Motor domain
IQ motif
α-helix coiled-coil
Myosin-homology 4 (MyTH4) 4 domain
Talin homoligy/ FERM Domain

(B)

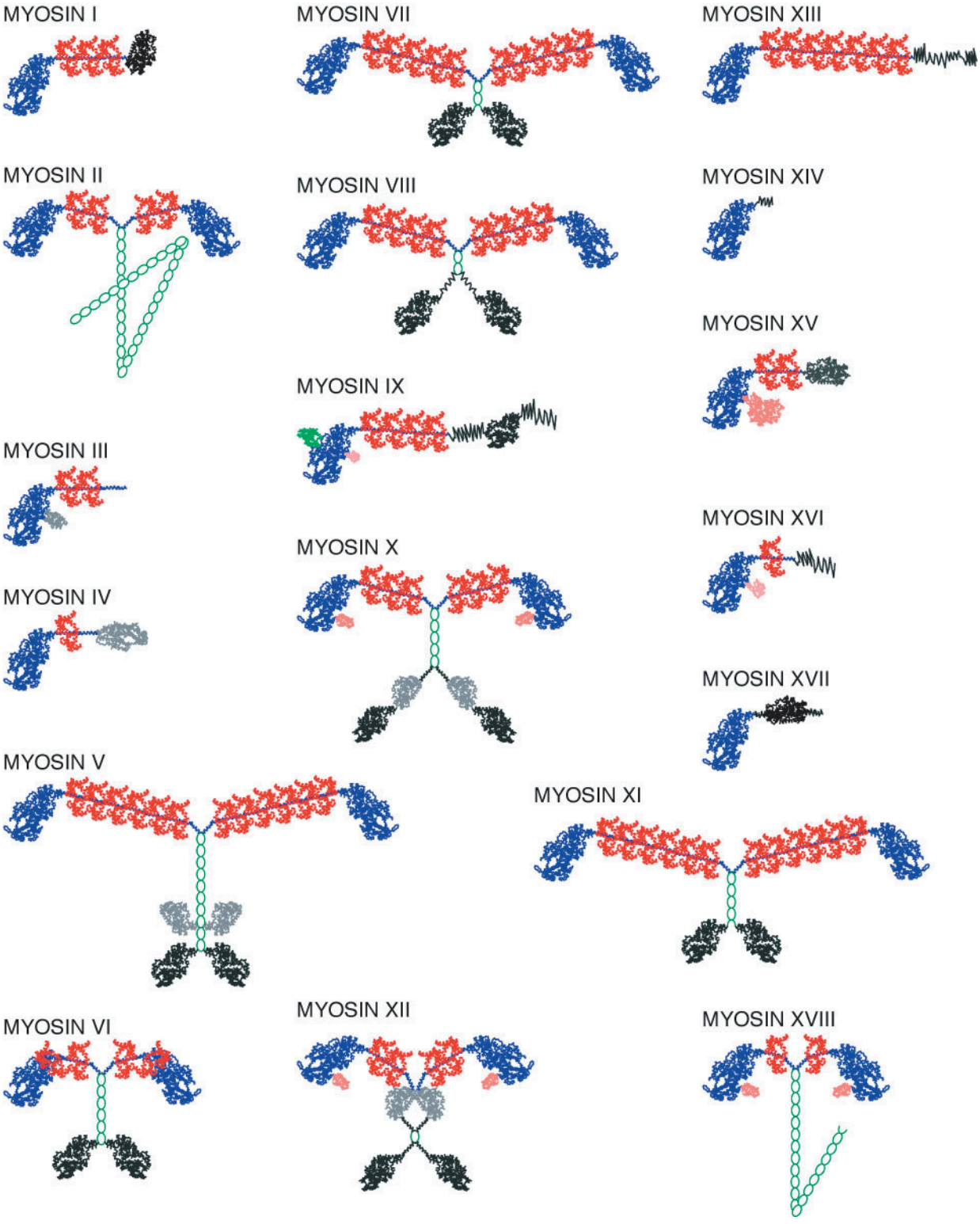
MYOSIN I
MYOSIN II
MYOSIN III
MYOSIN IV
MYOSIN V
MYOSIN VI
MYOSIN VII
MYOSIN VIII
MYOSIN IX
MYOSIN X
MYOSIN XI
MYOSIN XII
MYOSIN XIII
MYOSIN XIV
MYOSIN XV
MYOSIN XVI
MYOSIN XVII
MYOSIN XVIII

Fig. I-3. **Myosin superfamily.** A, Schematic representation of the domain structure of myosin superfamily members. The length of the molecules is drawn roughly proportional to the number of amino acids. While motor domains are conserved, tail regions are highly divergent. B, Model of structure of myosin superfamily. Three-dimensional structures of skeletal myosin motor domain (blue) and calmodulin (red) are used to represent the structure of myosin superfamily. Myosins that have putative coiled-coil region are considered as double-headed structure. Myosin XIII has longest neck because it has seven IQ motifs, while myosin-XIV and –XVII has no IQ motif. It should be noted that myosin VI binds two calmodulins, although it has only one IQ motif.

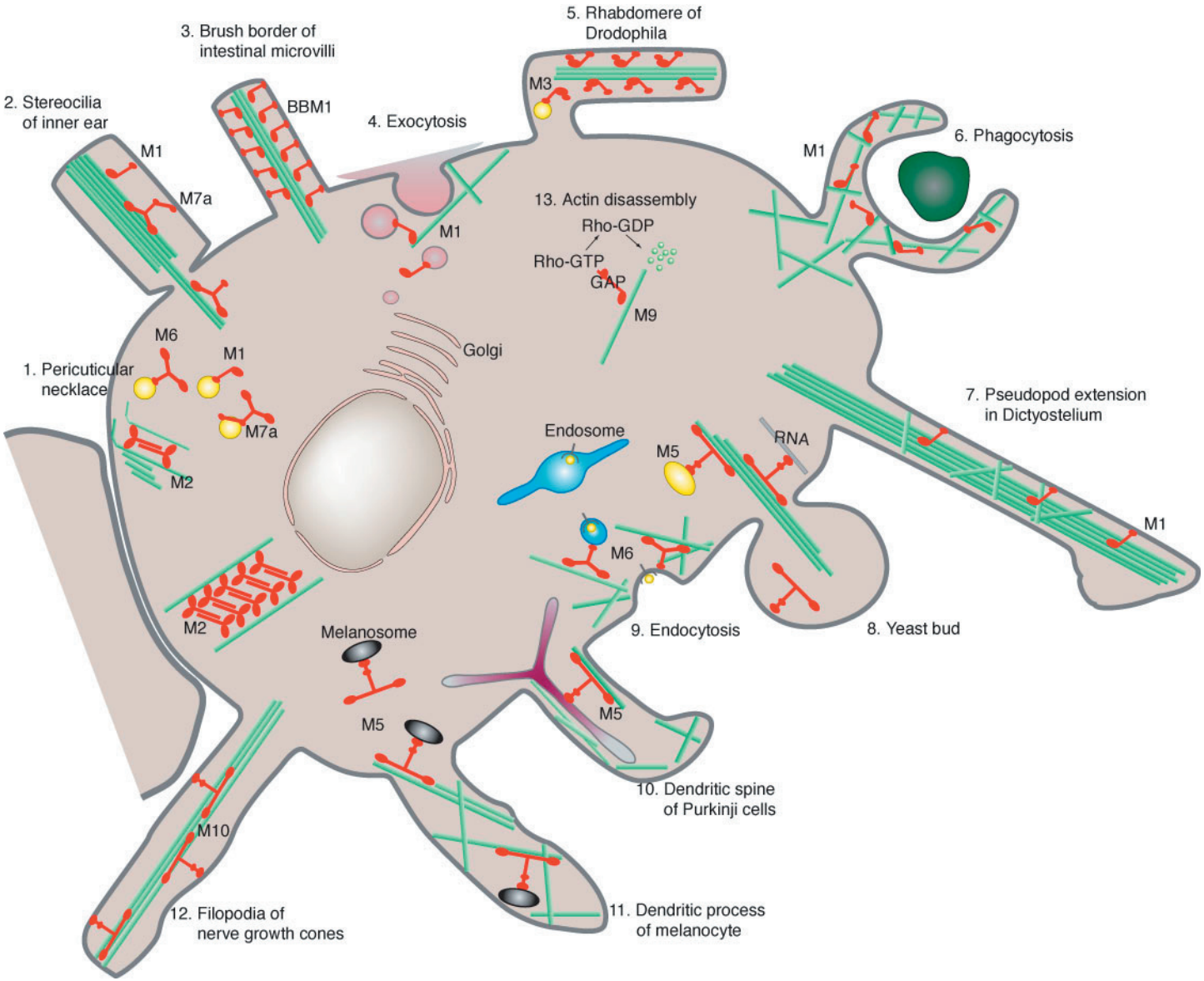
5. Rhabdomere of Drodophila
M3
3. Brush border of intestinal microvilli
BBM1
2. Stereocilia of inner ear
M1
M7a
4. Exocytosis
M1
13. Actin disassembly
Rho-GDP
Rho-GTP
GAP
M9
M1
6. Phagocytosis
M6
M1
1. Pericuticular necklace
M7a
Golgi
M2
Endosome
M5
RNA
7. Pseudopod extension in Dictyostelium
M1
M6
M2
Melanosome
9. Endocytosis
8. Yeast bud
M5
M5
10. Dendritic spine of Purkinji cells
M10
12. Filopodia of nerve growth cones
11. Dendritic process of melanocyte

Fig. I-4. **Super cell showing function of myosin superfamily.** Potential functions for myosins are shown. (1), M1, M6, and M7 exist in the pericuticular necklace (at the base of the stereocilia), a structure between the actin-rich cuticular plate and the circumferential actin band associated with the junctional complex. (2), M1β is shown as the adaptation motor of stereocilia in the hair cells of the inner ear, whereas M6 and M7 anchor and/or stabilize stereocilia. (3), Brush border M1 (BBM1) tethers the microvillar core bundle to the plasma membrane of intestinal microvilli. (4), M1s may assist endocytosis in yeast, *Dictyostelium*, and vertebrate cells. (5), M3 is required for rhabdomere integrity and phototransduction in the *Drosophila* eye. (6) and (7), M1s may play a role in phagocytosis in *Dictyostelium* and macrophages in addition to pseudopod extension in *Dictyostelium*. (8), In yeast, M5s may support organelle and RNA transport. (9), M6 plays a role in endocytosis. M5 may transport smooth ER through dendritic spines of Purkinje cells (10) as well as transport melanosomes though the dendritic processes of melanocytes (11). (12), M10 may assist extension of filopodia of nerve growth cones (12). (13), M9b is a rhoGAP, which inactivates rho and possibly modulates actin organization.

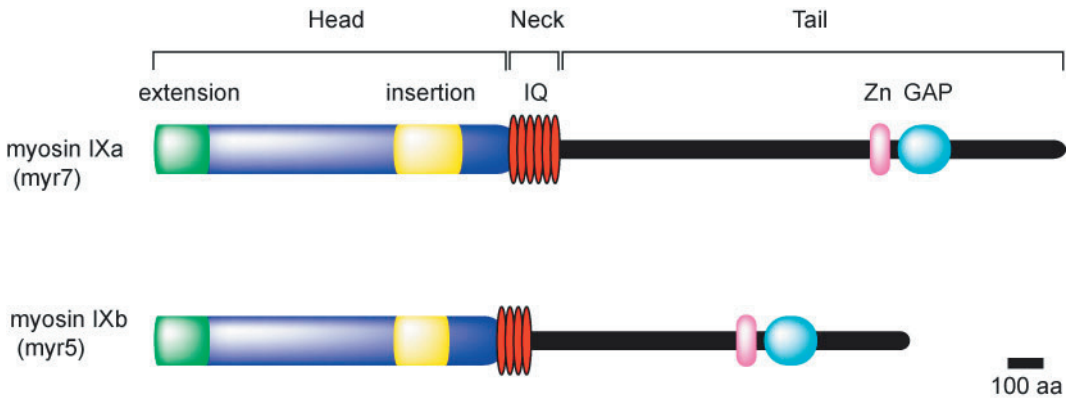

Fig. I-5. **Domain structure of myosin IX subfamily.** Both myosin IX isoforms contain unique extension (green) with 50 % homology and insertion (yellow) with 40 % homology. The number of IQ motifs (red) is different. Myosin IXb has 4 IQs, while myosin IXa has 6 IQs. Zn^{2+} binding motif (Zn, pink) and RhoGAP (GAP, light blue) are shown in C-terminal tail region. Homology of tail region of isoforms is 30 %.

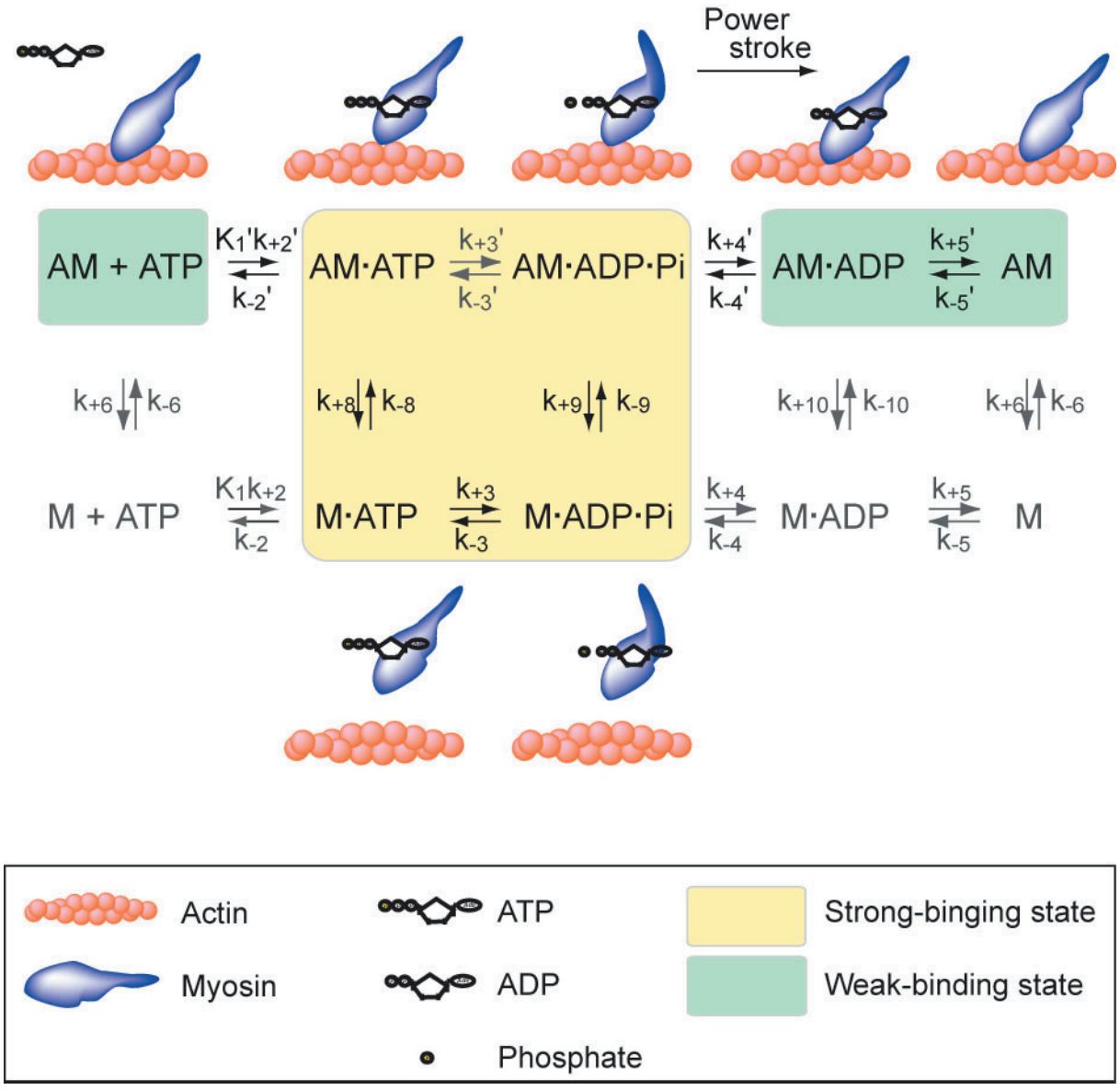

Fig. I-6. **Myosin ATPase cycle.** A, actin. M, myosin. In the absence of ATP, myosin binds tightly to actin (AM). ATP binding (AM•ATP) induces a conformational change in myosin that weakens its actin affinity and causes myosin to detach from actin (M•ATP). A second conformational change allows hydrolysis of ATP to ADP and inorganic phosphate (M•ADP•P). The M•ADP•P state rebinds to the actin filament (AM•ADP•P) and a force-generating power-stroke accompanies phosphate release (AM•ADP). ADP is released (AM) and the cycle repeats upon ATP binding.

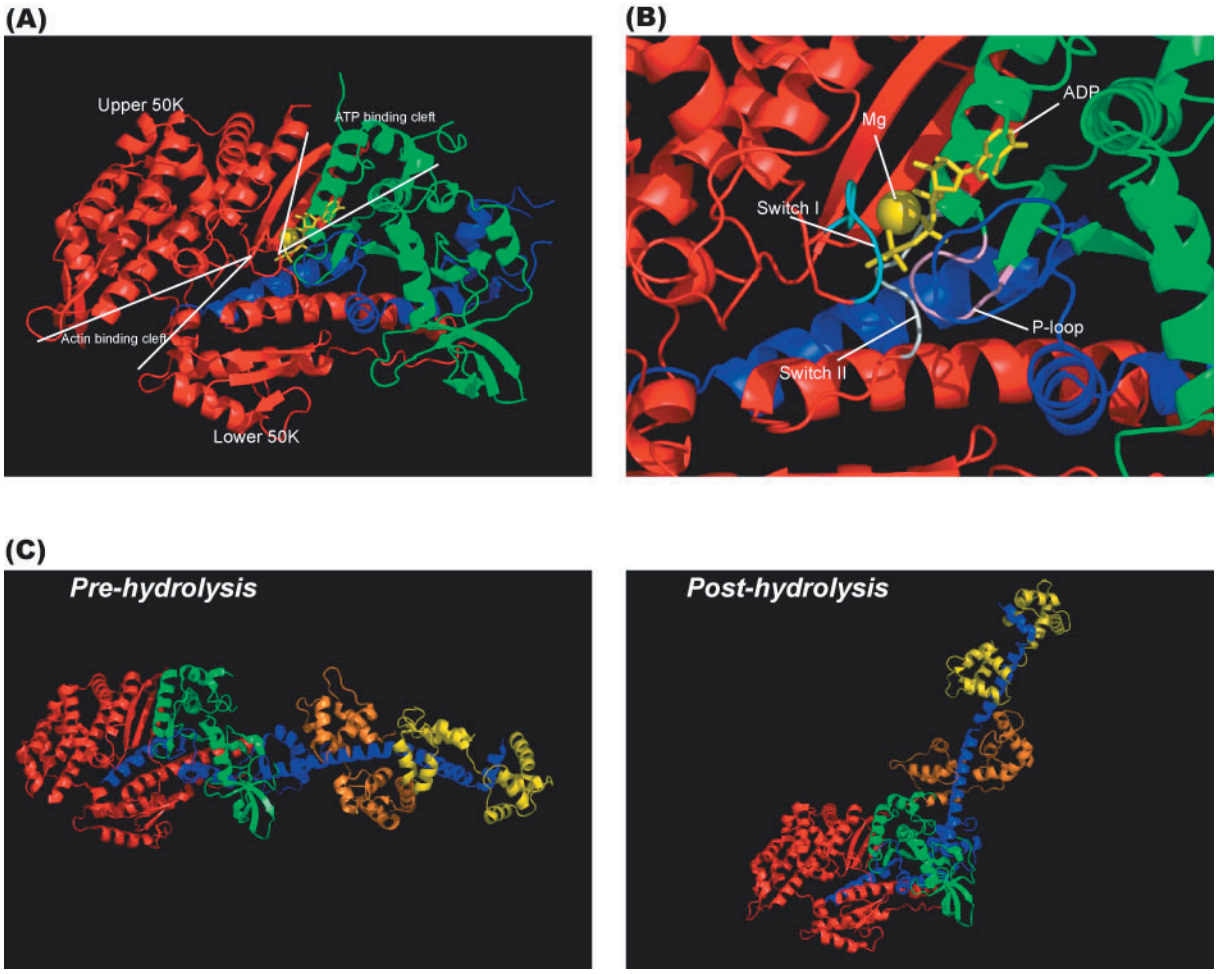

Fig. I-7. **Three-dimensional structures of myosin.** A, 3D-strycture of motor domain of Dictyostelium myosin II with ADP and vanadate, which is phosphate analogue. Limited proteolysis breaks the motor domain into three fragments, named after their apparent molecular masses – 25K (N-terminal, green), 50K (middle, red), and 20K (C-terminal, blue). ADP and Mg^{2+} are indicated by yellow. Structure data is obtained from protein data bank (PDB) using PDB ID = 1VOM. B, Magnified view around ATP binding site. P-loop, Switch I, and Switch II are colored as pink, cyan, and white respectively. C, Two structural states of Scallop S1. Pre-hydrolysis state: nucleotide free (PDB ID = 1DFK), post-hydrolysis state: ADP•V (PBD ID = 1DFL). Two light chains are indicated by yellow and orange. Long lever arm rotates about 60°.

CHAPTER TWO: KINETIC ANALYSIS OF TRUNCATED MYOSIN IXB.

INTRODUCTION

Myosin IXb is a member of the myosin superfamily and found in a variety of tissues including lung, testis, spleen, and liver (Reinhard et al., 1995; Wirth et al., 1996; Chieregatti et al., 1998). Myosin IXb is quite unique among the myosin superfamily in that the tail region contains a GTPase-activating protein (GAP) domain for the small GTP-binding protein, Rho (Reinhard et al., 1995; Post et al., 1998). Thus, unlike proposed cargo-carrying functions for other myosins, Myosin IXb may be a motor protein carrying its Rho-GAP tail to required sites to down-regulate Rho-dependent signaling. Quite recently, it was reported that myosin IXb binds to BIG1, a guanine nucleotide exchange factor for ADP-ribosylation factor (Arf1) (Saeki et al., 2005). BIG1 forms a heterodimer with BIG2 (Morinaga et al., 1996; Togawa et al., 1999), and BIG2 harbors protein kinase A binding sites (Li et al., 2003). It has been reported BIG1 changes its localization from the cytosol to membrane/cytoskeletal components by the stimulation of cAMP signaling (Li et al., 2003). Therefore, it is expected that myosin IX plays a role in translocation of a protein and/or protein complexes.

The studies of myosin IXb revealed that the expressed myosin IX motor domain with four light chain binding sites (Inoue et al., 2002), and the naturally isolated myosin IX (Post et al., 1998) show processive movement that undergoes multiple ATPase cycles before dissociating from actin filament. Consistent with this finding, myosin IXb does not dissociate from actin in the presence of ATP. The mechanism of the unique feature of myosin IX is largely unknown. However, the unique region on the motor domain of myosin IXb might be a key component for the processive movement of a single-headed myosin IXb. There is a large insertion (140 amino acid) in the

middle of motor domain. Since this domain is located at the actin-binding site, so called loop-2, and rich in highly charged residues, it would effect on the actin binding properties.

The mechanism of processive movement can be explained by the studies of kinetics of the ATPase cycle (De La Cruz et al., 1999; De La Cruz et al., 2001). Myosin molecule goes through a characteristic ATPase cycle that is closely correlated with the mechanical cycle of myosin. The key steps are, 1) rapid ATP binding to actomyosin ($K'_1 k'_{+2}$), 2) the hydrolysis of ATP ($k_{+3}+k_{-3}$), 3) the release of phosphate (Pi) (k'_{+4}), and 4) the release of ADP (k'_{+5}) (**Scheme II-1**).

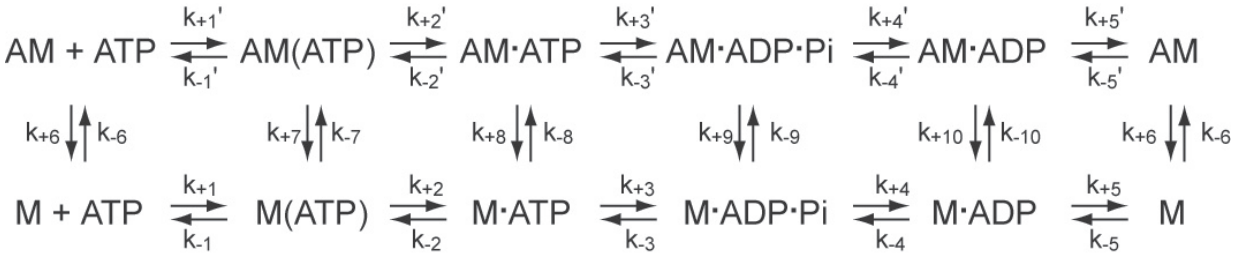

Scheme II-1

During the ATPase cycle, myosin populates either the weak-binding state or the strong binding state. The rate-limiting step of non-processive motor, such as myosin II, is Pi release (k'_{+4}), thus non-processive myosins spend in a large fraction of the weak binding during ATPase cycle. Therefore those myosins can work together in asynchronous ensemble with high speed. On the other hand, the rate-limiting step for myosin V is ADP release (k'_{+5}), thus processive myosins spend the strong-binding state in a large fraction during the ATPase cycle. Because the fraction of strong-binding state for a single head of myosin V is greater than 0.5, double-headed myosin can move processively through a coordinated interaction of two motor domains with actin filament. However, this model cannot account for the processive movement of a single-headed myosin IX. Of interest is how a single-headed myosin IX moves processively on actin filament.

Several questions have to be answered to explain processive movement of a single-headed myosin IX: (1) how much is duty ratio for myosin IX? Duty ratio has to be 1 for a single-headed myosin IX to be processive. (2) Which state is rate limiting? For other processive myosins, the rate-limiting step is AM•ADP state, which is strongly bound state. Question is whether or not AM•ADP state is strongly bound to actin and rate-limiting step is AM•ADP state as myosin V and myosin VI. (3) The weak binding state is identical to other myosin? Other characterized myosins dissociate from actin at the weakly bound state. However, the presence of weakly bound state during ATPase cycle is not consistent with previous observation that myosin IX does not dissociate from actin in the presence of ATP. To elucidate the mechanism by which a single-headed myosin IX moves processively on actin filament, we studied the kinetic characteristics of myosin IX ATPase.

METHODS

Reagents and Proteins.

2'-deoxymantATP (dmantATP) was kindly provided by Dr. Howard D. White (Eastern Virginia Medical School, VA). Rabbit skeletal muscle actin was purified according to Spudich and Watt (Spudich and Watt, 1971), and the actin concentration was determined by absorbance at 290 nm, ε_{290}=26,600 $M^{-1}cm^{-1}$. ATP and ADP concentration were determined by absorbance at 259 nm, ε_{259}=15,400 $M^{-1}cm^{-1}$. The dmantATP concentration was measured at 255 nm using an ε_{255}=23,300 $M^{-1}cm^{-1}$.

Recombinant human Calmodulin (CaM) was cloned from human testis total RNA (clontech). The cDNA was synthesized by reverse transcription with random oligonucleotides. The CaM fragment (accession # BC008437) was amplified with a set of primers, 5'-GCTACT AGTATGGCTGAC CAACTGACTGAAGAG-3' and 5'-ACACTCGAGTCACTTTGCTGTCATCATTTGTAC-3', containing SpeI and XhoI site, respectively. The CaM fragment was digested with *Spe*I and XhoI, and then ligated into pFastbac vector for expression in insect, Sf9 cells. The CaM fragment was introduced to PET30 vector for expression in E. coli. CaM was expressed in E. coli, and purified as described (Ikebe et al., 1998).

Preparation of recombinant Myosin IXb.

The myosin IXb construct used (M9bIQ4) was prepared previously (Inoue et al., 2002). The construct contains nucleotides 1-3,889, encoding residues 1-1296 of human myosin IXb (**Fig. II-1A**). To express recombinant myosin IXb, 300 ml of Sf9 cells (approximately 1 x 10^9) were co-infected with two separate viruses expressing the myosin IXb heavy chain and CaM. The cells were cultured at 27 °C in 175-cm^2 flasks and harvested after 60 h. Cells were lysed in 10 ml of lysis buffer (50 mM HEPES pH 8.0, 0.15 M KCl, 0.5 mM EGTA, 5 mM $MgCl_2$, 5 mM ATP, 5 mM

beta-mercaptoethanol, 1 mg/ml Trypsin inhibitor, and 0.01 mg/ml leupeptin). After centrifugation at 100,000 x *g* for 30 min, the supernatant was mixed with Ni-NTA agarose (Qiagen, Germany) in a conical tube on a rotating wheel for 30 min at 4 °C. The resin suspension was then loaded onto a column, and washed with a 20-fold column volume of buffer containing 30 mM HEPES pH 8.0, 30mM Imidazole, 0.6 M KCl, 0.5 mM EGTA, 5 mM beta-mercaptoethanol, and 0.01mg/ml leupeptin. M9bIQ4 was eluted with buffer containing 0.2 M Imidazole-HCl pH 7.5, 30 mM KCl, 1 mM EGTA, 5 mM beta-mercaptoethanol, and 0.01mg/ml leupeptin. Protein concentration was determined by densitometry of Coomassie-staining gel. Typically 0.3 mg of protein is obtained from 300 ml culture. Protein was used within 6 hours.

Gel Electrophoresis

SDS-polyacrylamide gel electrophoresis was carried out on a 5–20% polyacrylamide gel using the discontinuous buffer system of Laemmli (Laemmli, 1970). Molecular mass markers used were smooth muscle myosin heavy chain (200 kDa), β-galactosidase
(116 kDa), phosphorylase b (97.4 kDa), bovine serum albumin (66 kDa), ovalbumin (45 kDa), carbonic anhydrase (29 kDa), myosin regulatory light chain (20 kDa), and lactalbumin (14.2 kDa). Gels were stained with Coomassie Brilliant Blue R-250.

Steady-state ATPase assay

The ATPase assays were performed at 25 °C in 30mM HEPES, pH7.5, 30mM KCl, 1mM EGTA, 2mM $MgCl_2$, 1mM DTT, and 10μM CaM, otherwise described in figure legend. The reaction was initiated by the addition of [γ-^{32}P]-ATP. Liberated ^{32}P was measured as described previously (Ikebe and Hartshorne, 1985).

Actin binding assay

Various concentrations of actin (1 – 20 μM) were mixed with 0.3 - 0.5μM M9bIQ4 in 30mM

HEPES, pH7.5, 30mM KCl, 1mM EGTA, 2mM $MgCl_2$, 1mM DTT, and 10μM CaM and allowed to sit for 5 min at room temperature. 2 mM ATP was added, and incubated for 5min at room temperature. For the binding assay of M•ADP•P state, 0.1mM ADP and 1mM Vi were incubated with M9bIQ4 for 1hr on ice, then various concentrations of actin were incubated with the ternary complex of M9bIQ4•ADP•Vi for 5min at room temperature. The samples were centrifuged in the Beckman TL-100 at 350,000 x *g* for 5 min. Equal proportions of supernatant and dissolved pellet were run on SDS polyacrylamide gels. The gels were stained with Coomassie Brilliant Blue R-250. The band intensities were quantified using the ImageJ software package to determine the percentage of M9bIQ4 bound to pelleted actin.

To confirm that bound M9bIQ4 contains ADP•Vi, the amount of [^{3}H]-ADP trapped in actoM9bIQ4 was measured. M9bIQ4 was incubated with [^{3}H]-ADP in the presence and absence of 1 mM Vi for 1hr on ice, then 20μM actin and 2mM cold ADP were added to the mixture. If [^{3}H]-ADP•Vi is not stably trapped in the active site of M9bIQ4, [^{3}H]-ADP is replaced by non-radioactive ADP. After incubation for 5 min at room temperature, the samples were ultra-centrifuged. The pellet was washed with the buffer containing 1 mM ADP, and the amount of [^{3}H]-ADP in dissolved pellet was counted by scintillation counter. The concentration of bound M9bIQ4 in dissolved pellet was also determined by densitometry of SDSPAGE gel, and the percent of trapped [^{3}H]-ADP in the M9bIQ4 was calculated.

Photoaffinity labeling of Myosin IXb with ATP

Photoaffinity labeling was performed as described by Maruta and Korn, with some modification. Myosin IXb was mixed with 0.1mM [α-^{32}P]- or [γ-^{32}P]-ATP (9 Tbq/mmol) in 100μl of 30mM HEPES, pH7.5, 30mM KCl, 1mM EGTA, 2mM $MgCl_2$, 1mM DTT, and 0.5mg/ml BSA. The mixtures were irradiated at a distance of 3cm for 2min with UV light at 254nm. The proteins were precipitated by the addition of 5% TCA containing 1% sodium pyrophosphate and collected

by centrifugation. The pellets were dissolved in 20μl of SDS-loading buffer, and then run on SDSPAGE. Incorporation of ^{32}P into myosin heavy chain was analyzed by phosphor imager.

Kinetic experiments

All transient kinetic experiments were done in 30mM HEPES, pH7.5, 30mM KCl, 1mM EGTA, 2mM $MgCl_2$, 1mM DTT, and 10μM CaM at 25 °C using Kin-Tek SF-2001 stopped flow. The concentration of M9bIQ4 after mixing was 0.2-0.6μM, and actin was added at 1.2 times the M9bIQ4 concentration when appropriated. Fluorescence change of dmantATP was measured by fluorescence energy transfer (FRET) by exciting nearby tryptophan residues at 280nm, and emission was detected with 400nm long-pass filter (Oriel). For 90° light scattering, the excitation beam was passed through a 360 nm interference filter.

All of the transients shown are the average of 3 - 6 independent mixings. Single exponential data was fit to the equation $I(t) = c + I\ (\exp\text{-}k_{obs}t)$, and two exponential data was fit to $I(t) = c + I_1(\exp\text{-}k_{obs1}t) + I_2(\exp\text{-}k_{obs2}t)$, where I(t) is the fluorescent signal at time t, c is constant and I, I_1 and I_2 are the amplitude coefficients of reactions with rate constant k_{obs}, k_{obs1}, k_{obs2}.

Quenched flow measurements were performed with Kin-Tek RQF-3 apparatus (KinTek Corp.). Samples of M9bIQ4 or actoM9bIQ4 were mixed with an equal volume of [^{32}P]-ATP. After aging in the delay line, reactions were stopped by mixing with a solution containing 0.3N perchloric acid. Liberated ^{32}P was measured.

Kinetic modeling and simulation were performed based on **Scheme II-1** using STELLA software version 8.1.1 (isee systems, NH).

RESULTS

Expression and Purification of M9bIQ4

The purified M9bIQ4 construct was composed of a high molecular mass band and a low molecular mass band, and free from 200-kDa Sf9 conventional myosin and 43-kDa of actin (**Fig. II-1B**). The high molecular mass band (150 kDa) is consistent with the calculated molecular mass. The small molecular mass band showed mobility shift with the change in [Ca^{2+}] that is characteristic of calmodulin, suggesting that the small subunit is indeed calmodulin.

Steady-state ATPase activity of M9bIQ4.

The actin activated ATPase activity is not significantly activated by actin filament (**Table II-1, Fig. II-2**). Steady-state ATPase activity at saturating ATP concentration (V_{max}) is 0.22 s^{-1} with K_{ATP} of 7.95 μM in the absence of actin, and 0.29 s^{-1} with K_{ATP} of 6.30 μM in the presence of actin. We confirmed the binding of M9bIQ4 to actin by co-sedimentation assay, and M9bIQ4 co-precipitated with actin in the absence of ATP with high affinity (< 0.2 μM). Therefore, lack of activation of ATPase by actin is not due to failure of the binding of M9bIQ4 to actin.

As demonstrated for other characterized processive myosins, myosin V and myosin VI, ATPase activity of processive myosins is inhibited by ADP because of slow dissociation of ADP from the strongly actin binding form of myosin (De La Cruz et al., 2000a; Yoshimura et al., 2001). Thus, we examined if ADP inhibits the ATPase activity of M9bIQ4. In contrast to myosin V and myosin VI, the ATPase activity of M9bIQ4 was not changed with time in the absence and presence of ATP regeneration system (**Fig. II-3**), suggesting that the ATPase of M9bIQ4 is not inhibited by ADP. To further confirm this notion, the ATPase activity of M9bIQ4 was measured as a function of ADP (**Fig. II-4**). In the presence of 0.5 mM ATP, the ATPase activity of M9bIQ4 is not inhibited by 1mM ADP, which is consistent with the observation of no inhibition of the ATPase activity in the

absence and presence of ATP regeneration system. This would be due to the lower affinity of ADP compared with that of ATP. Thus we used lower concentration of ATP to determine the affinity of ADP to M9bIQ4. In the presence of 25 μM ATP, the ATPase activity shows inhibitory effect by ADP (**Fig. II-4**), and K_{ADP} of 16 μM is obtained.

ATP binding to M9bIQ4 and actoM9bIQ4.

The data of steady-state ATPase activity shows that single-headed myosin IX has lower affinity to ADP unlike other characterized processive myosins, suggesting that the mechanism of processive movement for myosin IXb would be different from these myosins. For known processive myosins, ADP release step is slow, and this is the rate-determining step. Of interest is if ADP release is the rate-limiting step for myosin IX. Because the each kinetic step of the ATP hydrolysis cycle is closely correlated to the cross bridge cycle, it is critical to determine rates and kinetic constants for the ATPase cycle of myosin IX to clarify the mechanism of processive movement of single headed myosin IX. Therefore, we further performed the transient kinetic analysis of M9bIQ4. **Table II-2** summarizes the values obtained. The fluorescent nucleotide 2'-deoxymantATP (dmantATP) is used as a probe to measure the rate of nucleotide binding. The dmantATP binding is modeled as two-step binding reaction according to **Scheme II-2** and **Scheme II-3**,

$$M + ATP \underset{}{\overset{K_1}{\rightleftharpoons}} M(ATP) \underset{k_{-2}}{\overset{k_{+2}}{\rightleftharpoons}} M{\cdot}^{*}ATP$$

Scheme II-2

$$AM + ATP \overset{K_1'}{\rightleftharpoons} AM(ATP) \underset{k_{-2}'}{\overset{k_{+2}'}{\rightleftharpoons}} AM{\cdot}^{*}ATP$$

Scheme II-3

, where M(ATP) and AM(ATP) are the collision complex in rapid equilibrium (K_1, K_1') and

isomerize (k_{+2}. k_{+2}') to the high fluorescence M•*ATP and AM•*ATP. MantATP was excited by energy transfer from adjacent tryptophan residues. A fluorescence enhancement of dmantATP upon binding to M9bIQ4 was best fit to single exponential (**Fig. II-5, inset**). The rates are linearly related to the dmantATP concentration. The apparent second order rate constants for dmantATP binding to M9bIQ4 and actoM9bIQ4, given by the slope of the plot of the rate as a function of dmantATP concentration, are K_1k_{+2} = 1.08 $\mu M^{-1}s^{-1}$ and K_1'k_{+2}' = 1.07 $\mu M^{-1}s^{-1}$, respectively (**Fig. II-5**). The linear fits of the rates do not pass through the origin. The y-intercept indicates dissociation rate of dmantATP (k_{-2}, k_{-2}'). The dissociation rates for M9bIQ4 and actoM9bIQ4 are 2.22 s^{-1} and 3.43 s^{-1}, respectively.

There is a tryptophan residue on M9bIQ4 corresponding to chicken skeletal muscle myosin Trp510. This tryptophan is known to enhance the fluorescence upon ATP binding and/or hydrolysis. Thus we examined the tryptophan fluorescence enhancement of M9bIQ4. However, there is no detectable change of tryptophan fluorescence of M9bIQ4 with ATP binding.

ATP hydrolysis.

The rate of hydrolysis was measured directory by quench-flow. This is modeled as two-step reaction according to **Scheme II-4** and **Scheme II-5**.

$$M + ATP \underset{}{\overset{K_1}{\rightleftharpoons}} M(ATP) \underset{k_{-2}}{\overset{k_{+2}}{\rightleftharpoons}} M{\cdot}ATP \underset{k_{-3}}{\overset{k_{+3}}{\rightleftharpoons}} M{\cdot}ADP{\cdot}P$$

Scheme II-4

$$AM + ATP \underset{}{\overset{K_1'}{\rightleftharpoons}} AM(ATP) \underset{k_{-2}'}{\overset{k_{+2}'}{\rightleftharpoons}} AM{\cdot}ATP \underset{k_{-3}'}{\overset{k_{+3}'}{\rightleftharpoons}} AM{\cdot}ADP{\cdot}P$$

Scheme II-5

The first step is ATP binding to Myosin (K_1k_{+2} and $K_1'k_{+2}'$). The second step is hydrolysis of ATP (k_{+3} and k_{+3}'). All characterized myosins rapidly hydrolyze ATP to form M•ADP•P complex (Pi burst), which is followed by slow product release. Formation of the myosin•ADP•P complex is necessary for normal motor function for myosin II (White et al., 1993; White et al., 1997; Kambara et al., 1999). Experiment is done by double mixing method. M9bIQ4 is mixed with [γ-^{32}P]-ATP, holds in a delay line for the desired time, and then quenched by a second mix with acids. Formation of M•ADP•P can be determined by monitoring initial phosphate burst by denaturation of myosin. When excess ATP is incubated with myosin, timecourse would show an initial rapid phase of Pi burst followed by a slower linear phase of steady state rate. Alternatively when ATP concentration is less than that of myosin, Myosin hydrolyzes ATP only one cycle. Timecourse for single turnover would show two exponential of which the first rapid phase is due to rapid ATP binding and hydrolysis of ATP, and the second slow phase is from slow product dissociation. There are two advantages on single turnover measurement; (1) the rates obtained by single turnover experiment is independent of protein concentration, while second linear phase for multiple turnover is divided by protein concentration to obtain steady state rate. (2) Because of < micromolar ATP concentration, the data shows less signal-to-noise ratio. Therefore, single turnover of ATP hydrolysis of M9bIQ4 is measured. Unlike other myosins, time course of hydrolysis is best fit to a single exponential in the presence and absence of actin (**Fig. II-6**), suggesting that M9bIQ4 does not form M•ADP•P rapidly and rate of product off is faster than that of hydrolysis. The apparent hydrolysis rates of single turnover of ATP hydrolysis are 0.06 s^{-1} and 0.08 s^{-1} in the absence and presence of actin, respectively.

Upon **Scheme II-4** and **Scheme II-5**, if equilibrium of the first step (ATP binding to Myosin, K_1k_{+2} and $K_1'k_{+2}'$) is rapid compared to the second step, which is the formation of M•ADP•P, the observed rate constant of the formation of M•ADP•P is described as,

$$k_{obs} = k_{+3}\left(\frac{[\overline{M}] + [\overline{ATP}]}{K_D + ([\overline{M}] + [\overline{ATP}])}\right) + k_{-3}$$

, where $K_D = k_{-2}/K_1k_{+2}$, and [M] and [ATP] are [M] and [ATP] at the equilibrium, respectively. At high concentration of ATP, when $[ATP]_o >> K_D$, the observed rate constant is $k_{+3}+k_{-3}$. However, when $[ATP]_o$ is not in excess of K_D, the observed rate constant is dependent on K_D. Thus, we obtain apparent second order kinetics for a first order reaction, which is preceded by a rapid equilibrium of ATP binding. For myosin-I, -II, and -V, there is no ATP dissociation from myosin (k_{-2}). Therefore, hydrolysis can be described as $k_{+3}+k_{-3}$. On the other hand, ATP dissociates from myosin IX (**Fig. II-5, Table II-2**). Thus the observed rate constant is slower than steady-state ATPase activity at the given ATP condition.

Figure II-7 shows the simulation to obtain k_{+3} and k_{+3}' values from k_{obs} (**Fig. II-6**) using **Scheme II-4** and **Scheme II-5**, respectively. At given M9bIQ4 and ATP concentration, k_{+3} and k_{+3}' values should be 0.24 s^{-1} and 0.45 s^{-1} to obtain k_{obs} = 0.06 s^{-1} in the absence of actin and 0.08 s^{-1} in the presence of actin, respectively. **Table II-3** summarizes the true hydrolysis rate obtained from k_{obs} in different M9bIQ4 and ATP concentration. This simulation suggests that k_{+3} is 0.21 ~ 0.25 s^{-1} and k_{+3}' is 0.40 ~ 0.46 s^{-1}. These rates are similar to that of steady-state ATPase, suggesting that ATP hydrolysis is the rate limiting for M9bIQ4.

Predominant intermediate during ATPase cycle.

To further confirm that ATP hydrolysis is rate limiting, we performed photoaffinity labeling of M9 with ^{32}P-labeled ATP. UV-irradiation induces photolabeling of myosin by ATP in the active site. Myosin samples were irradiated by UV in the presence of [α-^{32}P]-ATP or [γ-^{32}P]-ATP, and the incorporation of ^{32}P into myosin heavy chain was analyzed by phosphor imager. For smooth muscle heavy meromyosin (SmHMM), radioactivity is detected if myosin is irradiated with [α-^{32}P]-

ATP, but not with [γ-^{32}P]-ATP (**Fig. II-8**). SmHMM rapidly hydrolyze ATP. The non-covalently associated Pi dissociated from myosin heavy chain upon acid quenching. Thus, [γ-^{32}P]-ATP, which cross-linked to active site would be expected to lose γ-^{32}P after hydrolysis. On the other hand, similar radioactivity is detected when myosin is irradiated with [γ-^{32}P]-ATP to that with [α-^{32}P]-ATP for M9 (**Fig. II-8**). This is consistent with the notion that M9bIQ4 does not have a rapid Pi burst, indicating that the predominant steady-state intermediate is M•ATP state for myosin IX. We could not detect the radioactivity when myosin IX is mixed with [α-^{32}P]-ATP and [γ-^{32}P]-ATP in the presence of actin (not shown), suggesting that the conformation of the ATP binding site is different between in the presence and in the absence of actin.

Actin binding properties.

We further examined details of unique actin binding properties of myosin IX. The rate of actin binding was measured by monitoring light scattering. The association of myosin with actin in the absence and presence of ADP is modeled as shown in **Scheme II-6** and **Scheme II-7**.

$$AM \underset{k_{-6}}{\overset{k_{+6}}{\rightleftharpoons}} A + M$$

Scheme II-6

$$AM{\cdot}ADP \underset{k_{-10}}{\overset{k_{+10}}{\rightleftharpoons}} A + M{\cdot}ADP$$

Scheme II-7

The time courses of M9bIQ4 and M9bIQ4•ADP binding to actin follow two exponential rates (**Fig. II-9, inset**). Fast phase is linearly related to actin concentration (**Fig. II-9**), while the rates of slow phase show little actin dependence (not shown). The apparent second order rate constant for

M9bIQ4 binding to actin determined by slope is 5.2 $\mu M^{-1}s^{-1}$ in the absence of ADP (k_{+6}) and 5.4 $\mu M^{-1}s^{-1}$ in the presence of ADP (k_{+10}).

The rate of actoM9bIQ4 dissociation by ATP was measured by monitoring light scattering. The mechanism of ATP induced dissociation is modeled as **Scheme II-8**.

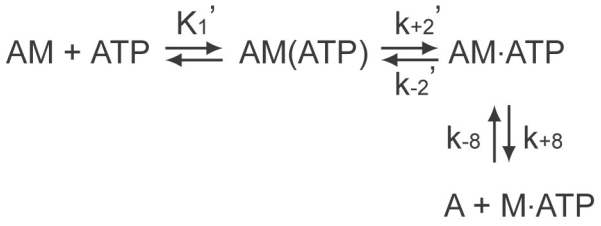

Scheme II-8

The first step is binding of ATP to actoM9S1 (K_1k_{+2}). The second step is dissociation of M9bIQ4 from actin (k_{+8}). Mixing ATP with actoM9S1 results in a decrease in light scattering (**Fig. II-10A**). The time courses follow two exponentials. Fast phase depends hyperbolically on ATP concentration (**Fig. II-10B**), while the rates of slow phase show no ATP dependence (not shown). The maximum rate is $k_{+8}+k_{-8}[A] = 13.0\ s^{-1}$. This is extremely slow compared to other characterized myosin that the rate of dissociation is typically >500 s^{-1}.

Light scattering was monitored to measure ADP dissociation from actoM9bIQ4. The actoM9bIQ4•ADP complex was mixed with ATP. In the presence of excess ATP, the dissociation of M9bIQ4 from actin should be limited by the rate of ADP release (k_{+5}') as described by **Scheme II-9**.

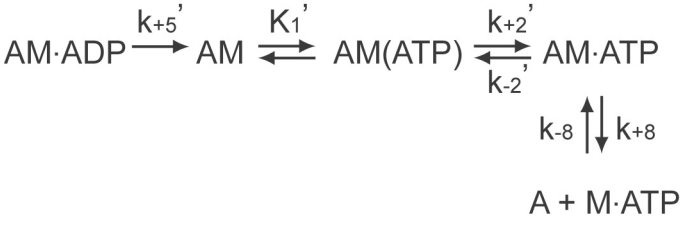

Scheme II-9

Premixing actoM9bIQ4 with 0.25mM ADP decreases the maximum rate of ATP-induced dissociation of M9bIQ4 from actin to 3.34 s^{-1} (**Fig. II-10B, C**). Thus the dissociation rate of ADP from actoM9bIQ4 is k_{+5} = 3.34 s^{-1}, which is 10-fold faster than steady-state ATPase activity. Therefore, the result suggests that ADP release is not the rate-determining step for M9bIQ4. Since the affinity of ADP to actoM9bIQ4 (K_{ADP}) is 16 μM (**Fig. II-4**), the association rate constant for ADP to actoM9bIQ4 is calculated to be 0.21 $\mu M^{-1}s^{-1}$.

Unlike other myosins, myosin IX binds to actin in the presence of ATP (Post et al., 1998; Inoue et al., 2002). Thus, we determined the binding affinity of M9bIQ4 to actin by co-sedimentation with increased actin concentration in the presence of ATP (**Fig. II-11A**). The band intensities of M9bIQ4 in the supernatant and pellet were quantified by densitometry, and the percent of bound M9bIQ4 was plotted as a function of actin concentration (**Fig. II-11B**). The points in graph are fit to hyperbola that assume 100% binding at infinite actin concentration, because M9bIQ4 shows complete binding to actin in the absence of ATP. The affinity of M9bIQ4 to actin in the presence of ATP is K_d = 2.33 μM. Since the predominant intermediate is M•ATP (**Fig. II-6, II-7, and II-8**), K_d value is considered as K_8 (= k_{-8}/k_{+8}). Since $k_{+8} + k_{-8}$[actin] is equal to 13.08 s^{-1}, where [actin] = 0.6 μM (**Fig. II-10B**), the values of k_{+8} and k_{-8} are calculated to be 5.45 $\mu M^{-1}s^{-1}$ and 12.7 s^{-1}, respectively.

For Other Myosins, M•ATP and M•ADP•P bind to actin weakly. However, M9bIQ4•ATP state

has much higher binding affinity than other myosin. Of interest is if M•ADP•P state of myosin IX binds weakly to actin. We determined the affinity of M•ADP•P state of myosin IX. It is shown that myosin forms stable ternary complex with ADP and phosphate analogue, vanadate (Vi) (Goodno, 1979; Goodno and Taylor, 1982). Because Vi ion adopts trigonal bipyramidal coordination, it is proposed that Vi mimics the conformation of phosphate groups at the transition state expected for phosphoryl transfer (Lindquist et al., 1973; Westheimer, 1987). In myosin, it is believed that M•ADP•Vi complex mimics M•ADP•P state (Goodno, 1979; Goodno and Taylor, 1982). The half-life for dissociation of M•ADP•Vi complex of myosin II at 0 °C is ~4days (Goodno, 1979; Goodno, 1982; Werber et al., 1992). Actin increases the rate of release of vanadate by 10^5 compared to that of M•ADP•Vi alone, although the release of vanadate is still slow. Therefore, we confirmed the binding of ADP•Vi to actoM9bIQ4 using [^{3}H]-ADP. M9bIQ4 with excess [^{3}H]-ADP and Vi was incubated with 20μM actin, and then the amount of trapped [^{3}H]-ADP on M9bIQ4 of actin bound fraction was counted by scintillation counter. As shown in **Figure II-12A**, nearly 100% of M9bIQ4 of bound fraction trapped [^{3}H]-ADP in the presence of Vi, whereas little [^{3}H]-ADP is trapped without Vi. These results suggest that M•ADP•P state of M9bIQ4 has high affinity to actin. Actin co-sedimentation assay was performed in the presence of ADP and Vi. As shown in **Figure II-12B**, M9bIQ4 co-precipitated with actin. When bound M9bIQ4 is plotted as a function of actin concentration, the affinity of M9bIQ4•ADP•P is obtained. The obtained K_9 is 1.2 μM (**Fig. II-12C**).

DISCUSSION

Overview of M9bS1 ATPase.

M9bIQ4 has a low K_{actin} (2.3μM) and has a little (~ 1.3 times) actin-activation of steady-state ATPase rate (**Table II-1**). For other characterized myosins, actin accelerates the product release (i.e. Pi release or ADP release). Since M9bIQ4 has a rate-limiting step at hydrolysis step (**Fig. II-6, II-7, and Table II-3**), this is not a case for M9bIQ4. The rate of hydrolysis is faster in the presence of actin (k_{+3}' = ~ 0.45 s^{-1}) than that in the absence of actin (k_{+3} = ~ 0.2 s^{-1}). Therefore, the low actin-activation of M9bIQ4 is the result of the actin-activation of the hydrolysis rate. The predominant pathway under physiological condition is: (a) ATP binding to actoM9; (b) M9 dissociates from actin upon ATP binding but rapidly re-associates at high actin concentration; (c) hydrolysis is slow, and determining the rate of steady-state ATPase; (d) the M•ADP•P complex dissociates from actin but rapidly re-associates at high actin concentration; (e) Pi is released from M9 while M9 binds to actin; (f) ADP is released from actin-bound M9. Because the hydrolysis is the rate limiting, and M9•ATP complex associates with actin at saturated ATP and actin concentration (**Fig. II-11**), the predominant steady-state intermediate is AM•ATP state. This is also confirmed by the photoaffinity labeling of Myosin IX with ATP.

ATP binding

The binding of ATP to M9bIQ4 and actoM9bIQ4, determined by dmantATP fluorescence change, is fast (**Fig. II-5, Table II-2**). The rate of ATP binding to actoM9IQ4 is also determined by the light scattering of ATP-induced dissociation of actoM9bIQ4 (**Fig. II-10**). The association rate constant for ATP binding to actoM9IQ4 obtained from the initial slope is 0.43 $\mu M^{-1}s^{-1}$, which is similar to the rate constant obtained from dmantATP fluorescence. The rate of ATP binding at physiological ATP concentration (Roth and Weiner, 1991) is 860 ~ 2000 s^{-1}, which is at least > 3000-fold faster than the rate limiting step. Therefore, the nucleotide free state of M9bIQ4 is not significantly

populated.

The intrinsic tryptophan fluorescence of myosin is enhanced upon nucleotide binding and is further enhanced by the hydrolysis of ATP. This property has been exploited to examine the rates of the reaction steps in skeletal and smooth muscle myosin in both the absence and presence of actin (Lymn and Taylor, 1971; Bagshaw et al., 1974; Marston and Taylor, 1980; Rosenfeld and Taylor, 1984; Cremo and Geeves, 1998). The structural basis of nucleotide-dependent intrinsic fluorescence changes in myosin II has been previously investigated in skeletal muscle (Park et al., 1997), smooth muscle (Yengo et al., 1998; Yengo et al., 1999; Yengo et al., 2000; Yengo et al., 2002a), and the slime-mold Dictyostelium discoideum (Batra and Manstein, 1999; Malnasi-Csizmadia et al., 2000; Kovacs et al., 2002). In all three isoforms, a tryptophan residue located on the rigid relay loop (W501 in D. discoideum non-muscle myosin II, W510 in skeletal muscle myosin, and W512 in smooth muscle myosin) has been shown to be the largest contributor to the observed intrinsic fluorescence enhancement associated with nucleotide binding and/or hydrolysis. The rigid relay loop is a region of the myosin II molecule thought to be critically involved in the conduction and amplification of structural changes at myosin's active site to both the lever arm and actin binding interface (Houdusse and Sweeney, 2001). The tryptophan residue corresponding to chicken skeletal muscle myosin Trp510 is highly conserved among myosin superfamily, and the fluorescence enhancement upon ATP binding has been reported with unconventional myosins, myosin-I (El Mezgueldi et al., 2002), -V (De La Cruz et al., 1999; Trybus et al., 1999). Among the myosin superfamily, only myosin VI does not have the corresponding tryptophan residue. When tryptophan residue is introduced to the corresponding site, myosin VI showed fluorescence enhancement upon ATP binding (Sato et al., 2004), suggesting that the conformational change of this region is conserved among myosin superfamily. However, we could not observed the change of fluorescence for M9bIQ4, although Myosin IX has the tryptophan residue at the corresponding site (not shown). This would be due to slow hydrolysis of myosin IXb.

Hydrolysis

The hydrolysis rate of M9bIQ4 on actin is nearly identical to the maximal steady-state actin activated ATPase rate, suggesting that the equilibrium favor is M•ATP state. This is confirmed by the photoaffinity labeling of myosin IXb with ATP showing that the predominant intermediate is M•ATP state for myosin IX. Taken together, these results suggest that hydrolysis is rate limiting of myosin IXb ATPase cycle. This is the first myosin shown that hydrolysis is the rate-limiting step.

It is previously shown that at very low ionic strength conditions (1 mM MOPS and 0.4 mM $MgCl_2$) and saturating actin concentration, the hydrolysis step could be rate limiting for actin bound skeletal muscle myosin ATPase (White et al., 1997). The forward rate of the hydrolysis step (k_{+3}') was slower when myosin binds to actin than in the absence of actin (k_{+3}). Rate constants for the hydrolysis step in the presence of actin were $k_{+3}' = 0.7\ s^{-1}$ and $k_{-3}' = 7\ s^{-1}$. At physiological condition, myosin dissociates from actin upon binding of ATP. Thus, myosin hydrolyzes ATP while dissociating, then rebinds to actin at M•ADP•P state. Therefore, if the weak binding states (M•ATP and M•ADP•P) of myosin had a high actin affinity, ATP hydrolysis would occur while attaching to actin. Indeed this is the case for myosin IX, since the affinity of M•ATP and M•ADP•P to actin was significantly high for Myosin IX (**Fig. II-11** and **Fig. II-12**).

Mechanism of ATP hydrolysis

ATP hydrolysis of myosin is tightly coupled with the change of its conformation. The transition-state structures, crystallized when either ATP or ADP•P analogs are bound to myosin (Fisher et al., 1995; Smith and Rayment, 1996; Dominguez et al., 1998; Houdusse et al., 2000), show that ATP hydrolysis requires interactions among Switch I, Switch II and the γ-phosphate that result in the closure of the γ-phosphate pocket, preventing Pi release (**Fig II-13**). However, there is no proton acceptor within 5.5 Å of the vulnerable P-O linkage of bound ATP. It was proposed that

two molecules of water bound in the γ-phosphate pocket by hydrogen-bond with Switch I and Switch II (Fisher et al., 1995; Smith and Rayment, 1996) play a role in this catalytic event. One of the hydrogen atoms of the water, w_1, initially bonded to an oxygen atom of the γ-phosphate group, then interacts with the oxygen atom of a new, intruding water, w_2. The other hydrogen atom remains bonded to the main chain carbonyl oxygen of Ser-237 (residue number is based on the sequence of Dictyostelium myosin II) on Switch I. A result of making this critical conjecture is that w_1 ends up partially positioned and oriented to carry out its attack on the γ−phosphorus. Therefore, water network plays a critical role in ATP hydrolysis. Comparison of X-ray crystal structures revealed that the myosin motor domain bends at Ile-455 and Gly-457 (residue numbers are based on the sequence of Dictyostelium myosin II) located at the Switch II pre- and post-hydrolysis. This suggests that a flexible hinge region in the myosin motor domain has a critical role in the coupling of ATP hydrolysis to mechanical work. Previously we showed the mutation of the conserved residues on Switch II, Asp454, severely disrupted the normal ATPase activity of smooth muscle myosin (Kambara et al., 1999). Asp454 form the hydrogen bond with water, w_3, which also forms hydrogen bond with Mg^{2+} ion coordinated with the tri-phosphate moiety of ATP. The substitution of Asp454 with Ala (D454A) disrupts this hydrogen bond. The D454A can form a rigor complex with actin, but ATP does not induce dissociation of D454A from actin. Although the structure of the actin-binding interface is preserved, the ATP-induced conformational change required to reduce actin affinity is disrupted. Although D454A shows significant basal Mg^{2+}-ATPase activity, it has neither actin-activated ATPase activity nor an initial Pi burst. These results suggest that w_3 also play a role in hydrolysis of ATP. Quite interestingly, the enzymatic character of D454A is similar to that of M9bIQ4. The mutation abolishes the hydrogen bonding of the side chain of residue 454 to the w_3. Therefore, it would be expected that the conformation around Switch II of Myosin IX is different from other myosins, and maybe the residue of myosin IXb corresponding to Asp454 of Dictyostelium myosin II is not able to form the hydrogen bond with the w_3.

Phosphate release

When single-turnover kinetic measurement of ATP hydrolysis was performed using rapid chemical quench methods, the observed kinetics of hydrolysis would be two exponentials if product release is rate limiting. The rapid initial phase is due to rapid binding and hydrolysis of ATP. The slower phase is from slow product dissociation. If the hydrolysis step is rate limiting for myosin ATPase, a single exponential may be observed. We showed in **Fig. II-6** that the kinetics shows a single exponential, suggesting that the product release is faster than hydrolysis. The phosphate release can be measured directly using a fluorescent probe for Pi, based on a phosphate binding protein (PiBP) (Brune et al., 1994; White et al., 1997). Myosin is mixed with ATP, aged to form M•ATP•P, and then mixed with actin in the presence of MDCC-labeled-PiBP. The fluorescence of MDCC-PiBP increases as it binds released phosphate from myosin. However, we could not use this method because M9bIQ4 does not form a significant amount of M•ADP•P state.

The rate of phosphate release from all previously characterized myosins is increased by actin binding (White et al., 1997; De La Cruz et al., 2000b; De La Cruz et al., 2001) with exception of no actin activation of phosphate release from myo1eIQ (El Mezgueldi et al., 2002). The authors proposed that the lack of actin activation is caused by the low affinity of the M•ADP•Pi state for actin. Other myosins bind actin in the presence of ATP with equilibrium dissociation constants < 50 μM at low ionic strength conditions (Furch et al., 1998; Joel et al., 2001), whereas myo1eIQ binds with a dissociation constant > 50 μM. The ionic component of actin binding has been shown to be mediated by positive charges in surface loop-2 of myosin (Furch et al., 1998). The two conserved lysines at the C-terminal end of loop-2 is shown to be crucial for actin activation of phosphate release (Joel et al., 2001). Substitution of two conserved lysines with alanines on smooth muscle myosin HMM abolished the actin-induced phosphate release, while the intrinsic myosin ATPase activity and the rate of ATP binding and hydrolysis of the mutant are similar to wild type. Furthermore, the rate of ADP release from actoHMM and the ability to strongly bind

to actin were also native. The affinity of M•ADP•P to actin is significantly high for myosin IX (**Fig. II-12**), and Myosin IX contains conserved lysine residues at the C-terminal end of loop-2. Therefore, it is possible that actin accelerates phosphate release from actoM9 and the rate of Pi release is fast.

ADP release

The ADP dissociation rate from myosin IX on actin (3 s^{-1}) is 10-fold faster than the steady-state actin-activated ATPase rate (0.3 s^{-1}), implying that ADP release is not the rate-limiting step in the ATPase cycle of myosin IX. M9bIQ4 has low affinity to ADP (16 μM). Consistent with this observation, 100 μM ADP did not inhibit the ATPase activity of M9bIQ4 (**Fig. II-3**). Therefore, the ATPase rate is not inhibited at physiological ADP (12–50μM) concentrations (Roth and Weiner, 1991). ADP release is rate limiting for other processive myosin, resulting in the formation of predominant intermediate at M•ADP state, which is strongly bound to actin. These myosins are tuned to have high duty ratio (> 0.5 for a head of double-headed myosin) to prevent from diffusing away from actin filament. In current criteria, AM and AM•ADP states are defined as strongly bound state with actin, and myosin has to populate at the strongly bound state for most of time during ATPase cycle to be processive. However, M9•ADP is not significantly populated during ATPase cycle, since M9•ATP state is predominant intermediate and ADP release rate is faster than that of steady-state ATPase activity. Myosin IXb is tuned to be processive by alternating binding state of AM•ATP and AM•ADP•P not to diffuse away from actin filament as shown **Fig. II-11** and **Fig. II-12**.

Actin binding properties

One of the unique features of myosin IX compare with other characterized myosin is that a single-headed myosin IX has the high affinity to actin during ATPase cycle. A series of actin co-sedimentation analysis (**Fig. II-11, II-12, Table II-2**) clearly showed that myosin IX does not

dissociate from actin at physiological actin concentration.

The notable finding is that the K_{actin} of M•ATP state (K_8) is 2.3 μM (**Fig. II-11, Table II-2**), which is much tighter than that of conventional myosin II (> 30 μM) (Konrad and Goody, 1982; Berger and Thomas, 1991; Resetar and Chalovich, 1995), and myosin VI (25 μM) (Sato et al., 2004). Furthermore, the dissociation rate (k^{+8}) is very slow compared to other myosins (250 – 1500 s^{-1}). The M•ATP state of myosin V, shows high affinity to actin (4 μM) (Yengo et al., 2002b), which is similar to myosin IX. However, myosin V dissociates from actin quickly (> 750 s^{-1}) upon ATP binding, and the hydrolysis (k_{+3}+k_{-3}) of myosin V is 750 s^{-1} in the absence of actin. Therefore, AM•ATP is not populated during ATPase cycle. Slow hydrolysis of myosin IX in the absence of actin allows myosin IX to stably form M9•ATP state. The affinity of M9•ATP to actin (K_8) is still weaker than that of M9 (K_6) and M9•ADP (K_{10}) states, suggesting that the conformation of actin-myosin interacting interface and the weak binding state is distinct from other myosins. It would be necessary to weaken the affinity (but must be high enough to prevent myosin diffusing away from actin) to make a movement.

It is possible that the large insertion at loop-2 region play a role in the strong affinity of myosin IX to actin, since it has been shown that loop-2 play a role in the binding of myosin with actin. Although there is no high-resolution structure of the actomyosin interface with myosin bound strongly to actin, elements of the interface have been inferred from docking the high-resolution structures of myosin into the electron density maps of strongly bound actomyosin complexes (Milligan, 1996). The actin-binding site of myosin is composed of five regions of myosin heavy chain (**Fig. II-14**). In the center of the interface, a helix-turn-helix motif of the lower 50-kDa subdomain of myosin is the main strong binding, stereospecific site participating in hydrophobic interactions with actin. Around this site, three different flexible loops of the myosin lower and upper 50 kDa subdomains (loop 2, loop 3 and the HCM loop) seem also to participate in the interactions. This actin-binding

interface is split by the large 50 kDa cleft, the opening and closing of which may be responsible for mediating the affinity between actin and myosin (Rayment et al., 1993b). As was predicted by Rayment *et al*. (Rayment et al., 1993b), recent studies of decorated actin suggest that the 50 kDa cleft is more closed in the strong binding state (Volkmann et al., 2000). Mutational studies that added additional positive charge to loop-2 (Furch et al., 1998), removed large segments of loop-2 (Rovner, 1998; Knetsch et al., 1999), or replaced loop-2 of one species with that from another (Uyeda et al., 1994; Rovner et al., 1995; Murphy and Spudich, 1999), all concluded that loop-2 affects the affinity for actin in the presence of ATP. Specially, Furch et al. (Furch et al., 1998) made a series of systematic changes to the loop-2 of *Dictyostelium* myosin-truncated S1. They increased the net charge from –1 to +12. The results show that the binding of ATP to the actoS1 construct and basal ATPase activity were unaffected by any of the changes. In contrast, increases in the number of positive charged residues dramatically increased the affinity of actin for the nucleotide free head (100-fold) and increased the apparent K_m of actin (25-fold) in ATPase. There is a large insertion (130 amino acids) at the site of loop-2 of myosin IX. This insert is in rich of arginine and lysine. Therefore, the insert of myosin IX would have high affinity to actin.

Steady-state distribution of Biochemical state.

We could simulate steady-state distribution of intermediates during ATPase cycle since we determined most of the rate and equilibrium constants. **Figure II-15** shows the steady-state distribution of intermediates at the physiological nucleotide concentration (Roth and Weiner, 1991) and the saturated actin concentration. The rates of steady-state ATPase as a function of actin concentration were similar to those obtained from the experiments (**Fig. II-2**). The M9•ATP state is the predominant intermediate and populates 82 % in this state. Myosin IX populates at the strong binding, AM•ADP state with 11 % during ATPase cycle. Kinetic model of the ATPase reaction yields an ATPase rate of 0.37 s^{-1}, which is very similar to the experimentally determined value of 0.29 s^{-1}.

How does a single-headed myosin IX move?

The steady state and transient kinetic data shown here strongly support the idea that a single-headed myosin IX does not dissociate from actin during ATPase cycle, thus moves processively on actin filament. Next question would be how and when myosin produces force to translocate actin filament.

It is widely believed that the neck region of myosin, or light chain binding domain, works as a rigid lever arm of power stroke (Uyeda et al., 1996; Geeves and Holmes, 1999; Highsmith, 1999). In the swinging lever arm hypothesis, force production would result from the amplification of small conformational changes in the motor domain (0.5 nm) that would be directly transmitted to a rotation of the extended neck region of the myosin head (11nm for myosin II). This concept suggests that the swing of the lever arm occurs while myosin is strongly bound to actin, as it would correspond to a force generating transition. Experimental support for the swinging lever arm model comes primarily from two types of studies. First, studies that show that the unitary displacement and/or velocity of the myosin are related to lever arm length (Uyeda et al., 1996; Warshaw et al., 2000). Second, studies of actomyosin complexes by electron microscopy have provided low-resolution structures of strong actin-binding states for a number of myosins (Rayment et al., 1993a; Schroder et al., 1993; Jontes et al., 1995; Whittaker et al., 1995; Carragher et al., 1998; Wells et al., 1999; Volkmann et al., 2000). An atomic model of the actin-myosin complex was then obtained by fitting the atomic structures of F-actin and myosin into three-dimensional cryo-electron microscope reconstitutions of decorated actin. For most of these, a significant rotation of the neck occurs upon ADP dissociation. Although both evidence support a role for the swinging of the lever arm in the generation of force and movement, they do not address whether force production is directly coupled to lever arm movement.

Kinetic studies show that binding of either an ADP-containing or a nucleotide-free head to F-actin is a two-step process (Taylor, 1991; Walker et al., 1999). The ADP-containing state that initially interacts with actin binds weakly before undergoing a transition to a strong binding state. This provides further evidence that none of the high-resolution structures, represents a strong actin-binding state. There are studies showing that Pi release occurs from a weak actin-binding conformation that precedes the strong actin-bound ADP state (force-generating state). A recent study of the kinetics of smooth muscle myosin II supports the same mechanism (Rosenfeld et al., 2000). Pi release would thus immediately follow lever arm movement, consistent with fluorescence experiments (Suzuki et al., 1998). The intriguing implication of assigning the near-rigor state bound to actin to be equivalent to the kinetic state defined by Sleep and Hutton (Sleep and Hutton, 1980) is that strong binding to actin does not occur until after the structural changes between the transition state and the ADP-containing near-rigor state have been completed. This would imply that the major movement of the lever arm is not coupled to force generation directly, as in current swinging lever arm hypotheses.

To adapt the lever arm mechanism, myosin needs to be a double-headed structure or scaffold to a cellular structure, such as cytoskeleton, membrane, and vesicles. If myosin is a single-headed, and does not associate with cellular structure on its tail domain, the lever arm cannot produce force to translocate actin. Myosin IX is a single-headed structure. It is largely unknown if myosin IX associates with some cellular structure. However, judging from its domain structure, myosin IX does not have such a domain. Recently it is shown that myosin IX play a role in signal transduction of RhoA cascade (Reinhard et al., 1995; Chieregatti et al., 1998; Post et al., 1998) and transport a signaling molecule (Saeki et al., 2005), suggesting that myosin IX would move without associating a cellular structure. Therefore, there must be another mechanism for a single-headed myosin IX to achieve movement.

Yanagida et al. proposed another mechanism for myosin movement, Brownian ratchet mechanism (**Fig. II-16**). That is to say that thermal motion causes the actin to move with respect to the myosin in concert with a weakly attached myosin flipping back and forth between the transition state and near-rigor state. If the actin moves far enough in the direction that allows the myosin to bind to actin in the near-rigor state, release Pi and attach strongly, then the actin will be physically constrained by the strongly bound myosin, thus biasing the Brownian motion (Yanagida et al., 2000). In the biased Brownian motion model, the lever arm merely functions as the ratchet, trapping Brownian motion of the actin filament and providing directionality. Yanagida *et al*. (Yanagida et al., 2000) further propose that the myosin can undergo multiple actin interactions per ATPase cycle. Although this view is not widely held, it could be possible if the myosin is attaching and detaching without reaching a strongly bound ADP state (i.e. detaching in the weakly bound near-rigor state). The asymmetry of the actin filament could bias the Brownian motion of the attachment/detachment in the same direction as the lever arm swing. Furthermore, if the lever arm stiffness is asymmetrical relative to directionality along an actin filament, this could also bias the Brownian motion. Once a strongly bound ADP state is reached, ADP dissociation and ATP binding would have to occur before the head could detach. As shown here, myosin IX predominantly populates AM•ATP state (82 %) and AM•ADP•P state (11 %) during ATPase cycle. These complexes do not dissociate from actin, but has weaker affinity to actin than M and M•ADP state, suggesting that the 'weak binding' state of myosin IX is distinct from previously characterized myosin. Taken together, it is possible that myosin IX adapts the Brownian ratchet mechanism. Further study is required to elucidate the mechanism of the movement of myosin IX.

Table II-1. Steady-state ATPase activity of M9bIQ4.

	Vmax (s^{-1})	K_{ATP} (μM)	K_{Actin} (μM)
- Actin	0.22 (0.012)	7.95 (0.77)	----------
+ Actin	0.29 (0.015)	6.30 (0.62)	2.3 (2.1)

Table II-2. Kinetic and equilibrium constants for M9bIQ4 actin-activated ATPase.

ATP binding		
K_1k_{+2} ($\mu M^{-1}s^{-1}$)	1.08 (0.21)	... mant
k_{+2} (s^{-1})	2.22 (0.71)	...mant
1/K1 (μM)	2.06	...calculation
$K_1'k_{+2}'$ ($\mu M^{-1}s^{-1}$)	1.07 (0.10)	...mant
k-2' (s^{-1})	3.43 (0.33)	...mant
$1/K_1'$ (μM)	3.21	...calculation
Hydrolysis		
k_{+3} (s^{-1})	0.21 ~ 0.25	...simulation
k_{+3}' (s^{-1})	0.4 ~ 0.45	...simulation
ADP release		
k_{+5}' (s^{-1})	3.34 (0.28)	...light scattering
k_{-5}' ($\mu M^{-1}s^{-1}$)	0.21	...calculation
K_5'	16.0 (1.3)	...steady-state
Actin binding		
k_{-6} ($\mu M^{-1}s^{-1}$)	5.16 (0.09)	...light scattering
K_6 (μM)	< 0.2	...co-sedimentation with actin
k_{+8} ($\mu M^{-1}s^{-1}$)	5.45	...calculation
k_{-8} (s^{-1})	12.7 (1.07)	...light scattering
K_8 (μM)	2.33 (0.29)	...co-sedimentation with actin
K_9 (μM)	0.99 (0.14)	...co-sedimentation with actin
k_{-10} ($\mu M^{-1}s^{-1}$)	5.37 (0.22)	...light scattering
K_{10} (μM)	< 0.2	...co-sedimentation with actin

Table II-3. Simulation for hydrolysis rate.
Different concentrations of M9bIQ4 and ATP are used to obtain apparent hydrolysis rate (k_{obs}). Rates of hydrolysis (k_{+3}) to fulfill experimentally determined kinetic constants (k_{obs}) in each condition are determined by simulation using STELLA software. Parameters used were K_1k_{+2} = 1.08 $\mu M^{-1}s^{-1}$, k-2 = 2.22 s^{-1}, $K_1'k_{+2}'$ = 1.07 $\mu M^{-1}s^{-1}$, k_{-2}' = 3.43 s^{-1}.

-Actin			
M9bIQ4 (μM)	ATP (μM)	k_{obs} (s^{-1})	simulated k_{+3} to obtain kobs
0.5	0.1	0.038	0.21
0.5	0.3	0.040	0.23
0.43	0.2	0.039	0.25
0.85	0.2	0.062	0.25
+Actin			
M9bIQ4 (μM)	ATP (μM)	k_{obs} (s^{-1})	simulated k_{+3} to obtain kobs
0.43	0.2	0.041	0.40
0.85	0.2	0.079	0.46

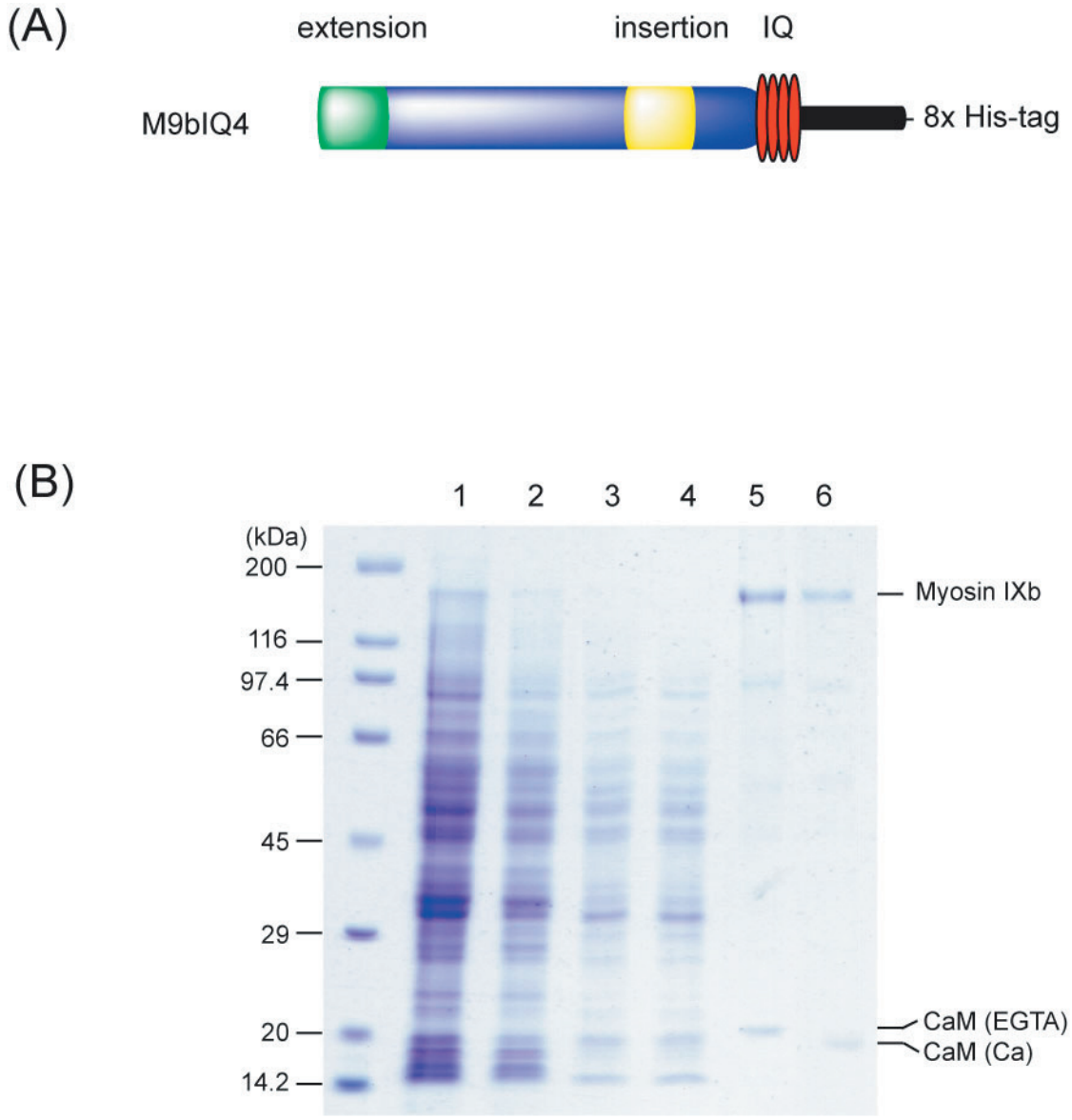

Fig. II-1. **Myosin IX construct.** A, schematic diagram of expressed truncated human myosin IXb (M9bIQ4). The molecule is monomeric. B, purification of M9bIQ4 from Sf9 cell extracts. Lane 1, total cell lysate; lane 2, pellet of cell homogenate after centrifugation; lane 3, supernatant of cell homogenate after centrifugation;lane 4, flow through fraction from Ni-NTA agarose column; lane 5 and 6, elution from Ni^{2+}-NTA agarose column. CaM undergoes its characteristic Ca^{2+}-dependent shift in mobility (lane 5, EGTA; lane 6, Ca^{2+}).

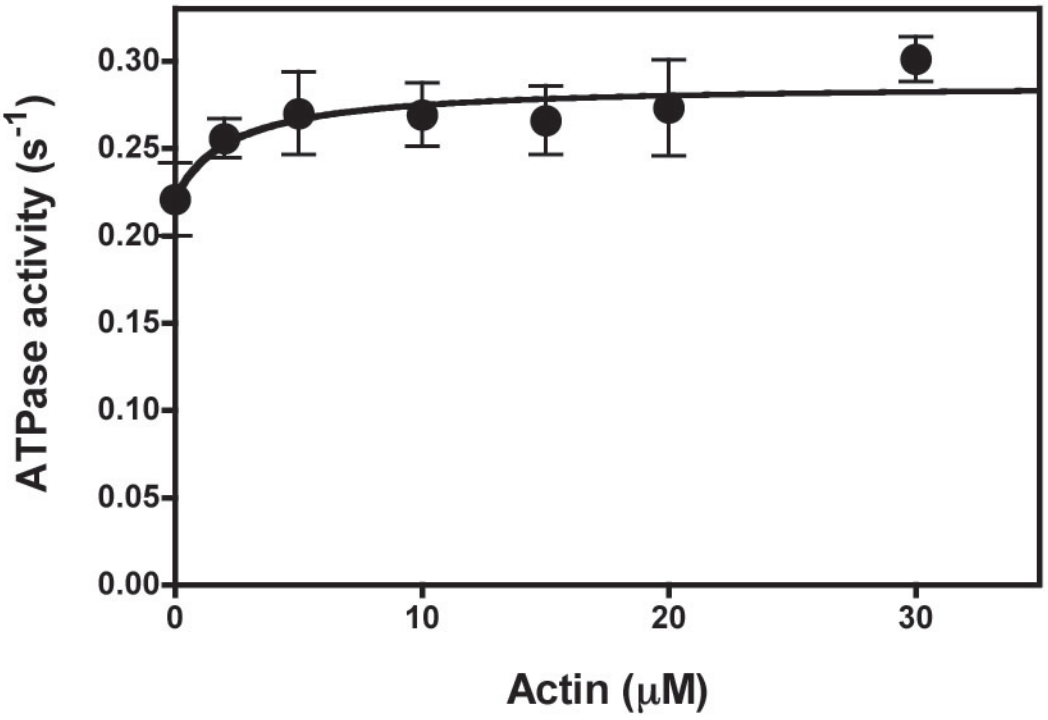

Fig. II-2. **The steady-state ATPase activity as a function of actin concentration.** The ATPase activity of M9bIQ4 was measured as a function of actin concentration in the presence of 0.3 mM ATP. Solid lines, calculated based on the equation $v = V_{max}[actin]/(K_{actin} + [actin]) + v_0$. According to the analysis, the basal ATPase activity, v_o is obtained for 0.22 s^{-1}. The maximum activation by actin (V_{max}) is 0.07 s^{-1}. The maximum ATPase activity at saturating actin concentration ($V_{max} + v_0$) is 0.29 s^{-1} with K_{actin} of 2.3 μM. The error bars indicate S.D. for n = 3 from three independent preparations.

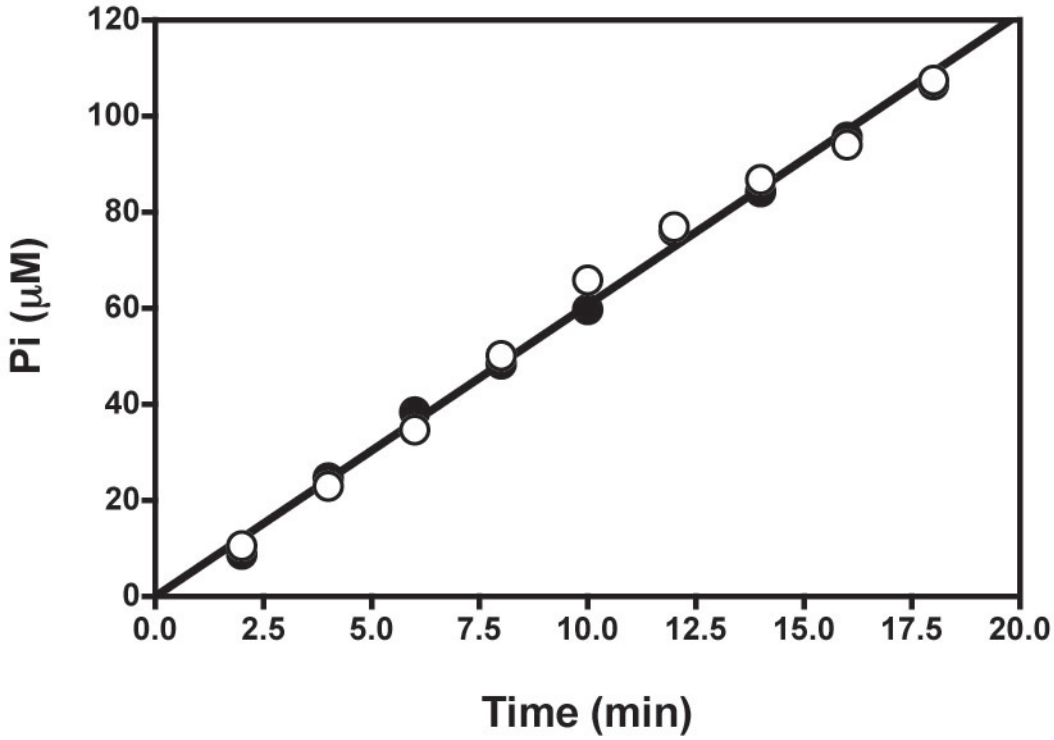

Fig. II-3. **The course of the steady-state ATPase activity of M9bIQ4 in the presence of actin with or without the ATP-regenerating system.** ATPase activity was measured in the presence (closed circles) and absence (open circles) of 20 units/ml pyruvate kinase and 2 mM phosphoenol pyruvate. 20 μM actin and 0.6 mM ATP were used in the assay.

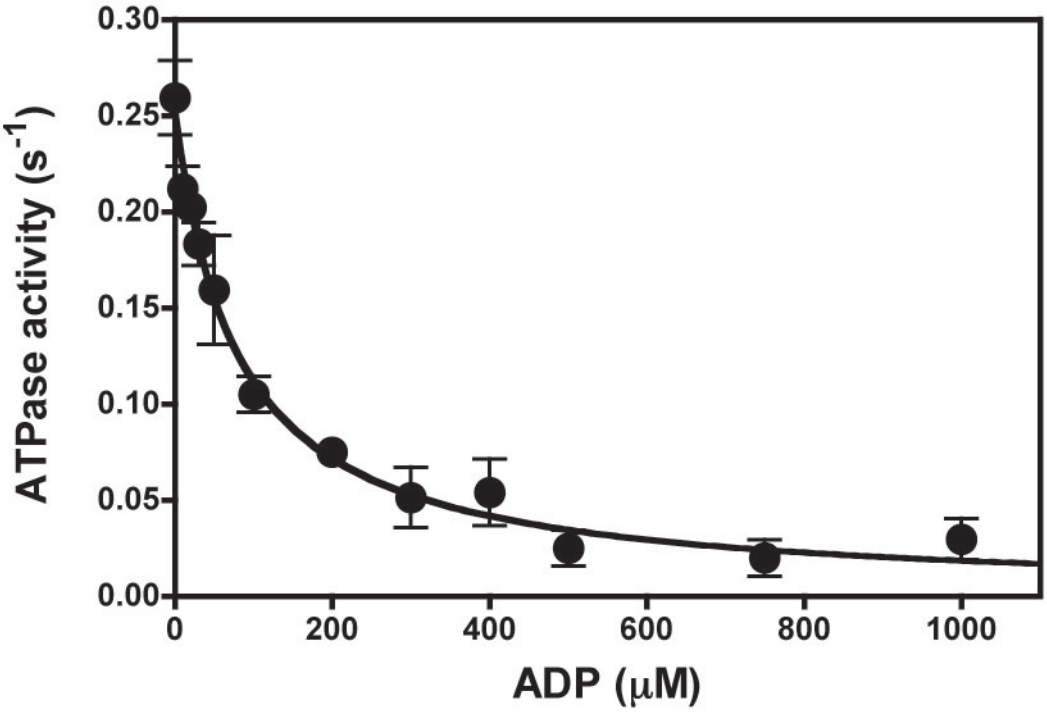

Fig. II-4. **Inhibition of the steady-state ATPase activity of M9bIQ4 in the presence of actin by Mg^{2+}-ADP.** The ATPase activity was measured in the presence of 25 μM ATP, 10 μM actin, and various concentration (0 – 1 mM) of ADP. The data was fit to the equation $v = V_{max}[ATP]/(K_{ATP}(1 + [ADP]/K_{ADP}) + [ATP])$, where [ATP] is 25 μM and K_{ATP} is 6.3 μM. According to the analysis, K_{ADP} was obtained for 16 μM. The error bars indicate S.D. for n = 3 from three independent preparations.

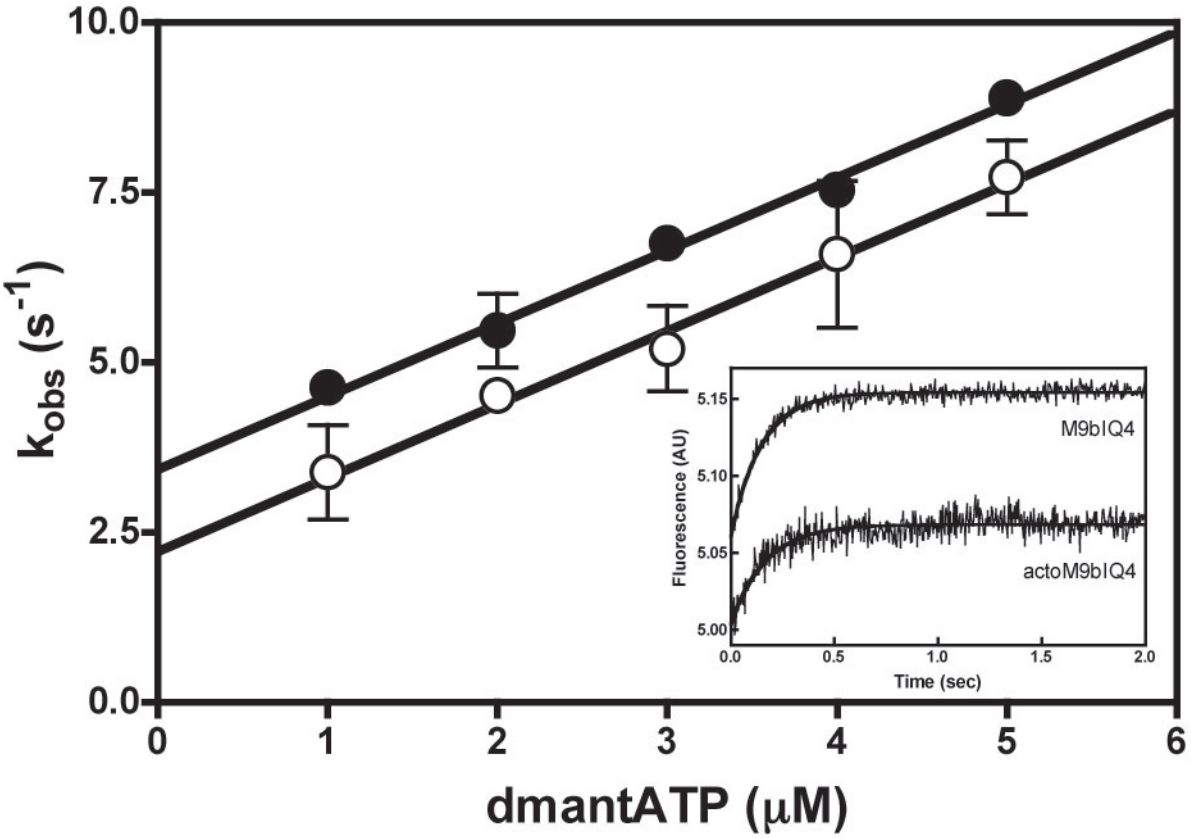

Fig. II-5. **Kinetics of dmantATP binding to M9bIQ4 and actoM9bIQ4.** Rates of dmantATP binding to M9bIQ4 (open circles) and actoM9bIQ4 (closed circles) as a function of nucleotide concentration are shown. The observed rates (k_{obs}) were obtained by fitting the fluorescence data at each nucleotide concentration to a single exponential. The apparent second order rate constant for dmantATP binding to M9bIQ4 and actoM9bIQ4 are 1.08 $\mu M^{-1}s^{-1}$ and 1.07 $\mu M^{-1}s^{-1}$, respectively. ATP-dissociation rates determined by y-intercept are 2.22 s^{-1} in the absence of actin and 3.43 s^{-1} in the presence of actin. The error bars indicate S.D. for n = 4 from three independent preparations. The inset shows dmantATP fluorescence transients obtained by mixing 0.25 μM M9bIQ4 or actoM9bIQ4 with 3 μM dmantATP. The fluorescence data are fit to a single exponential. The values of k_{obs} at these M9bIQ4 and dmantATP concentrations are 6.0 s^{-1} in the absence of actin and 6.78 s^{-1} in the presence of actin.

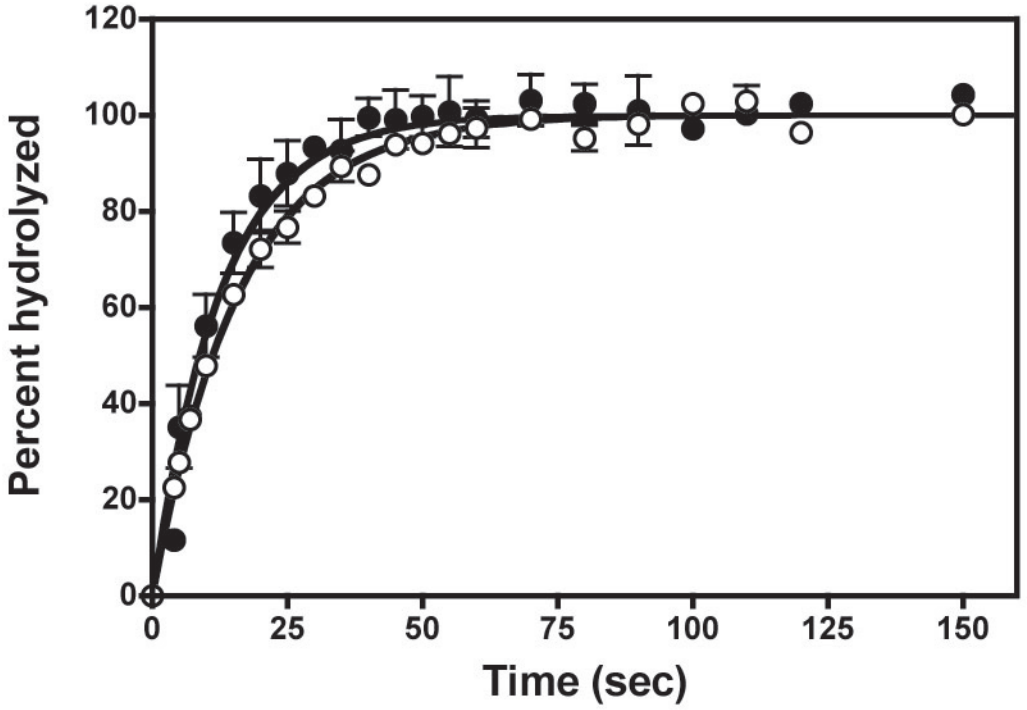

Fig. II-6. **Kinetics of ATP hydrolysis of M9bIQ4 and actoM9bIQ4.** Single turnover quench-flow measurements of hydrolysis is done upon mixing 0.85 μM M9bIQ4 (open circles) or actoM9bIQ4 (closed circles) with 0.2 μM [γ-^{32}P]-ATP. The solid lines are the best fits to a single exponential. The apparent rate constants are 0.06 s^{-1} in the absence of actin and 0.08 s^{-1} in the presence actin. The error bars indicate S.D. for n = 3 from two independent preparations.

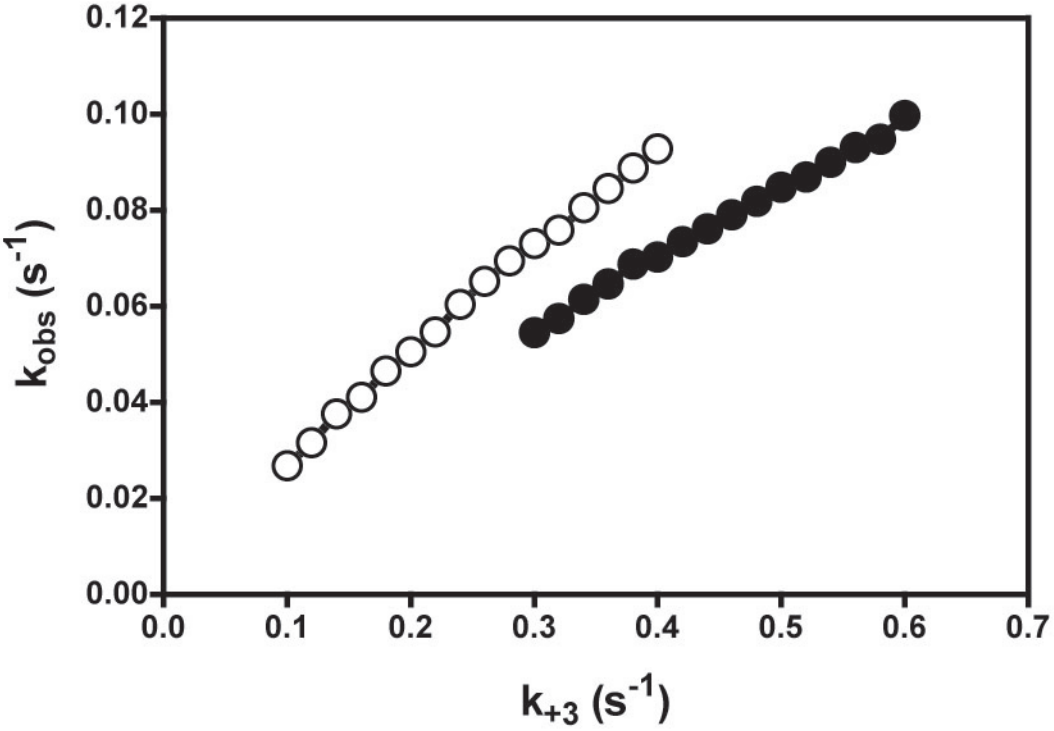

Fig. II-7. **Simulation for hydrolysis rate determined by the apparent rate of hydrolysis.** Rates of hydrolysis (k_{+3}) to fulfill experimentally determined kinetic constants (k_{app+3} = 0.06 s^{-1} and k_{app+3}' = 0.08 s^{-1}) are simulated using STELLA software. The experimentally determined kinetic constants (**Table II-2**) were fed into a kinetic model according to **Scheme II-3** and **Scheme II-4**. Parameters used were K_1k_{+2} = 1.08 $\mu M^{-1}s^{-1}$, k_{-2} = 2.22 s^{-1}, K_1'k_{+2}' = 1.07 $\mu M^{-1}s^{-1}$, k_{-2}' = 3.43 s^{-1}, [M9bIQ4 or actoM9bIQ4] = 0.85 μM, and [ATP] = 0.2 μM. Open circles, in the absence of actin. Closed circles, in the presence of actin. To obtain k_{app+3} = 0.06 s^{-1} and k_{app+3}' = 0.08 s^{-1}, k_{+3} and k_{+3}' should be 0.24 s^{-1} and 0.45 s^{-1}, respectively.

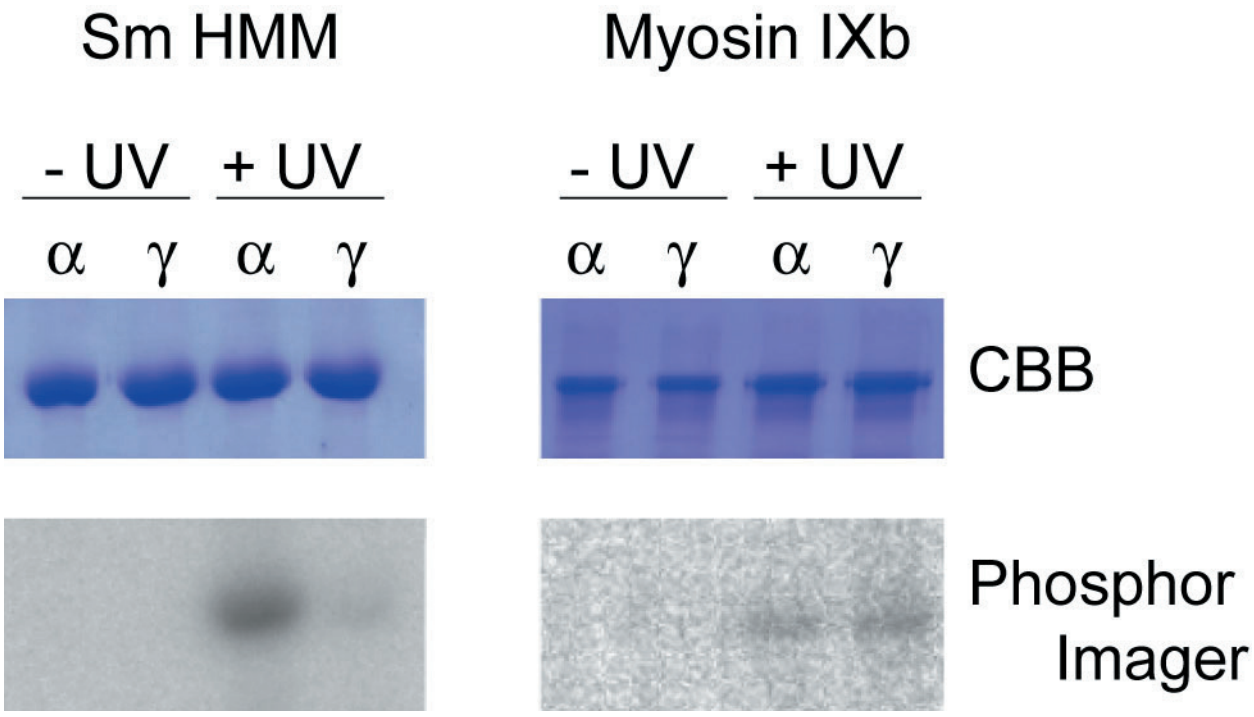

Fig. II-8. **Photoaffinity labeling of myosin IXb with ATP.** Predominant intermediate during ATPase is determined by photoaffinity labeling of myosin IXb using [α-^{32}P]-ATP or [γ-^{32}P]-ATP. Before (-UV) and after (+UV) irradiation, samples were subjected to SDSPAGE. Then, the incorporation of ^{32}P into myosin heavy chain was analyzed by autoradiography. Smooth muscle myosin heavymeromyosin (Sm HMM) was used for control. Top panels, Coomassie Brilliant Blue staining of the myosin heavy chain; lower panels, phosphor imager of the myosin heavy chain. α and γ represent labeling with [α-^{32}P]-ATP or [γ-^{32}P]-ATP.

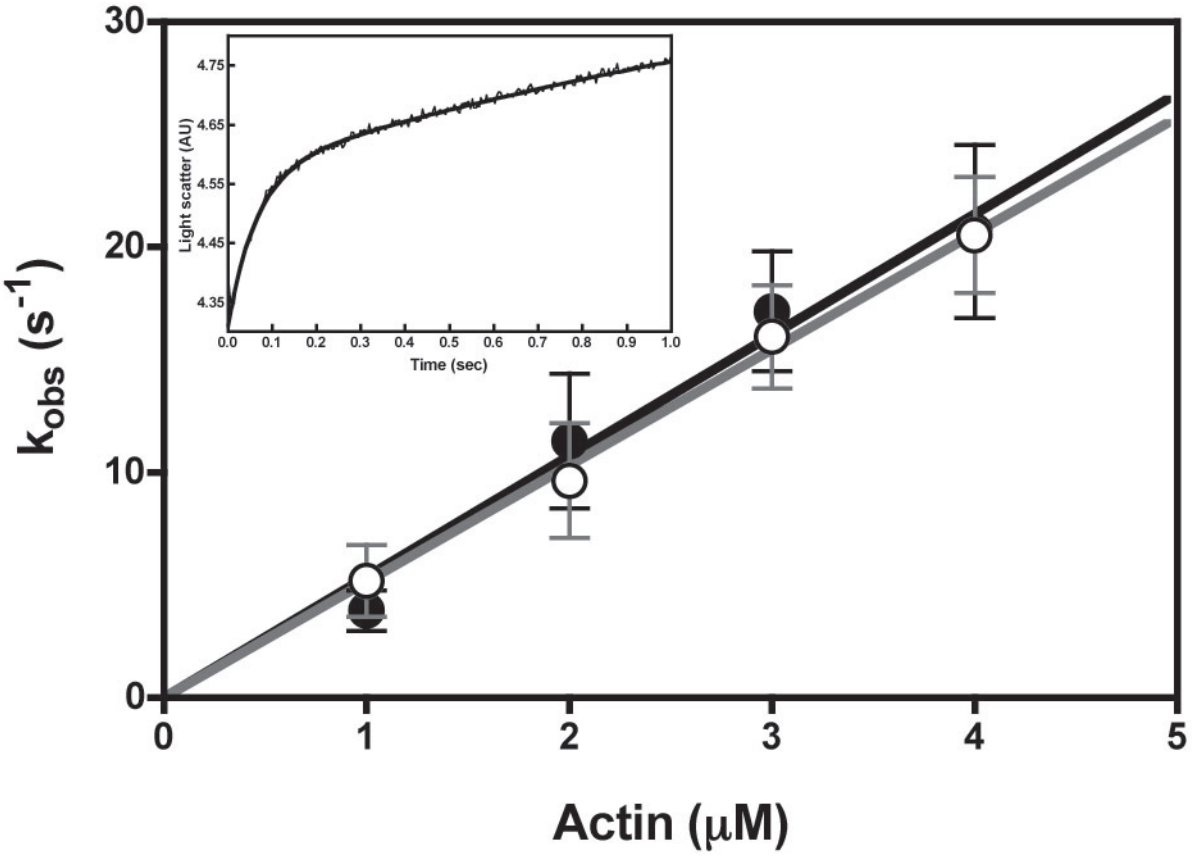

Fig. II-9. **Kinetics of M9bIQ4 association with actin filament in the presence and absence of ADP.** Rates of actin binding to M9bIQ4 in the absence of ADP (open circles with gray error bar) and in the presence of 0.1 mM ADP (closed circles with black error bar) as a function of actin concentration are shown. The observed rates (k_{obs}) were obtained by fitting the fluorescence data at each actin concentration to two exponentials. Solid lines are linear fits to the data, and starting from the origin. The apparent second order rate constants for actin binding to M9bIQ4 and actoM9bIQ4, determined by the slope, are 5.16 $\mu M^{-1}s^{-1}$ in the absence of ADP and 5.37 $\mu M^{-1}s^{-1}$ in the presence of ADP, respectively. The error bars indicate S.D. for n = 3 (in the absence of ADP) or n = 4 (in the presence of ADP) from three independent preparations. The inset shows timecourse of light scatter obtained by mixing 0.25 μM M9bIQ4 with 3 μM actin. The fluorescence data are fit to two exponential (solid line). The fast phase was k_{obs} = 15.43 s^{-1}, and the slow phase was 0.48 s^{-1}. The slow phase was not dependent on the actin concentration.

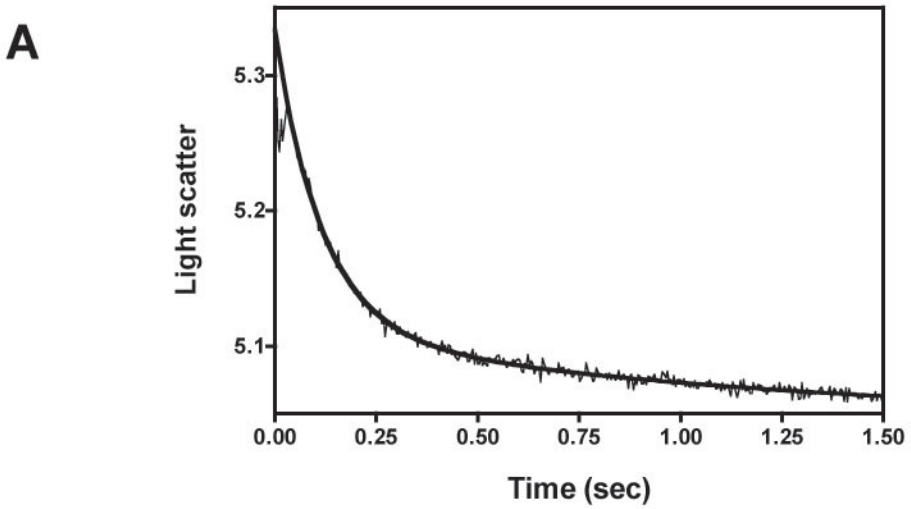
A
Light scatter
5.3
5.2
5.1
0.00
0.25
0.50
0.75
1.00
1.25
1.50
Time (sec)

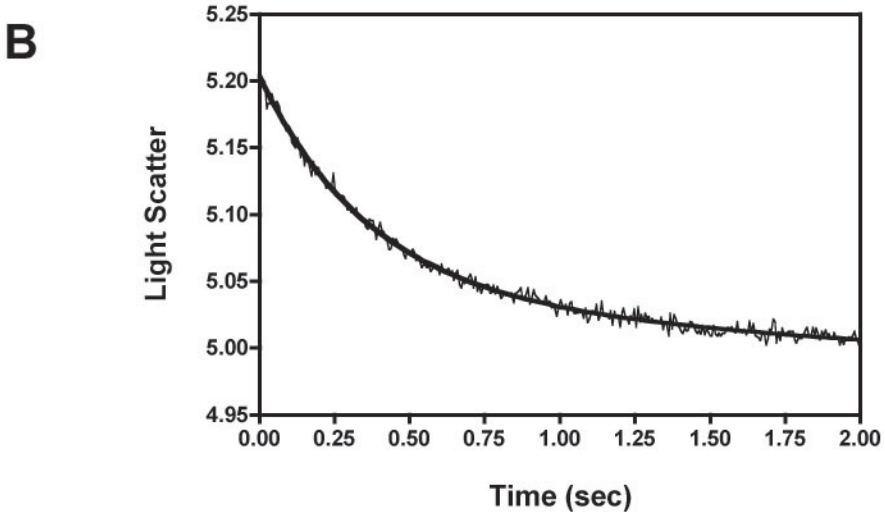
B
Light Scatter
5.25
5.20
5.15
5.10
5.05
5.00
4.95
0.00
0.25
0.50
0.75
1.00
1.25
1.50
1.75
2.00
Time (sec)

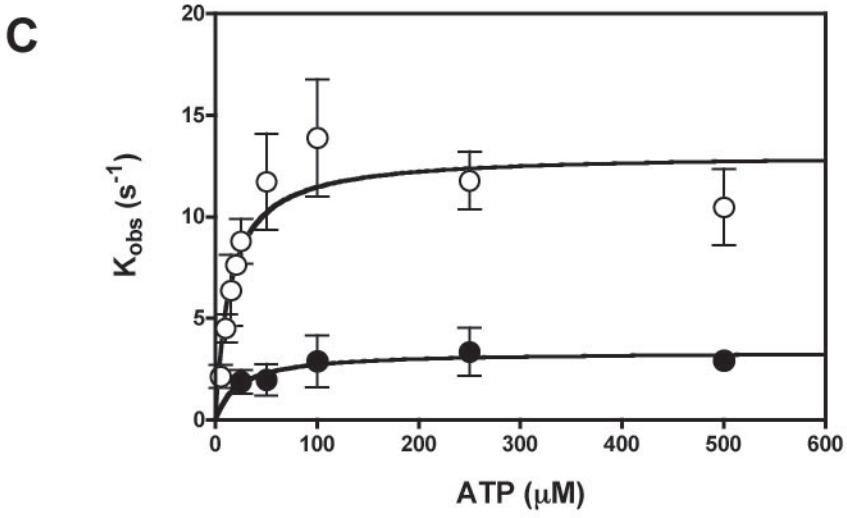
C
K_{obs} (s^{-1})
20
15
10
5
0
0
100
200
300
400
500
600
ATP (μM)

Fig. II-10. **ATP induced dissociation of M9bIQ4 from actin in the presence and absence of ADP.** A, Time course of dissociation of M9bIQ4 from actin by ATP. 0.5 μM actoM9bIQ4 was mixed with 25 μM ATP, and the decrease in light scattering as a function of time is fit to two exponentials (solid line). The fast phase was k_{obs} = 8.66 s^{-1}, and the slow phase was 0.87 s^{-1}. B, Time course of dissociation of M9bIQ4 from actin by ATP in the presence of ADP. 0.5 μM actoM9bIQ4 was mixed with 0.5 mM ATP in the presence of 0.25 mM ADP. The decrease in light scattering as a function of time is fitted to two exponentials (solid line). The fast phase was k_{obs} = 2.71 s^{-1}, and the slow phase was k_{obs} = 0.19 s^{-1}. C, Dissociation rates as a function of ATP concentration. All stopped-flow transients are fit to two exponentials, and the fast phases are plotted as a function of ATP concentration. The data are fit to rectangular hyperbolas. The maximum vales are 13.08 s^{-1} in the absence of ADP (open circles) and 3.34 s^{-1} in the presence of 0.2 mM ADP (closed circles). The slow phase was not dependent on ATP concentration. The error bars indicate S.D. for n = 4 from three independent preparations.

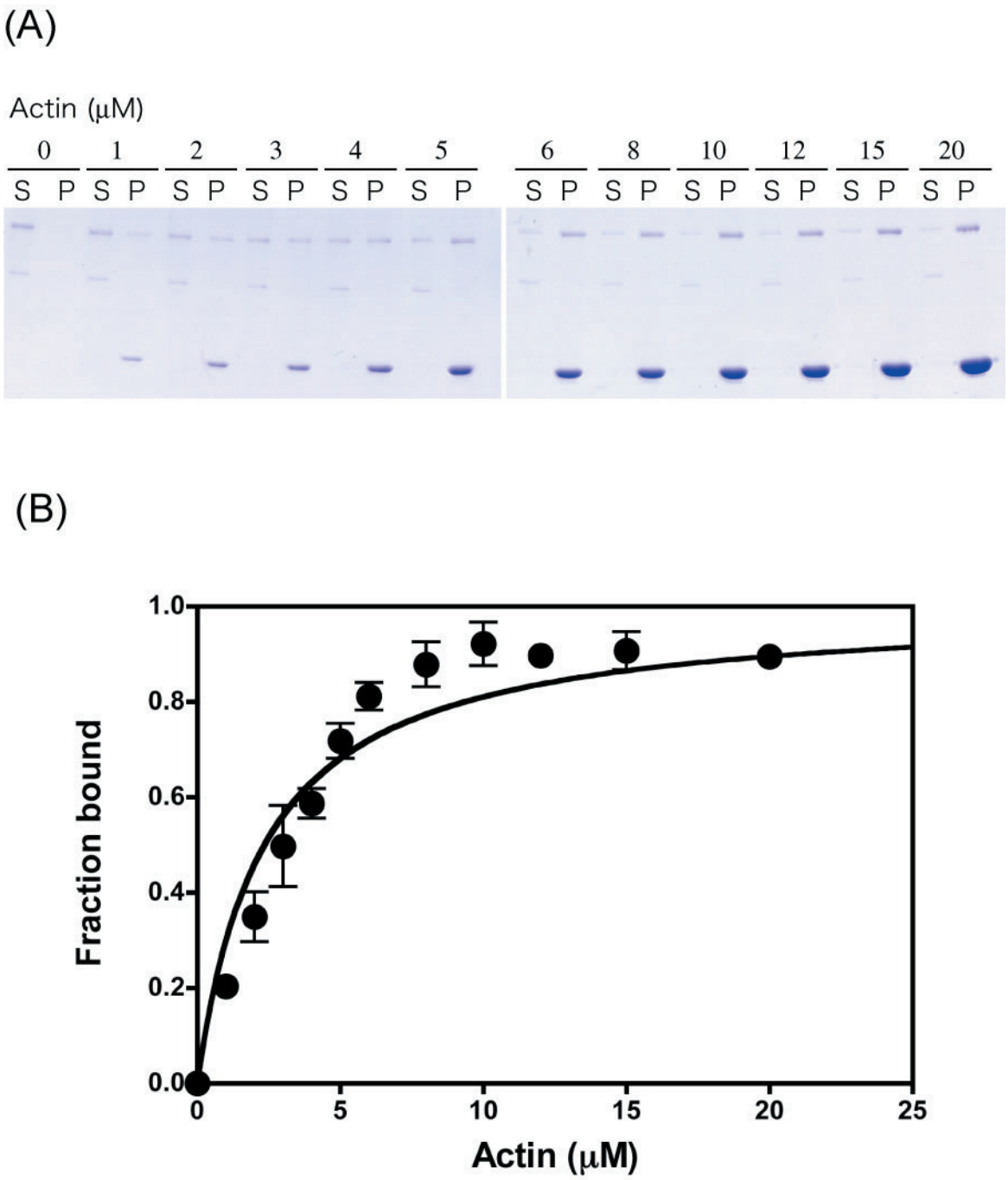

Fig. II-11. **Actin binding activity of M9bIQ4 in the presence of ATP.** Actin co-sedimentation assay of M9bIQ4 with actin was performed in the presence of 0.4 μM M9bIQ4, 1mM ATP, and various concentration (0 – 20 μM) of actin. Pellet and supernatant were analyzed by SDSPAGE. A, Coomassie staining of SDS gel. B, Fraction of bound M9IQ4 with actin was plotted as a function of actin concentration. The data was fit to hyperbola ($v = B_{max}[actin]/(K_{actin} + [actin])$, where $B_{max} = 1$. K_{actin} of 2.33 μM is obtained. The error bars indicate S.D. for n = 3 from three independent preparations.

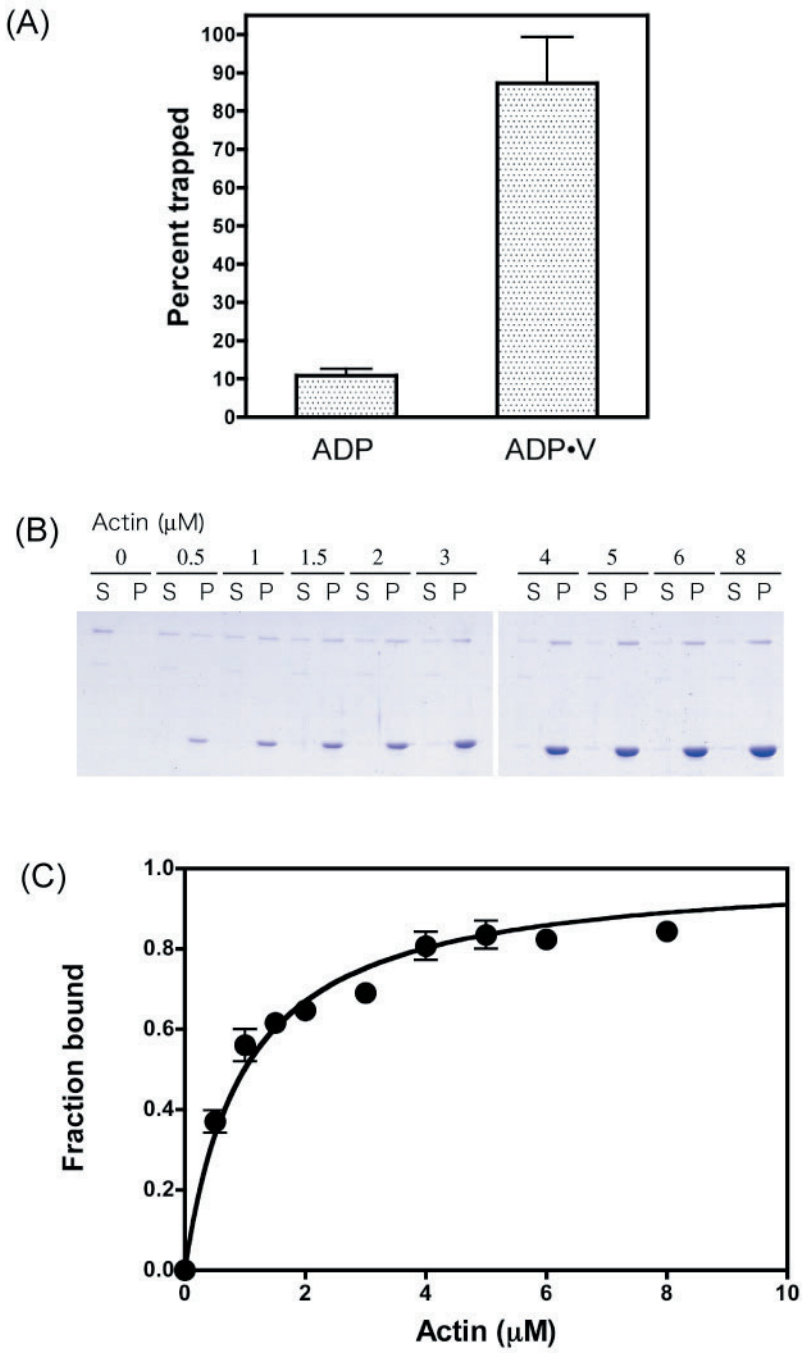

Fig. II-12. **Actin binding activity of M9bIQ4 in the presence of ADP and Vi.** Actin co-sedimentation assay of M9bIQ4 with actin was performed in the presence of 0.4 μM M9bIQ4, 0.1mM ADP, 1 mM Vi and various concentration (0 – 8 μM) of actin. Pellet and supernatant were analyzed by SDSPAGE. A, Trapped [^{3}H]-ADP in the absence and presence of vanadate. B, Coomassie staining of SDS gel. C, Fraction of bound M9IQ4 with actin was plotted as a function of actin concentration. The data was fit to hyperbola ($v = B_{max}[actin]/(K_{actin} + [actin])$, where $B_{max} = 1$. K_{actin} of 0.99 μM is obtained. The error bars indicate S.D. for n = 3 from three independent preparations. C, The amount of trapped [^{3}H]-ADP in the actin-bound fraction of M9bIQ4.

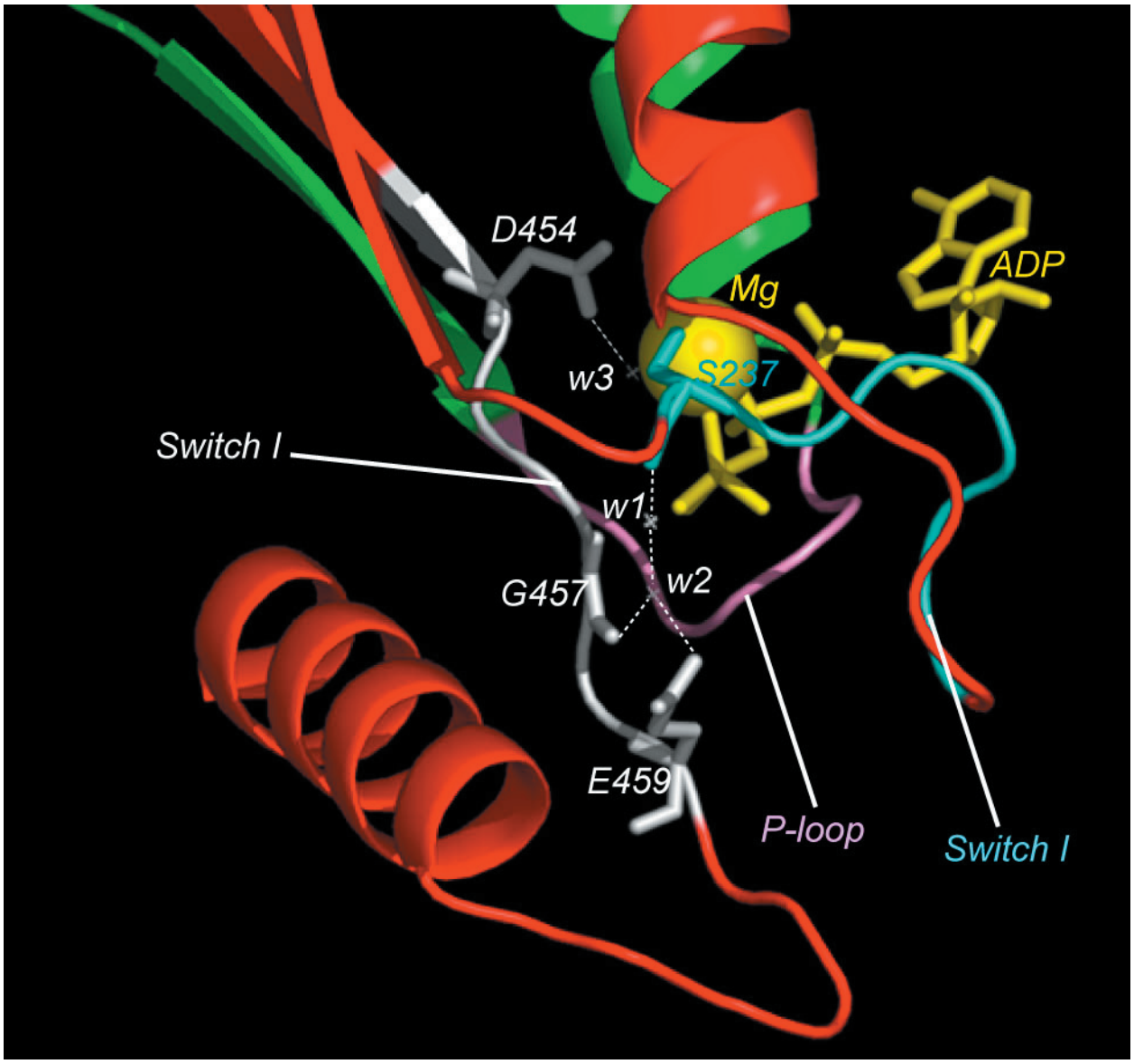

Figure II-13. **Three-dimensional structure of the switch II region of the myosin•ADP•Vi complex.** Structure data is obtained from protein data bank (PDB) using PDB ID of 1VOM. P-loop, Switch I, and Switch II are colored by pink, cyan, and white respectively. W1 forms hydrogen bond with S237 and w2. W2 forms hydrogen bond with w1, G457, and E459. W3 forms hydrogen bond with D454 and Mg. The sequences shown are based on the sequence of Dictyostelium myosin II.

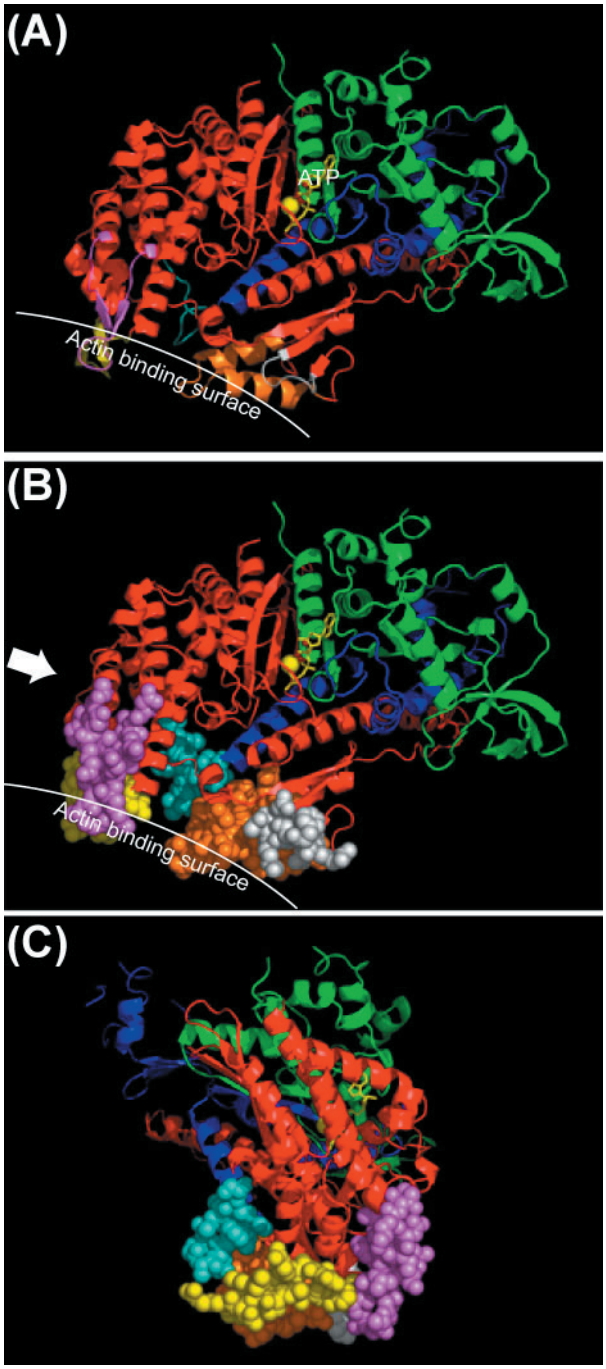

Figure II-14. **Three-dimensional structure of actin binding interface on myosin** A, Ribbon diagram of the 3D structure of Dictyostelium myosin II. B, Actin binding region is shown by spheres. Shown is the same orientation with panel A. C, Different orientation of (B). The molecule is observed from the arrow on panel B. Actin binding interface is composed of five regions, loop-2 (magenta), loop-3 (white), loop-4 (pink), HCM loop (yellow), helix-loop-helix (orange). Loop-2 shown is 11 residues. Myosin IXb has insertion of 130 residues at this region.

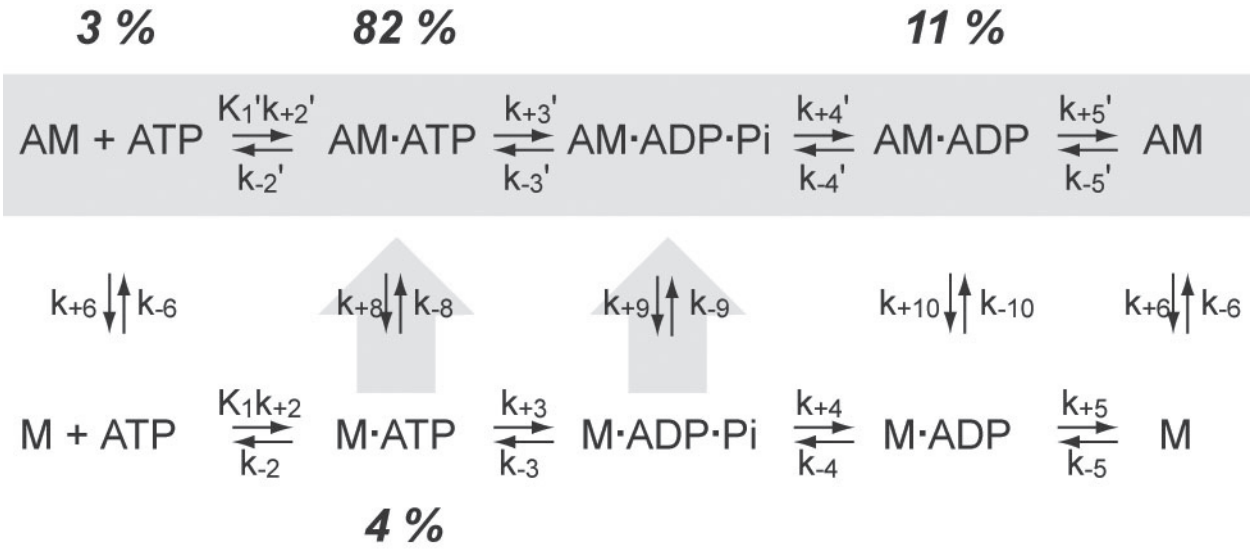

Figure II-15. **Models for steady-state distribution** Simulations were performed using experimentally determined kinetic constants (**Table II-2**) according to **Scheme II-1**. Parameters used were $K_1'k_{+2}' = 100\ s^{-1}$, $k_{-2}' = 3.43\ s^{-1}$, $k_{+8} = 5.45\ \mu M^{-1}s^{-1}$, $k_{-8} = 12.7\ s^{-1}$, $k_{+3}' = 0.43\ s^{-1}$, $k_{+3} = 0.23\ s^{-1}$, $k_{+9} = 5\ \mu M^{-1}s^{-1}$, $k_{-9} = 5\ s^{-1}$, $k_{+4}' = 100\ s^{-1}$, $k_{+5} = 3.32\ s^{-1}$, actin = 30 μM, and M9bIQ4 = 1 μM. Predominant intermediate is AM•ATP state (82 %). Other intermediates are AM•ADP (11 %), M•ATP (4 %), and AM (3 %).

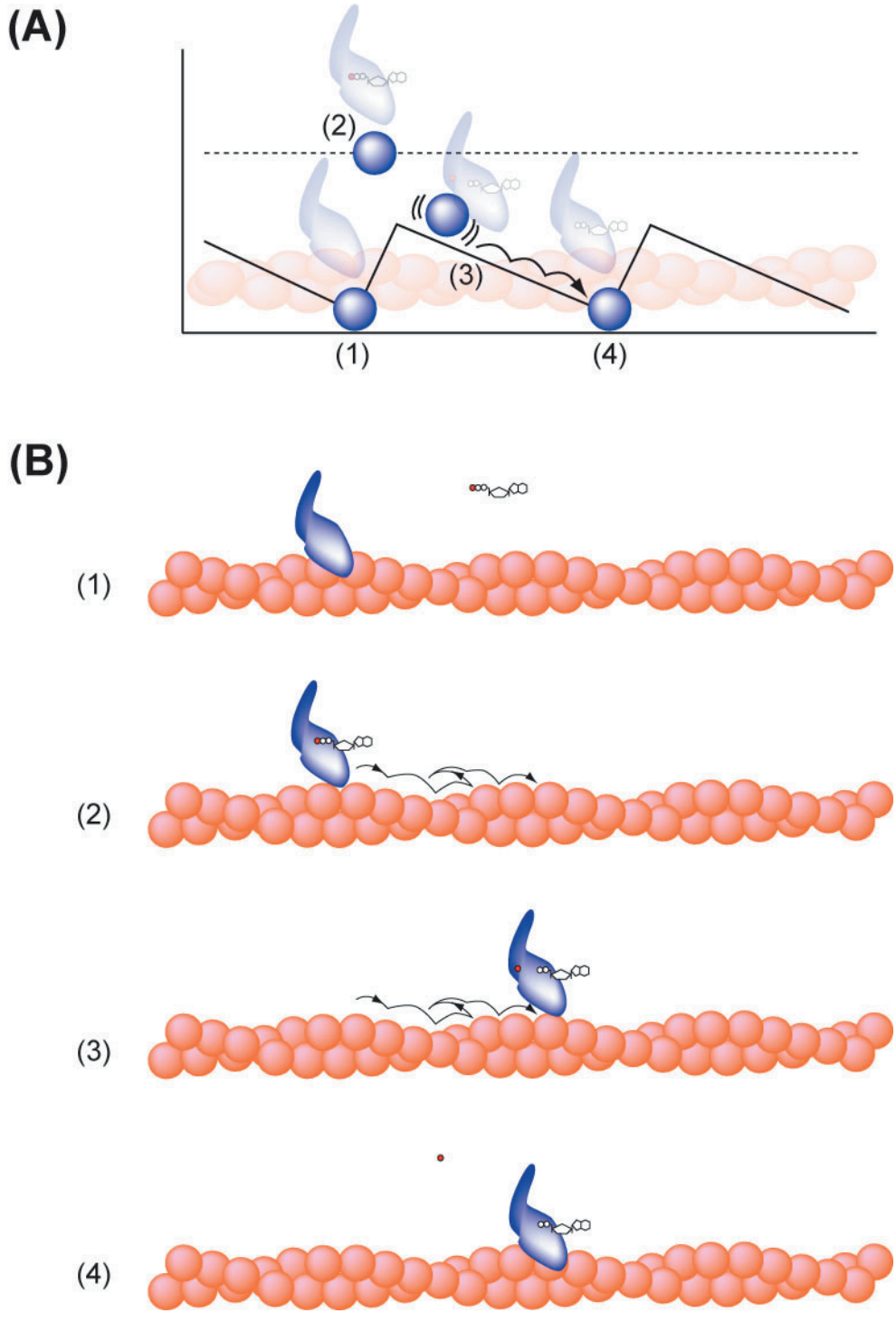
(A)
(2)
(3)
(1)
(4)
(B)
(1)
(2)
(3)
(4)

Figure II-16. **The biased Brownian ratchet model.** A, The mechanism is illustrated in terms of its possible energetics. In the absence of ATP, myosin is strongly bound to actin in its lowest energy state, unable to translocate (1). The binding of ATP switches myosin to a different conformational with a weaker affinity for actin (2), and allows it to diffuse along the actin filament. From the binding free energy point of view, this diffusion event depends on a downward slope in the energy profile (3). When myosin moves far enough, myosin binds to actin, concomitantly release products (4). B, the model of the processive movement for myosin IX. Myosin IX strongly binds to actin in the absence of ATP (1). Upon binding of ATP to myosin IX, the affinity of myosin IXb to actin is reduced allowing to move on actin filament (2). Possibly due to large insert at loop-2, myosin IXb does not diffuse away from actin filament. When myosin IXb reaches at the position of lowest energy state, it releases phosphate following by strong binding to actin.

CHAPTER THREE: CLONING OF FULL-LENGTH MYOSIN IXB AND INITIAL CHARACTERIZATION OF THE ATPASE ACTIVITY OF FULL-LENGTH MYOSIN IXB.

INTRODUCTION

Motor function of myosins is regulated by diverse mechanisms, such as phosphorylation of light chain or heavy chain, Ca^{2+}-binding to CaM light chain, conformational change by association with binding partner, and single headed-to-double headed transition. Since all characterized unconventional myosins have at least one CaM as light chain, those myosins seem to be regulated by calcium. The regulatory mechanism by calcium is well characterized for myosin V among the unconventional myosins. EGTA decreases the actin-activated ATPase activity of tissue-purified myosin V as well as its affinity for actin (Cheney et al., 1993; Nascimento et al., 1996; Tauhata et al., 2001). On the other hand, the actin-activated ATPase activity of any of the shorter baculovirus-expressed constructs is not altered by the presence of Ca (Trybus et al., 1999; Wang et al., 2000). There are common features between tissue-purified myosin V and truncated recombinant myosin V; Calcium causes dissociation of some CaM, and calcium inhibits actin movement in the in vitro motility assay regardless of whether the construct is an expressed monomer (Trybus et al., 1999), an expressed short-tailed dimer (Homma et al., 2000), or the tissue-purified full-length molecule (Cheney et al., 1993). These results suggest that full-length myosin V can adopt an inhibited structural state that is not possible with any shorter constructs. Consistent with this hypothesis, hydrodynamic data and EM suggest that the inhibited state is a compact conformation of the molecule that can be unfolded to an active state by calcium (Krementsov et al., 2004; Li et al., 2004; Wang et al., 2004). Quite recently it is shown that the binding of melanophilin at the tail of myosin Va activates actomyosin Va ATPase activity (Li et al., 2005). Taken together, the motor function of myosin V is regulated by conformational change of myosin itself by Ca and associating

with binding partner on the tail domain. Similar scenario would be applied for myosin IXb. We hypothesized that (1) the tail domain is required for the reguration of the motor activity by calcium, (2) cargo molecules may serve as regulator, and (3) Myosin IX tail containing GAP domain, rise an idea that Rho may regulate the motor activity.

It is previously shown that the actin translocating activity of tissue isolated myosin IXb is regulated by calcium mediated through CaM light chains (Post et al., 1998). In the presence of EGTA, myosin IX translocates actin filaments at 15 nm/sec, while the velocity is slowed to 10 nm/sec in the presence of 10 μM Ca. Therefore, calcium does not act as an on/off switch, rather may regulate a degree of processive movement. For further understanding of the function of myosin IXb, it is critical to express a full-length myosin IXb construct. The goals of this chapter are to express large, full-length myosin IXb construct, and perform the initial biochemical characterization of full-length myosin IXb.

METHODS

cDNA Cloning and sequencing

The construct of motor domain with four IQ motifs (M9bIQ4) was prepared previously. Therefore, we cloned tail potion of myosin IXb to make full-length myosin IXb construct. Total RNA was prepared from packed cells of the human leukaemic cell line HL60 using an RNeasy minikit (Qiagen), and cDNA was synthesized by reverse transcription with random oligonucleotides. The myosin IXb cDNA fragment, SP clone (encoding nucleotide 3741-4885, accession #NM004145) was amplified with a set of primers, 5'-GTTGGAGCGGCC GACTAGTCTGGCCCTGGACAGC-3' and 5'-TGGCGAACACGTGACTAGTGTGCTCCTGGACAGC-3', containing SpeI site. The amplified cDNA was random labeled with ^{32}P using the Megaprime labeling kit (Amersham Biosciences) and used as a probe to screen human promyelocytic leukemia lambda cDNA library (Stratagene). Plaque hybridization was carried out at 65 °C in Church buffer. The myosin IXb cDNA insert, SC clone (encoding nucleotide 4765-6894, accession #AF020267) were subcloned into pBluescript SK(+/-) from Uni-ZAP XR vector by in vivo excision according to manufacturer's protocol. The nucleotide sequence was analyzed with the PerkinElmer terminator ready reaction mix using a model 377 DNA sequencer (Applied Biosystems, Foster City, CA).

Production of Myosin IXb2 construct

The SP clone, the SC clone, and M9bIQ4 in pFastbac vector (Inoue et al., 2002) were used to construct full-length myosin IXb expression vector (**Fig. III-1** and **Fig. III-2**). The MluI site was introduced at nucleotide position 4798 by site-directed mutagenesis without changing the amino acid. The SP clone was amplified with a set of primers, 5'- G TTG GAG CGG CCG ACT AGT CTG GCC CTG GAC AGC -3' and 5'- CTT GGT GTA GCC ACG CGT GAA CTC ATC TAG -3', containing SpeI site and MluI site, respectively. The SC clone was amplified with a set of primers, 5'-CTA GAT GAG TTC ACG CGT GGC TAC ACC AAG -3' and 5'-CTT TGT CAG CTG TGG

ACT AGT GCC ATT GGT CTG GCC -3', containing MluI site and SpeI site, respectively. These PCR fragments were subcloned into pCR2.1 vectors. The SC fragment in pCR2.1 vector was digested with MluI and EcoRV, and the excised fragment was ligated into corresponding site on the SP clone in pCR2.1 vector. The SP/SC fragment in pCR2.1 vector was digested with SpeI, and the excised fragment was ligated into corresponding site on M9bIQ4 in pFastbac vector. Flag epitope (DYKDDDDK) was introduced at the N-terminus of the construct to facilitate purification.

Preparation of Full-length Myosin IXb Proteins

To express full-length myosin IXb, 250 ml of Sf9 cells (approximately 1 x 10^9) were co-infected with two separate viruses expressing the Myosin IXb heavy chain and CaM. Cells were cultured at 28 °C in 175-cm^2 flasks and harvested after 60 h. Cells were lysed in 10 ml of lysis buffer (30 mM Tris-HCl, pH 7.5, 0.15 M KCl, 1mM EGTA, 5 mM $MgCl_2$, 5 mM ATP, 1 mg/ml trypsin inhibitor, and 0.01 mg/ml leupeptin). After centrifugation at 100,000 x g for 30 min, the supernatant was loaded onto anti-flag affinity column, and washed with a 10-fold volume of buffer containing 30 mM Tris-HCl, pH 7.5, 0.3 M KCl, and 1 mM EGTA. Myosin IXb was eluted with buffer containing 30 mM Tris-HCl, pH 7.5, 30 mM KCl, 1 mM EGTA, 0.01 mg/ml leupeptin, and 0.01 ml/ml flag peptide. Protein concentration was determined by densitometry of Coomassie-staining gel. Typically 0.3 mg of protein is obtained from 300 ml culture. Protein was used within 6 hours.

Steady-state ATPase assay

The actin-activated ATPase assays were performed at 25oC in 30mM Tris-HCl, pH7.5, 30mM KCl, 1mM EGTA, 2mM $MgCl_2$, 1mM DTT. Otherwise described in figure legend. Liberated 32P was determined.

Actin binding

The binding of calmodulin to Myosin IXb was determined by actin co-sedimentation assay.

Myosin IX was incubated with in buffer containing 30 mM Tris-HCl pH7.5, 30mM KCl, 2 mM $MgCl_2$, 1 mM $CaCl_2$, 30 μM Actin, and various concentrations of EGTA at 25°C for 15 min. The samples were ultracentrifuged at 100,000 X g for 10min. The pellets were analyzed by SDSPAGE. The amount of the co-sedimented Myosin IXb heavy chain and calmodulin were determined by densitometry.

RESULTS

Cloning and sequencing of cDNAs encoding human myosin IXb.

The construct of motor domain with four IQ motifs (M9bIQ4) was prepared previously. Therefore, we cloned the tail potion of myosin IXb to make a full-length myosin IXb construct. The fragment of a middle portion of the construct (SP clone) could be amplified by PCR. However, we failed to obtain a fragment containing 3' end of myosin IXb by PCR. Therefore we performed screening human promyelocytic leukemia lambda cDNA library. From ~1 x 10^7 recombinant phage plaques, 8 positive clones were obtained. Among them, five clones covered the entire 3' region of open reading frame of human myosin IXb as shown in **Fig. III-1** and **Fig. III-2**. The sequencing analysis revealed that 3' end region from 5746-base of obtained sequence was different from the reported sequence (accession # NM004145. The sequence is already corrected by the authors.).

Two alternative splicing at C-terminus of myosin IXb are reported in orthologues of human myosin IXb, myr5 (rat) and Myo9b (mouse) (**Fig. III-3A**). We could get large fragment including 3' UTR region (SC clone) for human myosin IXb. By comparison the sequence of the obtained fragment with the genomic sequence and the sequence of orthologues, the large splicing variant found in rat and mouse would be exist in human by utilize an upstream alternative splice acceptor, inserting an additional 138 amino acids (**Fig. III-2** and **Fig. III-3**).

We isolated shorter isoform of full-length human myosin IXb cDNA of 6018 bp encoding a protein of 2006 amino acids with a molecular mass of 227 kDa. Sequencing analysis shows this clone does not contain the alternatively spliced exon of 48bp after residue Alanine 1915, and residue Glutamine 1612 is missing.

Preparation of full-length myosin IXb

The shorter isoform of myosin IXb construct was produced and expressed in Sf9 insect cells. Cells were co-infected with Myosin IXb expressing virus and calmodulin expressing virus. Myosin IXb is purified using FLAG-tag affinity chromatography (**Fig. III-4**). The purified Myosin IXb construct has bound calmodulin, which shows its characteristic calcium-dependent shift in mobility in SDSPAGE.

Steady-state ATPase activity of Myosin IXb.

To analyze myosin activities of purified full-length myosin IXb, steady-state ATPase activities were determined. Basal Mg^{2+}-ATPase activity was measured as a function of ATP concentration (**Fig. III-5A**). Steady-state ATPase activity at saturating ATP concentration is 0.031 s^{-1} in the absence of actin with K_{ATP} of 12 μM. Actin activated the ATPase of myosin IXb. In the presence of 20 μM actin, ATPase is activated to 0.15 s^{-1}. Actin does not effect on the affinity of myosin IXb to ATP. K_{ATP} of myosin IXb in the presence of actin is 13 μM (**Fig. III-5B**). Next we examined the effect of actin concentration on the Mg^{2+}-ATPase activity of full-length myosin IXb. The ATPase activity was activated ~ 10 fold by actin filament with K_{actin} of 10.5 μM (**Figure III-6**). As shown in **Chapter 2**, the ATPase activity of M9bIQ4 has high basal ATPase activity and is not significantly activated by saturating actin filament. Since the maximum ATPase activity in the presence of actin is similar between M9bIQ4 and full-length myosin IXb, it is plausible that tail domain of myosin IXb negatively regulates the basal ATPase activity of myosin IXb.

As demonstrated in **Chapter2**, ADP does not inhibit the ATPase activity of M9bIQ4 even though myosin IXb is a processive myosin. We confirmed if the ATPase activity of full-length myosin IXb is not inhibited by ADP. The ATPase activity of full-length myosin IXb did not change with time in the absence and presence of ATP regeneration system (**Fig. III-7**), suggesting that the ATPase of myosin IXb is not inhibited by ADP.

Regulation by Calcium

Tissue isolated myosin IXb shows the inhibition of actin-translocating activity by increasing [Ca2+] (Post et al., 1998). Thus, we examined if calcium inhibits the ATPase activity of myosin IXb (**Fig. III-8**). A detail analysis of the free Ca^{2+} concentration revealed inhibition for both the basal and actin-activated ATPase activity above pCa6. This concentration range coincides with the affinity of CaM for Ca^{2+}, supporting the notion that the observed inhibition is due to the binding of Ca^{2+} to the Myosin IXb light chain calmodulin. This Ca^{2+}- dependent inhibition of the ATPase activity of myosin IXb could be explained either by conformational change of CaM or by dissociation of CaM from the myosin IXb heavy chain. Calcium inhibits actin-translocating activity of myosin V by dissociation of some CaMs for an expressed monomer (Trybus et al., 1999), an expressed short-tailed dimer (Homma et al., 2000), or the tissue-purified full-length molecule (Cheney et al., 1993). Two of these papers (Cheney et al., 1993; Trybus et al., 1999) showed restoration of motility in the presence of excess Ca^{2+}-CaM. This observation suggests that calcium-dependent CaM dissociation causes the molecule to be ineffective as a motor. On the other hand, Calcium inhibits the ATPase activity of Myr3, a rat myosin I, but CaM remains bound to the Myr3 heavy chain. Addition of exogenous calmodulin had no effect on the ATPase activity of Myr3, suggesting that the inhibition of the ATPase activity of Myr3 is due to the conformational change of CaM by binding Ca^{2+}. To discriminate between these two possibilities, we performed an actin cosedimentation assay in the absence and presence of free Ca^{2+} (**Fig. III-9A, B**). This experiment allows for the separation of free calmodulins from calmodulins bound to the myosin IXb heavy chain. Comparable amounts of calmodulin were found to cosediment with myosin IXb and F-actin, suggesting that calmodulin light chain did not dissociate from myosin IX at high calcium concentration. Consistently, exogenous calmodulin did not rescue the inhibition of the ATPase activity of myosin IX by high Ca^{2+} (**Fig. III-9C**). These results indicate that the dissociation of calmodulin is not involved in the inhibition of the ATPase activity.

DISCUSSION

We could obtain a large, full-length myosin IXb cDNA. Sequence analysis revealed that myosin IXb could have two alternative splicing variants at C-terminal end found in rat and mouse. The additional sequence is rich in proline residue. Proline rich domain is known as target sequence of proteins that have SH3 domain. Therefore, it is likely that the physiological role of two isoforms would be different.

Regulation by the tail domain and the calcium binding to CaM light chains.

We could successfully express the full-length myosin IXb of 227 kDa. Our ability to express myosin IXb constructs in any size, the truncated myosin IXb (150kDa) and a larger molecular mass of the full-length myosin IXb (227kDa), allows us to show that full-length myosin IXb has some kind of regulation not observed with the truncated tail-less construct. The basal ATPase activity of full-length myosin IXb (0.03 s^{-1}) was activated ~10 fold by actin, while the basal ATPase activity of M9bIQ4 was raised to values that were comparable to the actin activated ATPase, suggesting that the tail domain of myosin IXb inhibits the basal ATPase activity of the myosin IXb head domain. Furthermore, Ca^{2+} inhibits the ATPase activity of the full-length myosin IXb in the presence and absence of actin. However, CaMs do not dissociate from myosin IX at high calcium concentration.

Similar regulation is found in a rat myosin I, myr3 (Stoffler and Bahler, 1998). The limited digestion of myr3 with mercuripapain produced a myr3 fragment truncated at its C-terminus by approximately 10 kDa. The C-terminally truncated myr3 shows increased basal ATPase activity as compared to the intact myr3. Moreover, when an antibody that recognizes the tail domain of myr3 is used as a substitute for a physiological binding partner, the basal ATPase activity of myr3 is increased in concentration dependent manner of antibody. These results indicate that myr3 is

subject to negative regulation by its own tail domain and passively positive regulation by a tail-domain binding partner. In addition, the ATPase activity of Myr3 was found to be negatively regulated by micromolar free Ca^{2+} concentration. CaM light chains remain association with myr3 heavy chain. Therefore, similar regulatory mechanism might be involved in the regulation of myosin IXb.

The studies of the effect of Ca^{2+} on other members of myosin superfamily also give us a clue for the inhibitory mechanism. The effect of Ca^{2+} on the ATPase activity of Myosin V was extensively studied. Ca^{2+} activates the ATPase activities of myosin V, and causes a partial dissociation of CaM light chains. On the other hand, any shorter, tail-less constructs have calcium-insensitive actin-activated ATPase activity. These results suggest that in solution, full-length myosin V can adopt an inhibited structural state that is not possible with any shorter construct. Hydrodynamic data and EM suggest that the inhibited state is a compact conformation of the molecule that can be unfolded to an active state by calcium. In addition, melanophilin, which binds to globular tail domain of myosin V, activates the actin-activated ATPase activity of myosin Va. It is proposed that a folded-to-extended conformational change, which is regulated by calcium and by cargo binding, is responsible for regulating myosin V's motor activity. Myosin IXb would be regulated by a folded-to-extended conformational change, which is dependent on Ca concentration and/or a binding partner.

The inhibition of the basal ATPase activity of myosin IXb is critical to avoid the waste of ATP consumption in cell. Presumably, myosin IXb is inactive state and does not consume ATP when it does not interact with actin, and upon actin binding the motor function of myosin IXb is activated. Of interest is how the tail region inhibits the basal ATPase activity of myosin IX. There are several possibilities for this inhibitory mechanism: (1) Myosin IX forms a folded conformation that the tail domain directly inhibits the binding of ATP to myosin IX. Inhibition is released by the binding

of actin to myosin IX. (2) Rate of hydrolysis is decreased for full-length myosin IX in the absence of actin. (3) Product release is decreased for full-length myosin IX in the absence of actin. Kinetic analysis of the ATPase of myosin IX would clarify this question.

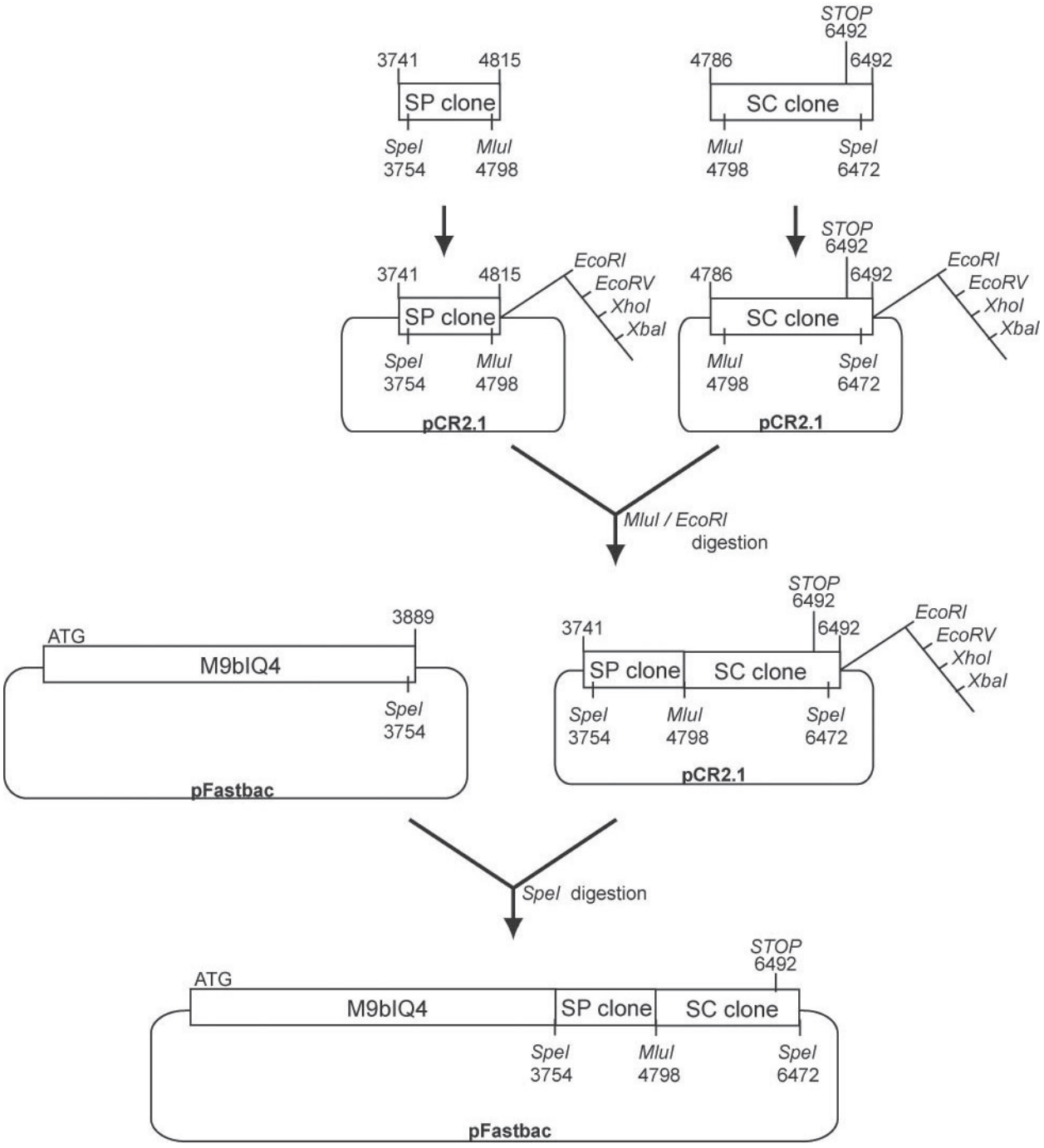

Figure III-1. **Construction of full-length human myosin IXb cDNA**.

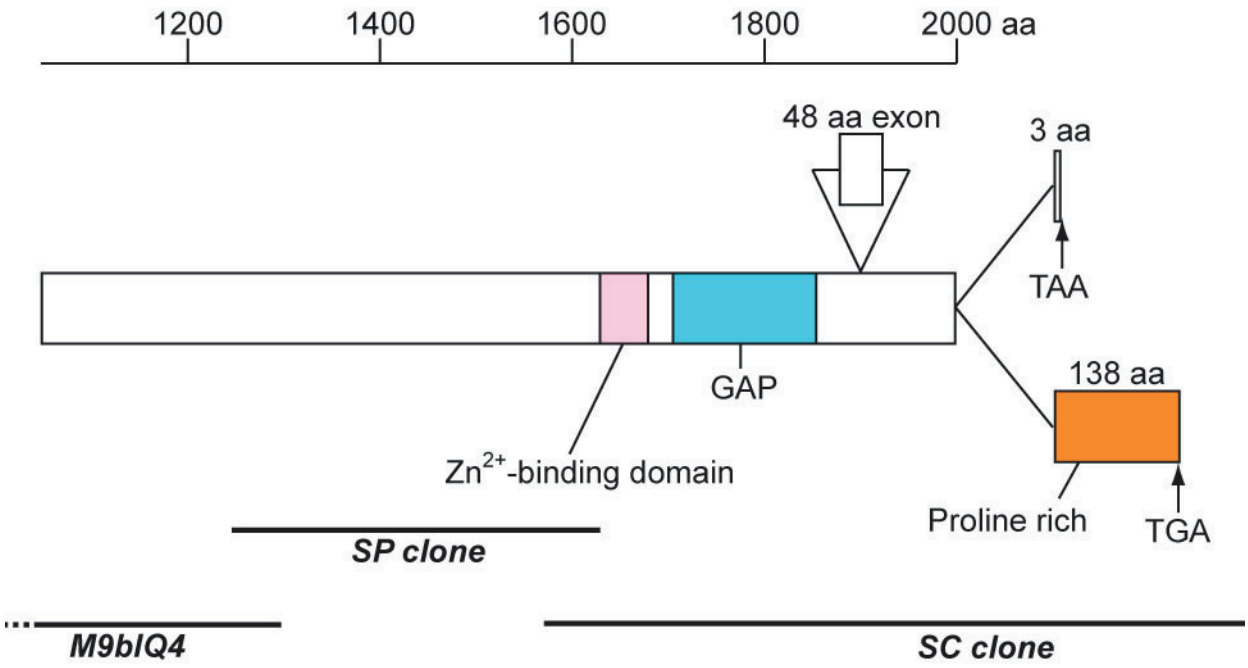

Figure III-2. **Schematic drawing of the tail region of human myosin IXb cDNA.**
Alternative splicing exon identified in this study is shown with the number of amino acids encoded. The alternative use of final exon results in two different length of cDNA. Longer isoform has additional 138 residues in which proline rich domain is found. Solid bars show the position of nucleotide sequence of each of the cloned cDNAs.

```
3754/1252
ACC AGC CTG GCC CTG GAC AGC AGG GTC AGC CCA CCG GCC CCC GGC AGC GCC CCC GAG ACC
 T   S   L   A   L   D   S   R   V   S   P   P   A   P   G   S   A   P   E   T

3814/1272
CCC GAG GAC AAG AGC AAA CCA TGT GGC AGC CCA AGG GTT CAG GAA AAG CCC GAC AGC CCC
 P   E   D   K   S   K   P   C   G   S   P   R   V   Q   E   K   P   D   S   P

3874/1292
GGA GGC TCC ACG CAG ATC CAG CGG TAC CTG GAC GCC GAG CGG CTG GCC AGC GCC GTG GAA
 G   G   S   T   Q   I   Q   R   Y   L   D   A   E   R   L   A   S   A   V   E

3934/1312
CTG TGG CGG GGC AAG AAG CTG GTG GCC GCC GCC AGC CCT AGT GCC ATG CTC AGC CAG TCC
 L   W   R   G   K   K   L   V   A   A   A   S   P   S   A   M   L   S   Q   S

3994/1332
CTG GAC CTC AGC GAC AGA CAC CGG GCC ACA GGG GCC GCC CTC ACG CCC ACA GAG GAG AGG
 L   D   L   S   D   R   H   R   A   T   G   A   A   L   T   P   T   E   E   R

4054/1352
CGC ACC TCC TTC TCC ACG AGC GAC GTC TCC AAG CTC CTC CCG TCC CTG GCC AAG GCT CAG
 R   T   S   F   S   T   S   D   V   S   K   L   L   P   S   L   A   K   A   Q

4114/1372
CCT GCA GCA GAA ACC ACG GAC GGA GAG CGA AGT GCG AAA AAG CCA GCT GTC CAG AAG AAG
 P   A   A   E   T   T   D   G   E   R   S   A   K   K   P   A   V   Q   K   K

4174/1392
AAG CCA GGC GAC GCA TCC TCC CTC CCA GAC GCA GGG CTG TCC CCG GGC TCT CAG GTC GAC
 K   P   G   D   A   S   S   L   P   D   A   G   L   S   P   G   S   Q   V   D

4234/1412
TCT AAA TCC ACG TTT AAG AGG CTT TTT CTG CAT AAA ACC AAG GAT AAA AAA TAC AGC CTG
 S   K   S   T   F   K   R   L   F   L   H   K   T   K   D   K   K   Y   S   L

4294/1432
GAG GGA GCA GAG GAG CTG GAG AAT GCA GTG TCC GGG CAC GTG GTG CTG GAA GCC ACC ACC
 E   G   A   E   E   L   E   N   A   V   S   G   H   V   V   L   E   A   T   T

4354/1452
ATG AAG AAG GGC CTG GAA GCC CCC TCC GGA CAG CAG CAT CGC CAC GCT GCA GGT GAG AAG
 M   K   K   G   L   E   A   P   S   G   Q   Q   H   R   H   A   A   G   E   K

4414/1472
CGC ACC AAG GAA CCA GGA GGC AAA GGG AAG AAG AAC CGA AAT GTC AAG ATT GGG AAG ATC
 R   T   K   E   P   G   G   K   G   K   K   N   R   N   V   K   I   G   K   I

4474/1492
ACA GTG TCA GAG AAG TGG CGG GAA TCG GTG TTC CGC CAG ATC ACC AAC GCC AAT GAG CTC
 T   V   S   E   K   W   R   E   S   V   F   R   Q   I   T   N   A   N   E   L

4534/1512
AAG TAC CTG GAC GAG TTC CTG CTC AAC AAG ATA AAT GAC CTC CGT TCC CAG AAG ACG CCC
 K   Y   L   D   E   F   L   L   N   K   I   N   D   L   R   S   Q   K   T   P

4594/1532
ATT GAG AGC TTG TTT ATC GAA GCC ACC GAG AAG TTC AGG AGC AAC ATC AAA ACG ATG TAC
 I   E   S   L   F   I   E   A   T   E   K   F   R   S   N   I   K   T   M   Y

4654/1552
TCT GTC CCG AAC GGG AAG ATC CAC GTG GGC TAC AAG GAT CTG ATG GAG AAC TAC CAG ATC
 S   V   P   N   G   K   I   H   V   G   Y   K   D   L   M   E   N   Y   Q   I

4714/1572
GTT GTC AGC AAC CTG GCC ACT GAG CGT GGC CAG AAG GAC ACC AAC CTG GTC CTC AAC CTC
 V   V   S   N   L   A   T   E   R   G   Q   K   D   T   N   L   V   L   N   L

4774/1592
TTC CAG TCA CTG CTA GAT GAG TTC ACC CGT GGC TAC ACC AAG AAC GAC TTC GAG CCA GTG
 F   Q   S   L   L   D   E   F   T   R   G   Y   T   K   N   D   F   E   P   V

4834/1612
AAG AGC AAA GCT CAG AAG AAG AAG CGG AAG CAG GAG CGT GCT GTC CAG GAG CAC AAC GGG
 K   S   K   A   Q   K   K   K   R   K   Q   E   R   A   V   Q   E   H   N   G
```

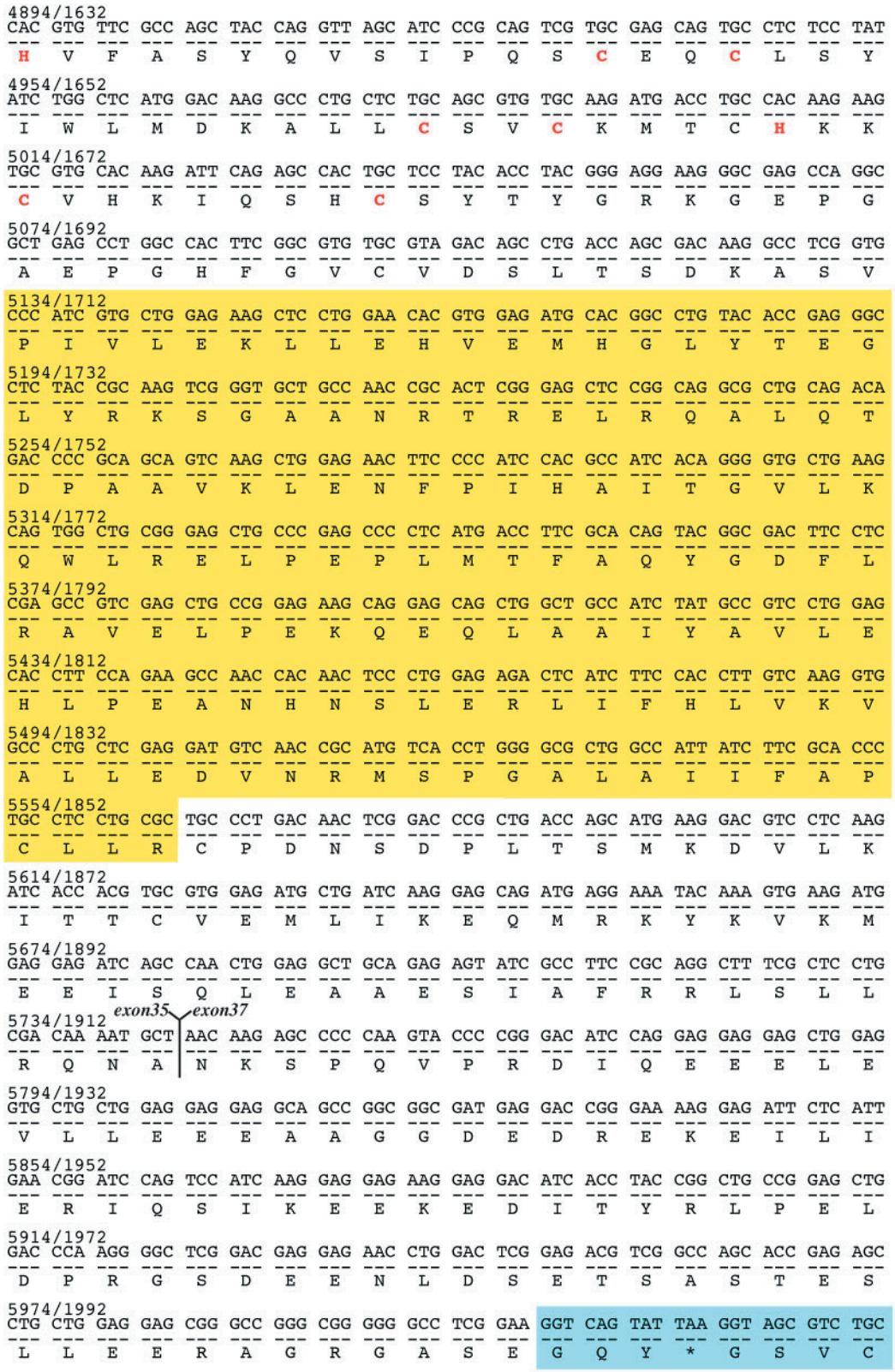
4894/1632
CAC GTG TTC GCC AGC TAC CAG GTT AGC ATC CCG CAG TCG TGC GAG CAG TGC CTC TCC TAT
H V F A S Y Q V S I P Q S C E Q C L S Y
4954/1652
ATC TGG CTC ATG GAC AAG GCC CTG CTC TGC AGC GTG TGC AAG ATG ACC TGC CAC AAG AAG
I W L M D K A L L C S V C K M T C H K K
5014/1672
TGC GTG CAC AAG ATT CAG AGC CAC TGC TCC TAC ACC TAC GGG AGG AAG GGC GAG CCA GGC
C V H K I Q S H C S Y T Y G R K G E P G
5074/1692
GCT GAG CCT GGC CAC TTC GGC GTG TGC GTA GAC AGC CTG ACC AGC GAC AAG GCC TCG GTG
A E P G H F G V C V D S L T S D K A S V
5134/1712
CCC ATC GTG CTG GAG AAG CTC CTG GAA CAC GTG GAG ATG CAC GGC CTG TAC ACC GAG GGC
P I V L E K L L E H V E M H G L Y T E G
5194/1732
CTC TAC CGC AAG TCG GGT GCT GCC AAC CGC ACT CGG GAG CTC CGG CAG GCG CTG CAG ACA
L Y R K S G A A N R T R E L R Q A L Q T
5254/1752
GAC CCC GCA GCA GTC AAG CTG GAG AAC TTC CCC ATC CAC GCC ATC ACA GGG GTG CTG AAG
D P A A V K L E N F P I H A I T G V L K
5314/1772
CAG TGG CTG CGG GAG CTG CCC GAG CCC CTC ATG ACC TTC GCA CAG TAC GGC GAC TTC CTC
Q W L R E L P E P L M T F A Q Y G D F L
5374/1792
CGA GCC GTC GAG CTG CCG GAG AAG CAG GAG CAG CTG GCT GCC ATC TAT GCC GTC CTG GAG
R A V E L P E K Q E Q L A A I Y A V L E
5434/1812
CAC CTT CCA GAA GCC AAC CAC AAC TCC CTG GAG AGA CTC ATC TTC CAC CTT GTC AAG GTG
H L P E A N H N S L E R L I F H L V K V
5494/1832
GCC CTG CTC GAG GAT GTC AAC CGC ATG TCA CCT GGG GCG CTG GCC ATT ATC TTC GCA CCC
A L L E D V N R M S P G A L A I I F A P
5554/1852
TGC CTC CTG CGC TGC CCT GAC AAC TCG GAC CCG CTG ACC AGC ATG AAG GAC GTC CTC AAG
C L L R C P D N S D P L T S M K D V L K
5614/1872
ATC ACC ACG TGC GTG GAG ATG CTG ATC AAG GAG CAG ATG AGG AAA TAC AAA GTG AAG ATG
I T T C V E M L I K E Q M R K Y K V K M
5674/1892
GAG GAG ATC AGC CAA CTG GAG GCT GCA GAG AGT ATC GCC TTC CGC AGG CTT TCG CTC CTG
E E I S Q L E A A E S I A F R R L S L L
exon35
exon37
5734/1912
CGA CAA AAT GCT AAC AAG AGC CCC CAA GTA CCC CGG GAC ATC CAG GAG GAG GAG CTG GAG
R Q N A N K S P Q V P R D I Q E E E L E
5794/1932
GTG CTG CTG GAG GAG GAG GCA GCC GGC GGC GAT GAG GAC CGG GAA AAG GAG ATT CTC ATT
V L L E E E A A G G D E D R E K E I L I
5854/1952
GAA CGG ATC CAG TCC ATC AAG GAG GAG AAG GAG GAC ATC ACC TAC CGG CTG CCG GAG CTG
E R I Q S I K E E K E D I T Y R L P E L
5914/1972
GAC CCA AGG GGC TCG GAC GAG GAG AAC CTG GAC TCG GAG ACG TCG GCC AGC ACC GAG AGC
D P R G S D E E N L D S E T S A S T E S
5974/1992
CTG CTG GAG GAG CGG GCC GGG CGG GGG GCC TCG GAA GGT CAG TAT TAA GGT AGC GTC TGC
L L E E R A G R G A S E G Q Y * G S V C

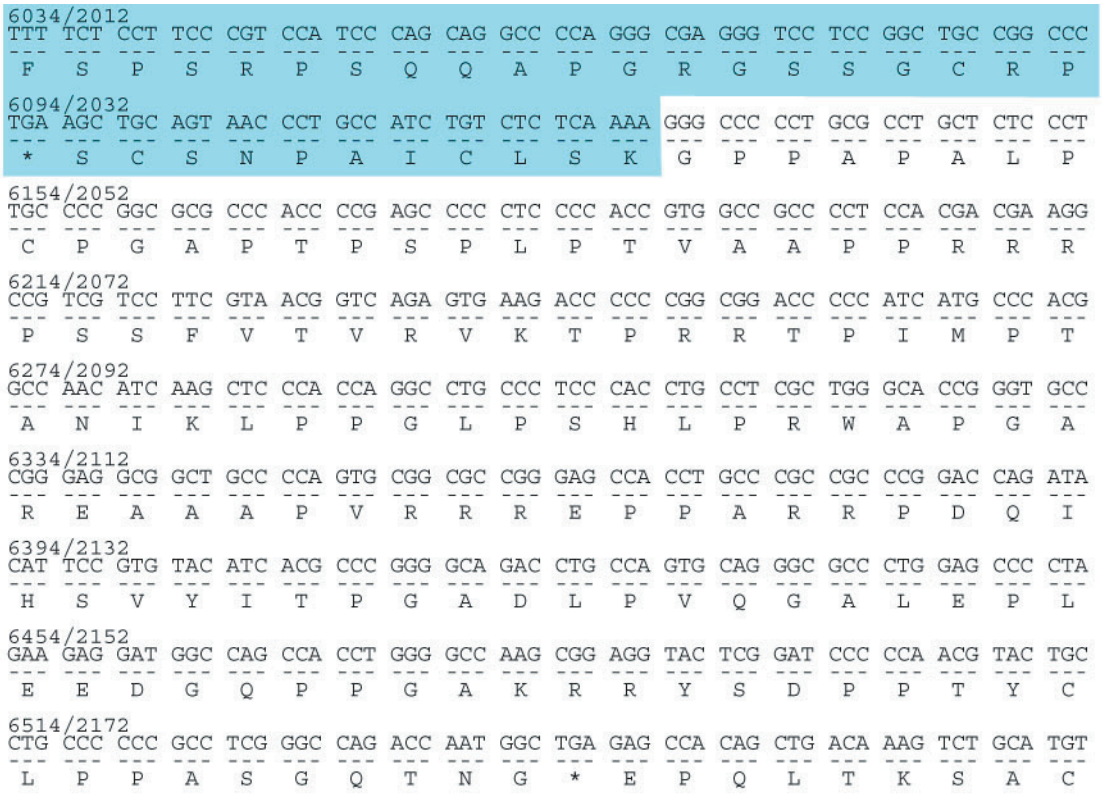

Figure III-3. **Sequence of cloned human cDNA.** Zinc-binding domain is indicated by red. GAP domain is highlighted by yellow box. Exon36 (16 amino acids) is spliced out in our construct. Alternative splicing exon at C-terminal region is shown by blue box. Shorter isoform is terminated at tyrosine 2006, while longer isoform terminated at Glysine 2181.

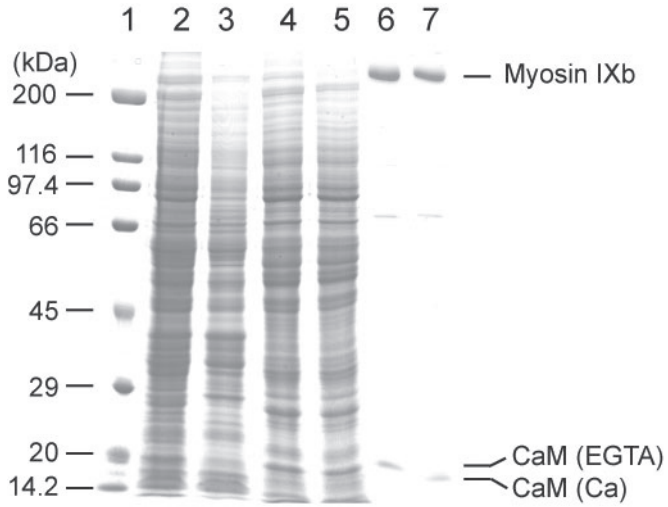

Figure III-4. **Purification of human myosin IXb construct.** Lane 1, molecular mass marker; lane 2; total cell lysate; lane 3, pellet of cell homogenate after centrifugation; lane 4, supernatant of cell homogenate after centrifugation; lane 5, flow though fraction from FLAG-tag affinity column; lane 6 and lane 7, elution from the column. CaM undergoes its characteristic Ca^{2+}-dependent shift in mobility (lane 6, EGTA; lane 7, Ca^{2+}).

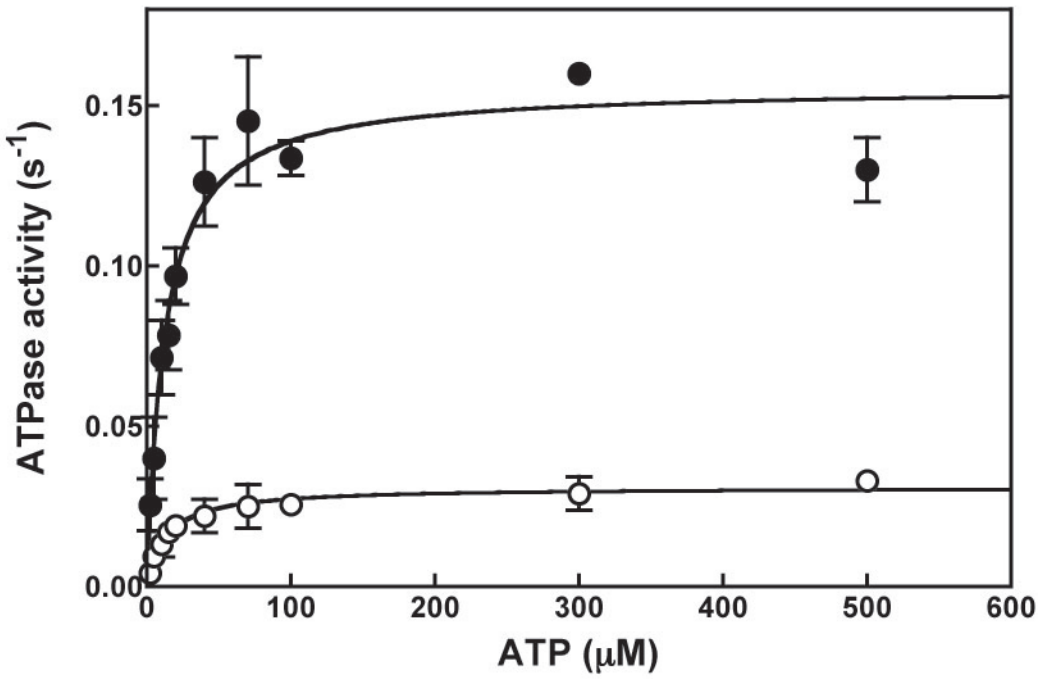

Figure III-5. **ATP dependence of steady-state ATPase activity of myosin IXb.** The ATPase activity of Myosin IXb was measured as a function of ATP concentration in the absence (open circles) or presence (closed circles) of 20 μM actin. Solid lines, calculated based on the equation $v = V_{max}[ATP]/(K_{ATP} + [ATP])$. According to the analysis, the basal ATPase activity is obtained for 0.03 s^{-1} with K_{ATP} of 12.2 μM. The maximum ATPase activity in the given actin concentration is 0.16 s^{-1} with K_{ATP} of 13.2 μM. The error bars indicate S.D. for n = 3 from three independent preparations.

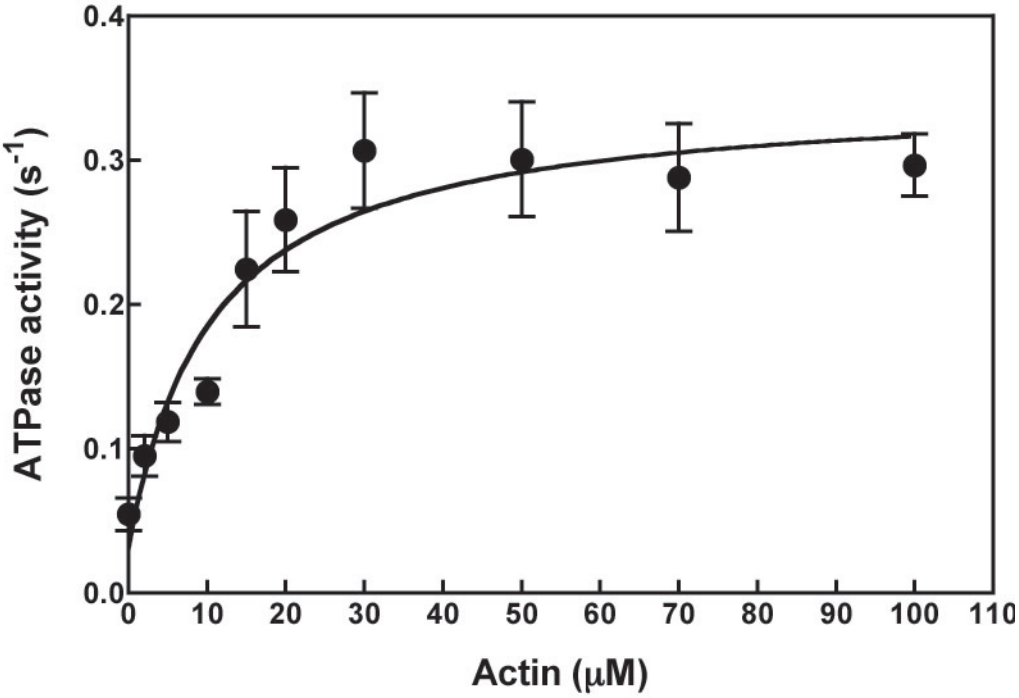

Figure III-6. **Actin dependence of steady-state ATPase activity of myosin IXb.** The ATPase activity of Myosin IXb was measured as a function of actin concentration in the presence of 0.3 mM ATP. Solid lines, calculated based on the equation $v = V_{max}[actin]/(K_{actin} + [actin]) + v_0$. According to the analysis, the basal ATPase activity, v_o is obtained for 0.03 s^{-1}. The maximum activation by actin (V_{max}) is 0.32 s^{-1}. The maximum ATPase activity at saturating actin concentration ($V_{max} + v_0$) is 0.35 s^{-1} with K_{actin} of 10.5 μM. The error bars indicate S.D. for n = 3 from three independent preparations.

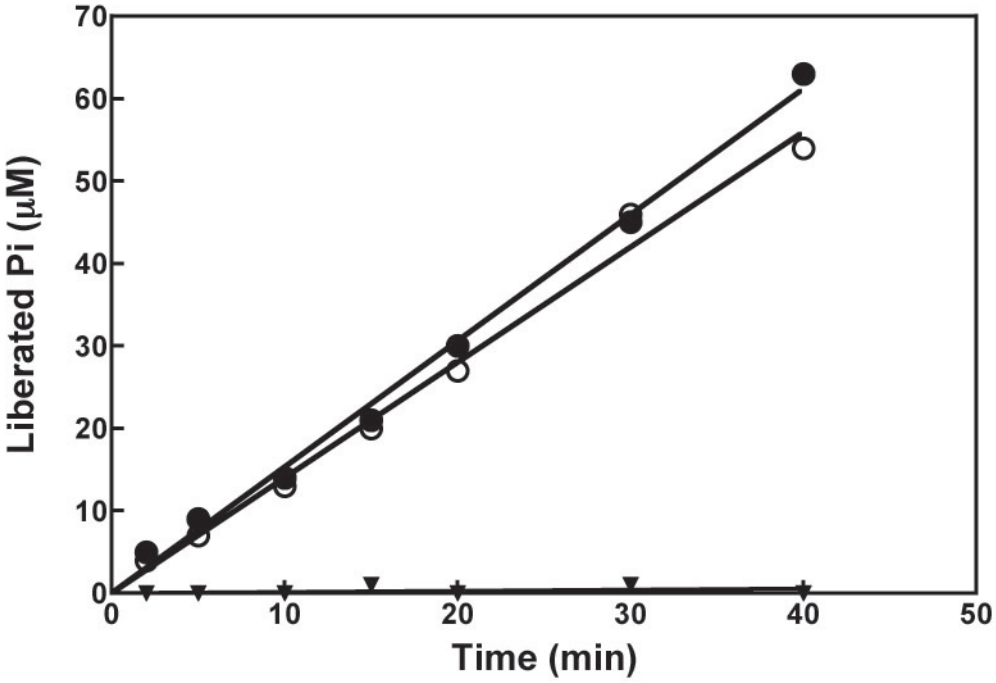

Figure III-7. **The course of the steady-state ATPase activity of Myosin IXb in the presence of actin with or without the ATP-regenerating system.** ATPase activity was measured in the presence (closed circles) and absence (open circles) of 20 units/ml pyruvate kinase and 2 mM phosphoenol pyruvate. 20 μM actin and 0.6 mM ATP were used in the assay. Actin does not show ATPase activity (triangles).

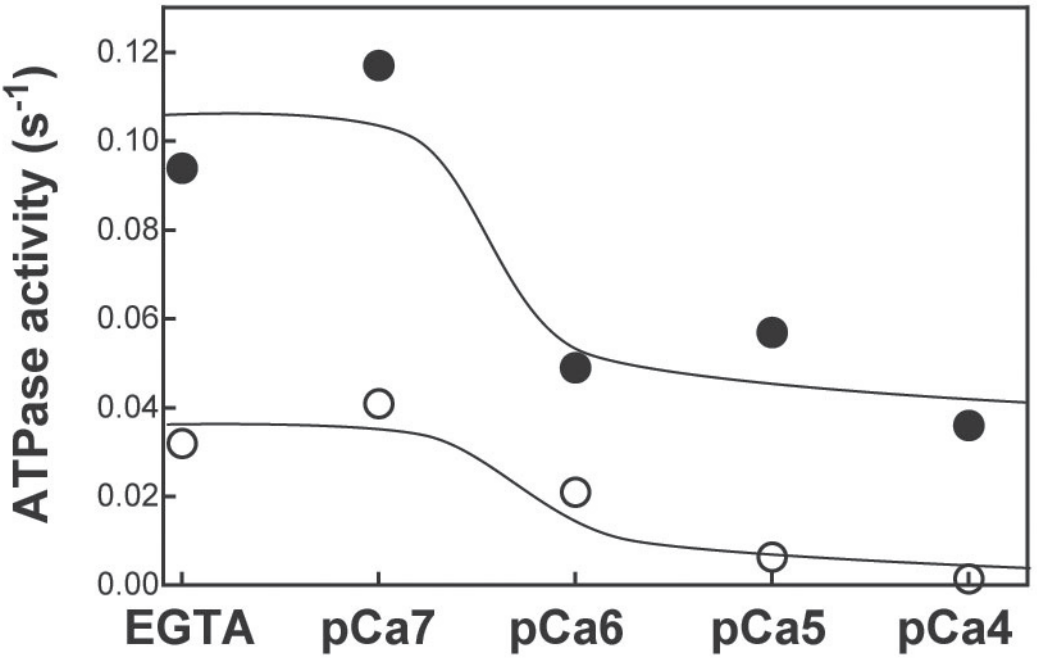

Figure III-8. **The effect of calcium on the ATPase activity of myosin IXb.** Myosin IXb was incubated with various Ca concentrations using Ca/EGTA buffer system. The ATPase activity was measured in the absence (open circles) and presence (closed circles) of 10 μM actin.

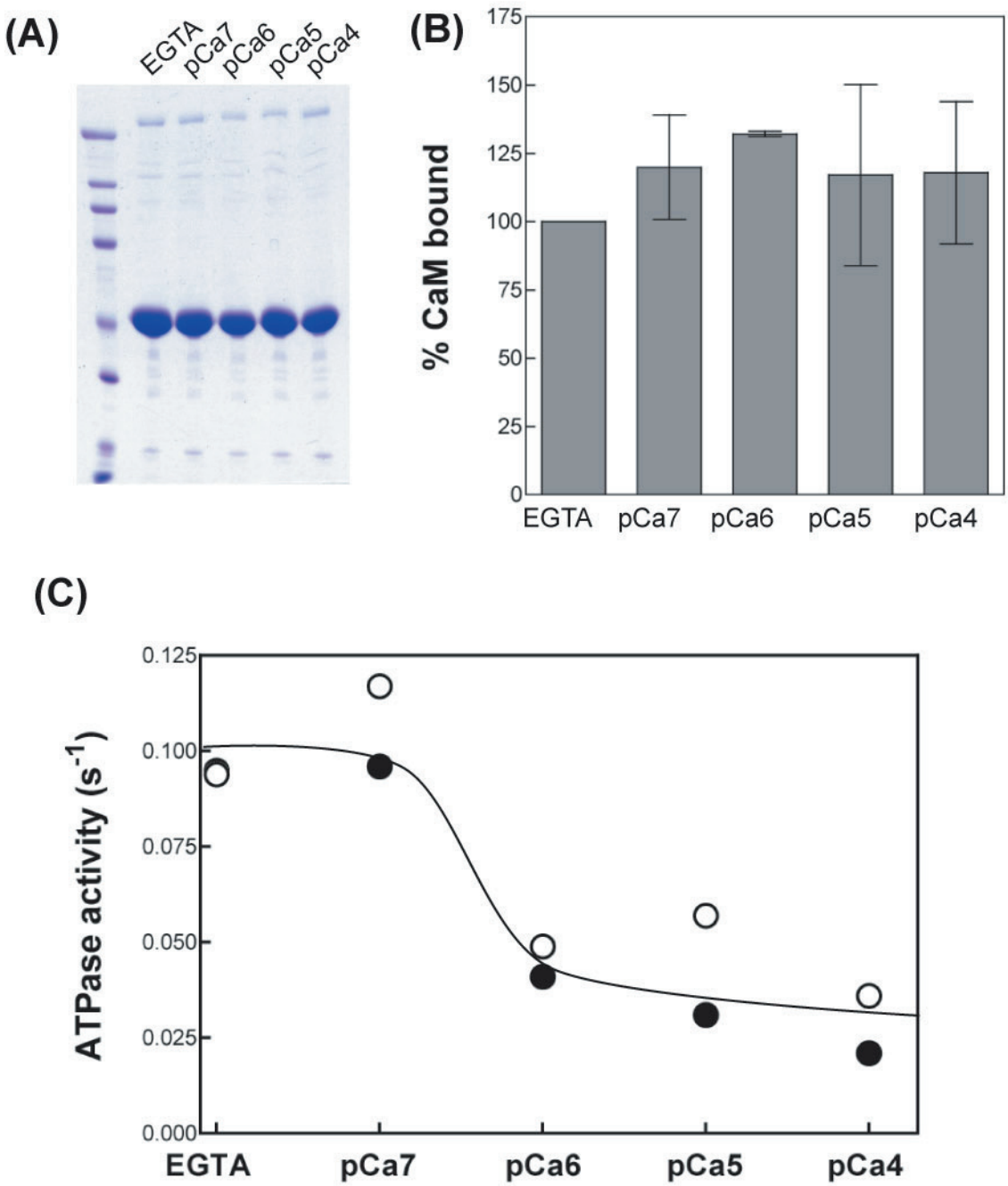

Figure III-9. **The effect of calcium on dissociation of calmodulin from myosin IXb heavy chain.** A, SDSPAGE shows the pellets of myosin IXb cosedimented with actin. B, fraction of bound CaM on the myosin IXb heavy chain. The concentration of heavy chain and CaM light chains are determined by densitometry of SDSPAGE gel from panel A. The experiment was done three times, and the bars represent SD. C, Effect of exogenous CaM on the ATPase activity of myosin IXb at various Ca^{2+} concentration. The ATPase activity was measured in the presence of 10 μM CaM. Open circles, without exogenous CaM. Closed circles, with exogenous CaM.

CHAPTER FOUR: CONCLUSION AND PERSPECTIVE

Studies for processive movement of myosin IX.

We determined the rates of key steps of ATPase cycle of myosin IXb. The most notable features of ATPase are; (1) the rate-limiting hydrolysis, (2) AM and AM•ADP strongly bind to actin, and the affinities are comparable to other myosins, and (3) M9•ATP and M9•ADP•P states are lower affinity to actin compared to that of AM and AM•ADP, but still high enough to prevent myosin IX from diffusing away from actin filaments. These results strongly support the finding that single-headed Myosin IXb moves processively on actin filaments. As discussed in the **Chapter 2**, proposed swinging lever arm model for force generation (power stroke) and hand-over-hand model for processive movement of double-headed myosin are not able to describe that of single-headed myosin IXb, but does a biased Brownian ratchet model. Therefore, characterization of the mechanism of processive movement for single-headed myosin IXb will be central to further research in this area. A critical experiment to answer the question is to measure the displacement of myosin IXb using total internal reflection fluorescence microscope (TIRFM) and a scanning probe (Kitamura et al., 1999). In this technique, single myosin molecules captured on the tip of the scanning probe were visualized by TIRFM, which produces clear images of single fluorophores at a high fluorescence-to-background ratio. If myosin IXb moves with a biased Brownian ratchet model, myosin IX would step 36 nm that coincides actin helical pitch.

Judging from very limited information, it is anticipated that processive myosin IX transports proteins such as BIG1 without dissociating from actin, but not vesicles like myosin V. Actin translocating activity (Inoue et al., 2002; Post et al., 2002) and kinetic data suggested that myosin IX is processive, then next question related to physiological function would be how far myosin IX can travel on actin filament without dissociating from actin track. This question will be answered by measuring run length of myosin IXb using TIRFM where the actin bundles are attached to the

glass surface and myosin molecule in solution is observed to move as single fluorescent spot along actin filament. Another question regarding processivity in cell is that if step size is dependent on loading. For myosin V and myosin VI, step size is not dependent on load. Because myosin IX is single headed structure, it is possible that myosin IX cannot travel for long distance without dissociation from actin under loaded condition. This question would be addressed by using dual bead optical trapping.

Does the processivity of myosin is regulated by association with binding partner protein? Even though myosin IX has high affinity to actin, the probability of processive movement might be less compare to double-headed processive myosins. If myosin IX is such a weak processive motor, binding of other molecules to myosin IX could attenuate diffusion of myosin IX from an actin track, thus could travel for long distance. Therefore, measuring run length in the absence and presence of binding partner is of interest in terms of regulation of processivity of myosin IX.

Of interest is how single-headed myosin IXb is tuned to move processively. To ensure that a myosin IXb molecule does not diffuse away from actin track, this myosin may use a mechanism similar to that originally proposed for the processive movement of the single-headed kinesin, KIF1A (Okada and Hirokawa, 2000; Kikkawa et al., 2001). This motor contains a highly charged surface loop in the motor domain that weakly tethers the motor to the microtubule preventing diffusion away from the microtubule surface. The electrostatic tether allows the motor to undergo one-dimensional diffusion along its track in search of its next strong binding site. The large, highly basic insertion at the actin contact site of Myosin IXb is an obvious candidate to participate in a similar mode of processive movement along the actin filament. Further characterization of the effect of the insertion of myosin IXb on processivity can be accomplished by using mutants expressed in baculovirus expression system. I would express only insertion region, and examine if this construct binds to actin filaments. Then processivity of myosin IXb mutant lacking the

insertion would be examined.

Studies for conformational change of myosin IX.

The second extension of this research is the characterization of conformational change of myosin IXb. As shown in **Chapter 3**, the ATPase activity of myosin IXb is regulated by its tail region and Ca^{2+}, maybe by folded-extended conformational change. This could be elucidated by studying rotary shadow electron microscopy and analytical centrifugation. Cryo-electron microscopy is another technique to see the structure of myosin IXb. Using this method, we can see the protein structure in aqueous environment in physiological conditions. Decorated actin filament with myosin IXb can be analyzed by cryo-EM and image reconstitution to gain structural insight. This technique will enable us to determine the identity of the subdomains in the reconstituted structure and the movement of the subdomains among various nucleotide bound forms of myosin IX. The decoration of myosin IX on actin filaments can be done in the presence and absence of ATP, in the presence of ADP, and in the presence of ADP and phosphate analogs such as vanadate. As shown in Chapter 2, all of intermediates do not dissociate from actin filaments during ATPase cycle. Therefore, we will detect the changes in the conformation of myosin IX while it associates with actin during the ATPase cycle.

Physiological function of myosin IXb.

What is a physiological role of myosin IX? How processive motor behavior could contribute to the biological function of myosin IX? The cellular function of the class IX myosins is currently unknown. However, it has been shown that myosin IX has GAP activity, which inactivates small G-protein RhoA. Thus it is likely that the class IX myosins are involved in rho-mediated signaling pathways.

RhoA was shown to regulate formation of stress fibers and focal adhesions in fibroblasts and to

regulate Ca^{2+} sensitivity of smooth muscle contraction (Hirata et al., 1992). Thus RhoA is involved in remodeling of the actin cytoskeleton. Reorganization of the actin cytoskeleton plays crucial roles in many cellular functions such as cell shape change, cell motility, cell adhesion, and cytokinesis. Filamentous actin is generally organized into a number of discrete structures: (1) actin stress fibers: bundles of actin filaments that traverse the cell and are linked to the extracellular matrix through focal adhesions; (2) lamellipodia: thin protrusive actin sheets that dominate the edges of cultured fibroblasts and many migrating cells; and (3) filopodia: fingerlike protrusions that contain a tight bundle of long actin filaments in the direction of the protrusion. They are found primarily in motile cells and neuronal growth cones. It is important, therefore, that the polymerization and depolymerization of cortical actin are tightly regulated. Rho proteins regulate stress fiber formation (Ridley and Hall, 1992; Miura et al., 1993), while other members of Rho superfamily, Rac and Cdc42 regulate lamellipodia formation (Ridley et al., 1992), and filopodium formation (Kozma et al., 1995; Nobes and Hall, 1995), respectively. Evidence has also accumulated that they may play additional roles in gene expression (Hill et al., 1995), cell growth (Yamamoto et al., 1993; Khosravi-Far et al., 1995; Qiu et al., 1995; Obaishi et al., 1998), and membrane trafficking (Adam et al., 1996; Komuro et al., 1996; Lamaze et al., 1996). In these cellular events, it is not known whether Rho proteins directly or indirectly regulate them through cytoskeletal reorganization and gene expression. It is possible that class IX myosins act to modulate one or more of above functions for rho. The Myosin IXb motor domain may serve to localize it to the site of rho functions, i.e. on actin.

It has been shown that rho is a negative regulator of human monocyte cell spreading (Aepfelbacher et al., 1996)**.** Studies in a leukocyte cell line suggest a model that Myosin IXb inactivates rho to allow monocyte spreading. TPA treatment of these cells induces their differentiation into macrophage-like cells. Myosin IXb is colocalized with F-actin in the cortex of rounded, undifferentiated cells, where activated GTP-bound rho would exist (Wirth et al., 1996). This pattern changes to a more

diffuse, cytoplasmic localization in spread, macrophage differentiated cells where inactivated GDP-bound rho would exist and is no longer colocalized with F-actin (Wirth et al., 1996). Myosin IXb may inactivate rho (causing depolymerization of actin) in order to allow actin remodeling and macrophage spreading to occur. Furthermore, differentiated cells show concentrated staining in a perinuclear spot, which is reminiscent of Golgi staining. Of particular interest is the potential association of myosin-IXb with the Golgi in differentiating cells, because Golgi membrane associate with the actin network and actin structure is important for the organization of the Golgi. Quite recently it has been shown that myosin IXb interacts with BIG1, a guanine nucleotide exchange factor for ADP-ribosylation factor (Arf1) (Saeki et al., 2005). The RhoGAP activity of myosin IXb is inhibited by BIG1 by competition between BIG1 and Rho in binding to myosin IXb. The Arf proteins play a role in the vesicle transport, and the Arf activity is activated by BIG1. Thus it is possible that myosin IX is involved in this event. Saeki et al. further hypothesized that myosin IXb moves BIG1 away from the Golgi.

Since it is likely that the Myosin IXb plays a role in down-regulating rho-mediated events, it will be critical to determine whether myosin IX is a substrate for kinases implicated in rho cascades. The rho family interacts with several kinases that phosphorylate other myosins. Rho interacts with protein kinase N (Amano et al., 1996b; Watanabe et al., 1996) and rho kinase (Kimura et al., 1996) that affects the phosphorylation state of myosin II regulatory light chain and induces fibroblast stress fiber formation, focal adhesion formation and smooth muscle contraction (Amano et al., 1996a; Amano et al., 1997; Kureishi et al., 1997). Rac and cdc42 bind to p65 PAK, which phosphorylates *Acanthamoeba* myosin I and activates enzymatic activity (Brzeska et al., 1997). Phosphorylation of myosin IX is possibly involved in regulation of physiological function, such as direction of movement, processivity, and localization in cell. Therefore it is critical to determine if myosin IX is phosphorylated by some kinases, and if there are, identifying the responsible kinases.

As a preliminary study, we examined if myosin IX is phosphorylated by any kinases. Purified full-length myosin IX was phosphorylated various kinases, and then samples are subjected to SDSPAGE followed by autoradiography. The radioactivity was detected at the band of myosin IX when myosin IX is incubated with ATP without addition of any kinases. Thus we could not evaluate if certain kinases phosphorylate myosin IX. This is because some kinase is co-purified with myosin IX, and the contaminated kinase in the purified myosin IX sample phosphorylates myosin IX. This implies that myosin IX could be phosphorylated by certain kinase. Further experiments will clarify the physiological function of myosin IX.

REFERENCES

Adam, T., Giry, M., Boquet, P. and Sansonetti, P.: Rho-dependent membrane folding causes Shigella entry into epithelial cells. Embo J 15 (1996) 3315-21.

Aepfelbacher, M., Essler, M., Huber, E., Czech, A. and Weber, P.C.: Rho is a negative regulator of human monocyte spreading. J Immunol 157 (1996) 5070-5.

Amano, M., Chihara, K., Kimura, K., Fukata, Y., Nakamura, N., Matsuura, Y. and Kaibuchi, K.: Formation of actin stress fibers and focal adhesions enhanced by Rho-kinase. Science 275 (1997) 1308-11.

Amano, M., Ito, M., Kimura, K., Fukata, Y., Chihara, K., Nakano, T., Matsuura, Y. and Kaibuchi, K.: Phosphorylation and activation of myosin by Rho-associated kinase (Rho-kinase). J Biol Chem 271 (1996a) 20246-9.

Amano, M., Mukai, H., Ono, Y., Chihara, K., Matsui, T., Hamajima, Y., Okawa, K., Iwamatsu, A. and Kaibuchi, K.: Identification of a putative target for Rho as the serine-threonine kinase protein kinase N. Science 271 (1996b) 648-50.

Bagshaw, C.R., Eccleston, J.F., Eckstein, F., Goody, R.S., Gutfreund, H. and Trentham, D.R.: The magnesium ion-dependent adenosine triphosphatase of myosin. Two-step processes of adenosine triphosphate association and adenosine diphosphate dissociation. Biochem J 141 (1974) 351-64.

Bahler, M., Kehrer, I., Gordon, L., Stoffler, H.E. and Olsen, A.S.: Physical mapping of human myosin-IXB (MYO9B), the human orthologue of the rat myosin myr 5, to chromosome 19p13.1. Genomics 43 (1997) 107-9.

Bar-Sagi, D. and Hall, A.: Ras and Rho GTPases: a family reunion. Cell 103 (2000) 227-38.

Batra, R. and Manstein, D.J.: Functional characterisation of Dictyostelium myosin II with conserved tryptophanyl residue 501 mutated to tyrosine. Biol Chem 380 (1999) 1017-23.

Berg, J.S., Powell, B.C. and Cheney, R.E.: A millennial myosin census. Mol Biol Cell 12 (2001) 780-94.

Berger, C.L. and Thomas, D.D.: Rotational dynamics of actin-bound intermediates in the myosin ATPase cycle. Biochemistry 30 (1991) 11036-45.

Brune, M., Hunter, J.L., Corrie, J.E. and Webb, M.R.: Direct, real-time measurement of rapid inorganic phosphate release using a novel fluorescent probe and its application to actomyosin subfragment 1 ATPase. Biochemistry 33 (1994) 8262-71.

Brzeska, H., Knaus, U.G., Wang, Z.Y., Bokoch, G.M. and Korn, E.D.: p21-activated kinase has substrate specificity similar to Acanthamoeba myosin I heavy chain kinase and activates Acanthamoeba myosin I. Proc Natl Acad Sci U S A 94 (1997) 1092-5.

Buss, F., Spudich, G. and Kendrick-Jones, J.: Myosin VI: cellular functions and motor properties. Annu Rev Cell Dev Biol 20 (2004) 649-76.

Carragher, B.O., Cheng, N., Wang, Z.Y., Korn, E.D., Reilein, A., Belnap, D.M., Hammer, J.A., 3rd and Steven, A.C.: Structural invariance of constitutively active and inactive mutants of acanthamoeba myosin IC bound to F-actin in the rigor and ADP-bound states. Proc Natl Acad Sci U S A 95 (1998) 15206-11.

Cheney, R.E. and Mooseker, M.S.: Unconventional myosins. Curr Opin Cell Biol 4 (1992) 27-35.

Cheney, R.E., O'Shea, M.K., Heuser, J.E., Coelho, M.V., Wolenski, J.S., Espreafico, E.M., Forscher, P., Larson, R.E. and Mooseker, M.S.: Brain myosin-V is a two-headed unconventional myosin with motor activity. Cell 75 (1993) 13-23.

Chieregatti, E., Gartner, A., Stoffler, H.E. and Bahler, M.: Myr 7 is a novel myosin IX-RhoGAP expressed in rat brain. J Cell Sci 111 (Pt 24) (1998) 3597-608.

Coluccio, L.M. and Geeves, M.A.: Transient kinetic analysis of the 130-kDa myosin I (MYR-1

gene product) from rat liver. A myosin I designed for maintenance of tension? J Biol Chem 274 (1999) 21575-80.

Cremo, C.R. and Geeves, M.A.: Interaction of actin and ADP with the head domain of smooth muscle myosin: implications for strain-dependent ADP release in smooth muscle. Biochemistry 37 (1998) 1969-78.

Dai, J., Ting-Beall, H.P., Hochmuth, R.M., Sheetz, M.P. and Titus, M.A.: Myosin I contributes to the generation of resting cortical tension. Biophys J 77 (1999) 1168-76.

De La Cruz, E.M., Ostap, E.M. and Sweeney, H.L.: Kinetic mechanism and regulation of myosin VI. J Biol Chem 276 (2001) 32373-81.

De La Cruz, E.M., Sweeney, H.L. and Ostap, E.M.: ADP inhibition of myosin V ATPase activity. Biophys J 79 (2000a) 1524-9.

De La Cruz, E.M., Wells, A.L., Rosenfeld, S.S., Ostap, E.M. and Sweeney, H.L.: The kinetic mechanism of myosin V. Proc Natl Acad Sci U S A 96 (1999) 13726-31.

De La Cruz, E.M., Wells, A.L., Sweeney, H.L. and Ostap, E.M.: Actin and light chain isoform dependence of myosin V kinetics. Biochemistry 39 (2000b) 14196-202.

Dominguez, R., Freyzon, Y., Trybus, K.M. and Cohen, C.: Crystal structure of a vertebrate smooth muscle myosin motor domain and its complex with the essential light chain: visualization of the pre-power stroke state. Cell 94 (1998) 559-71.

El Mezgueldi, M., Tang, N., Rosenfeld, S.S. and Ostap, E.M.: The kinetic mechanism of Myo1e (human myosin-IC). J Biol Chem 277 (2002) 21514-21.

Fisher, A.J., Smith, C.A., Thoden, J.B., Smith, R., Sutoh, K., Holden, H.M. and Rayment, I.: X-ray structures of the myosin motor domain of Dictyostelium discoideum complexed with MgADP.BeFx and MgADP.AlF4. Biochemistry 34 (1995) 8960-72.

Forkey, J.N., Quinlan, M.E., Shaw, M.A., Corrie, J.E. and Goldman, Y.E.: Three-dimensional

structural dynamics of myosin V by single-molecule fluorescence polarization. Nature 422 (2003) 399-404.

Furch, M., Geeves, M.A. and Manstein, D.J.: Modulation of actin affinity and actomyosin adenosine triphosphatase by charge changes in the myosin motor domain. Biochemistry 37 (1998) 6317-26.

Geeves, M.A. and Holmes, K.C.: Structural mechanism of muscle contraction. Annu Rev Biochem 68 (1999) 687-728.

Geeves, M.A., Perreault-Micale, C. and Coluccio, L.M.: Kinetic analyses of a truncated mammalian myosin I suggest a novel isomerization event preceding nucleotide binding. J Biol Chem 275 (2000) 21624-30.

Geli, M.I. and Riezman, H.: Role of type I myosins in receptor-mediated endocytosis in yeast. Science 272 (1996) 533-5.

Gerner, C., Frohwein, U., Gotzmann, J., Bayer, E., Gelbmann, D., Bursch, W. and Schulte-Hermann, R.: The Fas-induced apoptosis analyzed by high throughput proteome analysis. J Biol Chem 275 (2000) 39018-26.

Gillespie, P.G., Wagner, M.C. and Hudspeth, A.J.: Identification of a 120 kd hair-bundle myosin located near stereociliary tips. Neuron 11 (1993) 581-94.

Goodno, C.C.: Inhibition of myosin ATPase by vanadate ion. Proc Natl Acad Sci U S A 76 (1979) 2620-4.

Goodno, C.C.: Myosin active-site trapping with vanadate ion. Methods Enzymol 85 Pt B (1982) 116-23.

Goodno, C.C. and Taylor, E.W.: Inhibition of actomyosin ATPase by vanadate. Proc Natl Acad Sci U S A 79 (1982) 21-5.

Grewal, P.K., Jones, A.M., Maconochie, M., Lemmers, R.J., Frants, R.R. and Hewitt, J.E.: Cloning

of the murine unconventional myosin gene Myo9b and identification of alternative splicing. Gene 240 (1999) 389-98.

Highsmith, S.: Lever arm model of force generation by actin-myosin-ATP. Biochemistry 38 (1999) 9791-7.

Hill, C.S., Wynne, J. and Treisman, R.: The Rho family GTPases RhoA, Rac1, and CDC42Hs regulate transcriptional activation by SRF. Cell 81 (1995) 1159-70.

Hirata, K., Kikuchi, A., Sasaki, T., Kuroda, S., Kaibuchi, K., Matsuura, Y., Seki, H., Saida, K. and Takai, Y.: Involvement of rho p21 in the GTP-enhanced calcium ion sensitivity of smooth muscle contraction. J Biol Chem 267 (1992) 8719-22.

Hodge, T. and Cope, M.J.: A myosin family tree. J Cell Sci 113 Pt 19 (2000) 3353-4.

Homma, K., Saito, J., Ikebe, R. and Ikebe, M.: Ca(2+)-dependent regulation of the motor activity of myosin V. J Biol Chem 275 (2000) 34766-71.

Houdusse, A., Kalabokis, V.N., Himmel, D., Szent-Gyorgyi, A.G. and Cohen, C.: Atomic structure of scallop myosin subfragment S1 complexed with MgADP: a novel conformation of the myosin head. Cell 97 (1999) 459-70.

Houdusse, A. and Sweeney, H.L.: Myosin motors: missing structures and hidden springs. Curr Opin Struct Biol 11 (2001) 182-94.

Houdusse, A., Szent-Gyorgyi, A.G. and Cohen, C.: Three conformational states of scallop myosin S1. Proc Natl Acad Sci U S A 97 (2000) 11238-43.

Howard, J., Hudspeth, A.J. and Vale, R.D.: Movement of microtubules by single kinesin molecules. Nature 342 (1989) 154-8.

Hurley, J.H., Newton, A.C., Parker, P.J., Blumberg, P.M. and Nishizuka, Y.: Taxonomy and function of C1 protein kinase C homology domains. Protein Sci 6 (1997) 477-80.

Ikebe, M. and Hartshorne, D.J.: Effects of Ca2+ on the conformation and enzymatic activity of

smooth muscle myosin. J Biol Chem 260 (1985) 13146-53.

Ikebe, M., Kambara, T., Stafford, W.F., Sata, M., Katayama, E. and Ikebe, R.: A hinge at the central helix of the regulatory light chain of myosin is critical for phosphorylation-dependent regulation of smooth muscle myosin motor activity. J Biol Chem 273 (1998) 17702-7.

Inoue, A., Saito, J., Ikebe, R. and Ikebe, M.: Myosin IXb is a single-headed minus-end-directed processive motor. Nat Cell Biol 4 (2002) 302-6.

Joel, P.B., Trybus, K.M. and Sweeney, H.L.: Two conserved lysines at the 50/20-kDa junction of myosin are necessary for triggering actin activation. J Biol Chem 276 (2001) 2998-3003.

Jontes, J.D., Milligan, R.A., Pollard, T.D. and Ostap, E.M.: Kinetic characterization of brush border myosin-I ATPase. Proc Natl Acad Sci U S A 94 (1997) 14332-7.

Jontes, J.D., Wilson-Kubalek, E.M. and Milligan, R.A.: A 32 degree tail swing in brush border myosin I on ADP release. Nature 378 (1995) 751-3.

Jung, G., Wu, X. and Hammer, J.A., 3rd: Dictyostelium mutants lacking multiple classic myosin I isoforms reveal combinations of shared and distinct functions. J Cell Biol 133 (1996) 305-23.

Kalhammer, G., Bahler, M., Schmitz, F., Jockel, J. and Block, C.: Ras-binding domains: predicting function versus folding. FEBS Lett 414 (1997) 599-602.

Kambara, T., Rhodes, T.E., Ikebe, R., Yamada, M., White, H.D. and Ikebe, M.: Functional significance of the conserved residues in the flexible hinge region of the myosin motor domain. J Biol Chem 274 (1999) 16400-6.

Khosravi-Far, R., Solski, P.A., Clark, G.J., Kinch, M.S. and Der, C.J.: Activation of Rac1, RhoA, and mitogen-activated protein kinases is required for Ras transformation. Mol Cell Biol 15 (1995) 6443-53.

Kikkawa, M., Sablin, E.P., Okada, Y., Yajima, H., Fletterick, R.J. and Hirokawa, N.: Switch-based

mechanism of kinesin motors. Nature 411 (2001) 439-45.

Kimura, K., Ito, M., Amano, M., Chihara, K., Fukata, Y., Nakafuku, M., Yamamori, B., Feng, J., Nakano, T., Okawa, K., Iwamatsu, A. and Kaibuchi, K.: Regulation of myosin phosphatase by Rho and Rho-associated kinase (Rho-kinase). Science 273 (1996) 245-8.

Kitamura, K., Tokunaga, M., Iwane, A.H. and Yanagida, T.: A single myosin head moves along an actin filament with regular steps of 5.3 nanometres. Nature 397 (1999) 129-34.

Knetsch, M.L., Uyeda, T.Q. and Manstein, D.J.: Disturbed communication between actin- and nucleotide-binding sites in a myosin II with truncated 50/20-kDa junction. J Biol Chem 274 (1999) 20133-8.

Komuro, R., Sasaki, T., Takaishi, K., Orita, S. and Takai, Y.: Involvement of Rho and Rac small G proteins and Rho GDI in Ca2+-dependent exocytosis from PC12 cells. Genes Cells 1 (1996) 943-51.

Konrad, M. and Goody, R.S.: Kinetic and thermodynamic properties of the ternary complex between F-actin, myosin subfragment 1 and adenosine 5'-[beta, gamma-imido]triphosphate. Eur J Biochem 128 (1982) 547-55.

Kovacs, M., Malnasi-Csizmadia, A., Woolley, R.J. and Bagshaw, C.R.: Analysis of nucleotide binding to Dictyostelium myosin II motor domains containing a single tryptophan near the active site. J Biol Chem 277 (2002) 28459-67.

Kozma, R., Ahmed, S., Best, A. and Lim, L.: The Ras-related protein Cdc42Hs and bradykinin promote formation of peripheral actin microspikes and filopodia in Swiss 3T3 fibroblasts. Mol Cell Biol 15 (1995) 1942-52.

Krementsov, D.N., Krementsova, E.B. and Trybus, K.M.: Myosin V: regulation by calcium, calmodulin, and the tail domain. J Cell Biol 164 (2004) 877-86.

Kureishi, Y., Kobayashi, S., Amano, M., Kimura, K., Kanaide, H., Nakano, T., Kaibuchi, K. and Ito, M.: Rho-associated kinase directly induces smooth muscle contraction through myosin

light chain phosphorylation. J Biol Chem 272 (1997) 12257-60.

Laemmli, U.K.: Cleavage of structural proteins during the assembly of the head of bacteriophage T4. Nature 227 (1970) 680-5.

Lamaze, C., Chuang, T.H., Terlecky, L.J., Bokoch, G.M. and Schmid, S.L.: Regulation of receptor-mediated endocytosis by Rho and Rac. Nature 382 (1996) 177-9.

Li, H., Adamik, R., Pacheco-Rodriguez, G., Moss, J. and Vaughan, M.: Protein kinase A-anchoring (AKAP) domains in brefeldin A-inhibited guanine nucleotide-exchange protein 2 (BIG2). Proc Natl Acad Sci U S A 100 (2003) 1627-32.

Li, X.D., Ikebe, R. and Ikebe, M.: Activation of Myosin va function by melanophilin, a specific docking partner of Myosin va. J Biol Chem 280 (2005) 17815-22.

Li, X.D., Mabuchi, K., Ikebe, R. and Ikebe, M.: Ca2+-induced activation of ATPase activity of myosin Va is accompanied with a large conformational change. Biochem Biophys Res Commun 315 (2004) 538-45.

Lindquist, R.N., Lynn, J.L., Jr. and Lienhard, G.E.: Possible transition-state analogs for ribonuclease. The complexes of uridine with oxovanadium(IV) ion and vanadium(V) ion. J Am Chem Soc 95 (1973) 8762-8.

Lister, I., Schmitz, S., Walker, M., Trinick, J., Buss, F., Veigel, C. and Kendrick-Jones, J.: A monomeric myosin VI with a large working stroke. Embo J 23 (2004) 1729-38.

Lymn, R.W. and Taylor, E.W.: Mechanism of adenosine triphosphate hydrolysis by actomyosin. Biochemistry 10 (1971) 4617-24.

Malnasi-Csizmadia, A., Woolley, R.J. and Bagshaw, C.R.: Resolution of conformational states of Dictyostelium myosin II motor domain using tryptophan (W501) mutants: implications for the open-closed transition identified by crystallography. Biochemistry 39 (2000) 16135-46.

Marston, S.B. and Taylor, E.W.: Comparison of the myosin and actomyosin ATPase mechanisms of the four types of vertebrate muscles. J Mol Biol 139 (1980) 573-600.

Mehta, A.D., Rock, R.S., Rief, M., Spudich, J.A., Mooseker, M.S. and Cheney, R.E.: Myosin-V is a processive actin-based motor. Nature 400 (1999) 590-3.

Milligan, R.A.: Protein-protein interactions in the rigor actomyosin complex. Proc Natl Acad Sci U S A 93 (1996) 21-6.

Miura, Y., Kikuchi, A., Musha, T., Kuroda, S., Yaku, H., Sasaki, T. and Takai, Y.: Regulation of morphology by rho p21 and its inhibitory GDP/GTP exchange protein (rho GDI) in Swiss 3T3 cells. J Biol Chem 268 (1993) 510-5.

Montell, C. and Rubin, G.M.: The Drosophila ninaC locus encodes two photoreceptor cell specific proteins with domains homologous to protein kinases and the myosin heavy chain head. Cell 52 (1988) 757-72.

Morinaga, N., Tsai, S.C., Moss, J. and Vaughan, M.: Isolation of a brefeldin A-inhibited guanine nucleotide-exchange protein for ADP ribosylation factor (ARF) 1 and ARF3 that contains a Sec7-like domain. Proc Natl Acad Sci U S A 93 (1996) 12856-60.

Muller, R.T., Honnert, U., Reinhard, J. and Bahler, M.: The rat myosin myr 5 is a GTPase-activating protein for Rho in vivo: essential role of arginine 1695. Mol Biol Cell 8 (1997) 2039-53.

Murphy, C.T. and Spudich, J.A.: The sequence of the myosin 50-20K loop affects Myosin's affinity for actin throughout the actin-myosin ATPase cycle and its maximum ATPase activity. Biochemistry 38 (1999) 3785-92.

Nascimento, A.A., Cheney, R.E., Tauhata, S.B., Larson, R.E. and Mooseker, M.S.: Enzymatic characterization and functional domain mapping of brain myosin-V. J Biol Chem 271 (1996) 17561-9.

Nishikawa, S., Homma, K., Komori, Y., Iwaki, M., Wazawa, T., Hikikoshi Iwane, A., Saito, J., Ikebe, R., Katayama, E., Yanagida, T. and Ikebe, M.: Class VI myosin moves processively

along actin filaments backward with large steps. Biochem Biophys Res Commun 290 (2002) 311-7.

Nobes, C.D. and Hall, A.: Rho, rac, and cdc42 GTPases regulate the assembly of multimolecular focal complexes associated with actin stress fibers, lamellipodia, and filopodia. Cell 81 (1995) 53-62.

Novak, K.D., Peterson, M.D., Reedy, M.C. and Titus, M.A.: Dictyostelium myosin I double mutants exhibit conditional defects in pinocytosis. J Cell Biol 131 (1995) 1205-21.

O'Connell, C.B. and Mooseker, M.S.: Native Myosin-IXb is a plus-, not a minus-end-directed motor. Nat Cell Biol 5 (2003) 171-2.

Obaishi, H., Nakanishi, H., Mandai, K., Satoh, K., Satoh, A., Takahashi, K., Miyahara, M., Nishioka, H., Takaishi, K. and Takai, Y.: Frabin, a novel FGD1-related actin filament-binding protein capable of changing cell shape and activating c-Jun N-terminal kinase. J Biol Chem 273 (1998) 18697-700.

Okada, Y. and Hirokawa, N.: A processive single-headed motor: kinesin superfamily protein KIF1A. Science 283 (1999) 1152-7.

Okada, Y. and Hirokawa, N.: Mechanism of the single-headed processivity: diffusional anchoring between the K-loop of kinesin and the C terminus of tubulin. Proc Natl Acad Sci U S A 97 (2000) 640-5.

Ostap, E.M. and Pollard, T.D.: Biochemical kinetic characterization of the Acanthamoeba myosin-I ATPase. J Cell Biol 132 (1996) 1053-60.

Park, S., Ajtai, K. and Burghardt, T.P.: Mechanism for coupling free energy in ATPase to the myosin active site. Biochemistry 36 (1997) 3368-72.

Post, P.L., Bokoch, G.M. and Mooseker, M.S.: Human myosin-IXb is a mechanochemically active motor and a GAP for rho. J Cell Sci 111 (Pt 7) (1998) 941-50.

Post, P.L., Tyska, M.J., O'Connell, C.B., Johung, K., Hayward, A. and Mooseker, M.S.: Myosin-

IXb is a single-headed and processive motor. J Biol Chem 277 (2002) 11679-83.

Qiu, R.G., Chen, J., McCormick, F. and Symons, M.: A role for Rho in Ras transformation. Proc Natl Acad Sci U S A 92 (1995) 11781-5.

Raposo, G., Cordonnier, M.N., Tenza, D., Menichi, B., Durrbach, A., Louvard, D. and Coudrier, E.: Association of myosin I alpha with endosomes and lysosomes in mammalian cells. Mol Biol Cell 10 (1999) 1477-94.

Rayment, I. and Holden, H.M.: The three-dimensional structure of a molecular motor. Trends Biochem Sci 19 (1994) 129-34.

Rayment, I., Holden, H.M., Whittaker, M., Yohn, C.B., Lorenz, M., Holmes, K.C. and Milligan, R.A.: Structure of the actin-myosin complex and its implications for muscle contraction. Science 261 (1993a) 58-65.

Rayment, I., Rypniewski, W.R., Schmidt-Base, K., Smith, R., Tomchick, D.R., Benning, M.M., Winkelmann, D.A., Wesenberg, G. and Holden, H.M.: Three-dimensional structure of myosin subfragment-1: a molecular motor. Science 261 (1993b) 50-8.

Reinhard, J., Scheel, A.A., Diekmann, D., Hall, A., Ruppert, C. and Bahler, M.: A novel type of myosin implicated in signalling by rho family GTPases. Embo J 14 (1995) 697-704.

Resetar, A.M. and Chalovich, J.M.: Adenosine 5'-(gamma-thiotriphosphate): an ATP analog that should be used with caution in muscle contraction studies. Biochemistry 34 (1995) 16039-45.

Ridley, A.J. and Hall, A.: The small GTP-binding protein rho regulates the assembly of focal adhesions and actin stress fibers in response to growth factors. Cell 70 (1992) 389-99.

Ridley, A.J., Paterson, H.F., Johnston, C.L., Diekmann, D. and Hall, A.: The small GTP-binding protein rac regulates growth factor-induced membrane ruffling. Cell 70 (1992) 401-10.

Rief, M., Rock, R.S., Mehta, A.D., Mooseker, M.S., Cheney, R.E. and Spudich, J.A.: Myosin-V

stepping kinetics: a molecular model for processivity. Proc Natl Acad Sci U S A 97 (2000) 9482-6.

Rock, R.S., Ramamurthy, B., Dunn, A.R., Beccafico, S., Rami, B.R., Morris, C., Spink, B.J., Franzini-Armstrong, C., Spudich, J.A. and Sweeney, H.L.: A flexible domain is essential for the large step size and processivity of myosin VI. Mol Cell 17 (2005) 603-9.

Rock, R.S., Rice, S.E., Wells, A.L., Purcell, T.J., Spudich, J.A. and Sweeney, H.L.: Myosin VI is a processive motor with a large step size. Proc Natl Acad Sci U S A 98 (2001) 13655-9.

Rosenfeld, S.S. and Taylor, E.W.: The ATPase mechanism of skeletal and smooth muscle acto-subfragment 1. J Biol Chem 259 (1984) 11908-19.

Rosenfeld, S.S., Xing, J., Whitaker, M., Cheung, H.C., Brown, F., Wells, A., Milligan, R.A. and Sweeney, H.L.: Kinetic and spectroscopic evidence for three actomyosin:ADP states in smooth muscle. J Biol Chem 275 (2000) 25418-26.

Roth, K. and Weiner, M.W.: Determination of cytosolic ADP and AMP concentrations and the free energy of ATP hydrolysis in human muscle and brain tissues with 31P NMR spectroscopy. Magn Reson Med 22 (1991) 505-11.

Rovner, A.S.: A long, weakly charged actin-binding loop is required for phosphorylation-dependent regulation of smooth muscle myosin. J Biol Chem 273 (1998) 27939-44.

Rovner, A.S., Freyzon, Y. and Trybus, K.M.: Chimeric substitutions of the actin-binding loop activate dephosphorylated but not phosphorylated smooth muscle heavy meromyosin. J Biol Chem 270 (1995) 30260-3.

Rovner, A.S., Freyzon, Y. and Trybus, K.M.: An insert in the motor domain determines the functional properties of expressed smooth muscle myosin isoforms. J Muscle Res Cell Motil 18 (1997) 103-10.

Saeki, N., Tokuo, H. and Ikebe, M.: BIG1 is a binding partner of myosin IXb and regulates its Rho-GTPase activating protein activity. J Biol Chem 280 (2005) 10128-34.

Sato, O., White, H.D., Inoue, A., Belknap, B., Ikebe, R. and Ikebe, M.: Human deafness mutation of myosin VI (C442Y) accelerates the ADP dissociation rate. J Biol Chem 279 (2004) 28844-54.

Schroder, R.R., Manstein, D.J., Jahn, W., Holden, H., Rayment, I., Holmes, K.C. and Spudich, J.A.: Three-dimensional atomic model of F-actin decorated with Dictyostelium myosin S1. Nature 364 (1993) 171-4.

Sellers, J.R.: Myosins: a diverse superfamily. Biochim Biophys Acta 1496 (2000) 3-22.

Siemankowski, R.F., Wiseman, M.O. and White, H.D.: ADP dissociation from actomyosin subfragment 1 is sufficiently slow to limit the unloaded shortening velocity in vertebrate muscle. Proc Natl Acad Sci U S A 82 (1985) 658-62.

Sleep, J.A. and Hutton, R.L.: Exchange between inorganic phosphate and adenosine 5'-triphosphate in the medium by actomyosin subfragment 1. Biochemistry 19 (1980) 1276-83.

Smith, C.A. and Rayment, I.: X-ray structure of the magnesium(II).ADP.vanadate complex of the Dictyostelium discoideum myosin motor domain to 1.9 A resolution. Biochemistry 35 (1996) 5404-17.

Sokac, A.M. and Bement, W.M.: Regulation and expression of metazoan unconventional myosins. Int Rev Cytol 200 (2000) 197-304.

Spudich, J.A. and Watt, S.: The regulation of rabbit skeletal muscle contraction. I. Biochemical studies of the interaction of the tropomyosin-troponin complex with actin and the proteolytic fragments of myosin. J Biol Chem 246 (1971) 4866-71.

Stoffler, H.E. and Bahler, M.: The ATPase activity of Myr3, a rat myosin I, is allosterically inhibited by its own tail domain and by Ca2+ binding to its light chain calmodulin. J Biol Chem 273 (1998) 14605-11.

Suzuki, Y., Yasunaga, T., Ohkura, R., Wakabayashi, T. and Sutoh, K.: Swing of the lever arm of a myosin motor at the isomerization and phosphate-release steps. Nature 396 (1998) 380-3.

Svoboda, K., Schmidt, C.F., Schnapp, B.J. and Block, S.M.: Direct observation of kinesin stepping by optical trapping interferometry. Nature 365 (1993) 721-7.

Tang, N. and Ostap, E.M.: Motor domain-dependent localization of myo1b (myr-1). Curr Biol 11 (2001) 1131-5.

Tauhata, S.B., dos Santos, D.V., Taylor, E.W., Mooseker, M.S. and Larson, R.E.: High affinity binding of brain myosin-Va to F-actin induced by calcium in the presence of ATP. J Biol Chem 276 (2001) 39812-8.

Taylor, E.W.: Kinetic studies on the association and dissociation of myosin subfragment 1 and actin. J Biol Chem 266 (1991) 294-302.

Togawa, A., Morinaga, N., Ogasawara, M., Moss, J. and Vaughan, M.: Purification and cloning of a brefeldin A-inhibited guanine nucleotide-exchange protein for ADP-ribosylation factors. J Biol Chem 274 (1999) 12308-15.

Trybus, K.M., Krementsova, E. and Freyzon, Y.: Kinetic characterization of a monomeric unconventional myosin V construct. J Biol Chem 274 (1999) 27448-56.

Uyeda, T.Q., Abramson, P.D. and Spudich, J.A.: The neck region of the myosin motor domain acts as a lever arm to generate movement. Proc Natl Acad Sci U S A 93 (1996) 4459-64.

Uyeda, T.Q., Ruppel, K.M. and Spudich, J.A.: Enzymatic activities correlate with chimaeric substitutions at the actin-binding face of myosin. Nature 368 (1994) 567-9.

Volkmann, N., Hanein, D., Ouyang, G., Trybus, K.M., DeRosier, D.J. and Lowey, S.: Evidence for cleft closure in actomyosin upon ADP release. Nat Struct Biol 7 (2000) 1147-55.

Wakabayashi, K., Tokunaga, M., Kohno, I., Sugimoto, Y., Hamanaka, T., Takezawa, Y., Wakabayashi, T. and Amemiya, Y.: Small-angle synchrotron x-ray scattering reveals distinct shape changes of the myosin head during hydrolysis of ATP. Science 258 (1992) 443-7.

Walker, M., Zhang, X.Z., Jiang, W., Trinick, J. and White, H.D.: Observation of transient disorder during myosin subfragment-1 binding to actin by stopped-flow fluorescence and millisecond time resolution electron cryomicroscopy: evidence that the start of the crossbridge power stroke in muscle has variable geometry. Proc Natl Acad Sci U S A 96 (1999) 465-70.

Walker, M.L., Burgess, S.A., Sellers, J.R., Wang, F., Hammer, J.A., 3rd, Trinick, J. and Knight, P.J.: Two-headed binding of a processive myosin to F-actin. Nature 405 (2000) 804-7.

Wang, F., Chen, L., Arcucci, O., Harvey, E.V., Bowers, B., Xu, Y., Hammer, J.A., 3rd and Sellers, J.R.: Effect of ADP and ionic strength on the kinetic and motile properties of recombinant mouse myosin V. J Biol Chem 275 (2000) 4329-35.

Wang, F., Thirumurugan, K., Stafford, W.F., Hammer, J.A., 3rd, Knight, P.J. and Sellers, J.R.: Regulated conformation of myosin V. J Biol Chem 279 (2004) 2333-6.

Warshaw, D.M., Guilford, W.H., Freyzon, Y., Krementsova, E., Palmiter, K.A., Tyska, M.J., Baker, J.E. and Trybus, K.M.: The light chain binding domain of expressed smooth muscle heavy meromyosin acts as a mechanical lever. J Biol Chem 275 (2000) 37167-72.

Warshaw, D.M., Kennedy, G.G., Work, S.S., Krementsova, E.B., Beck, S. and Trybus, K.M.: Differential labeling of Myosin v heads with quantum dots allows direct visualization of hand-over-hand processivity. Biophys J 88 (2005) L30-2.

Watanabe, G., Saito, Y., Madaule, P., Ishizaki, T., Fujisawa, K., Morii, N., Mukai, H., Ono, Y., Kakizuka, A. and Narumiya, S.: Protein kinase N (PKN) and PKN-related protein rhophilin as targets of small GTPase Rho. Science 271 (1996) 645-8.

Wells, A.L., Lin, A.W., Chen, L.Q., Safer, D., Cain, S.M., Hasson, T., Carragher, B.O., Milligan, R.A. and Sweeney, H.L.: Myosin VI is an actin-based motor that moves backwards. Nature 401 (1999) 505-8.

Werber, M.M., Peyser, Y.M. and Muhlrad, A.: Characterization of stable beryllium fluoride, aluminum fluoride, and vanadate containing myosin subfragment 1-nucleotide complexes. Biochemistry 31 (1992) 7190-7.

Westheimer, F.H.: Why nature chose phosphates. Science 235 (1987) 1173-8.

White, H.D., Belknap, B. and Jiang, W.: Kinetics of binding and hydrolysis of a series of nucleoside triphosphates by actomyosin-S1. Relationship between solution rate constants and properties of muscle fibers. J Biol Chem 268 (1993) 10039-45.

White, H.D., Belknap, B. and Webb, M.R.: Kinetics of nucleoside triphosphate cleavage and phosphate release steps by associated rabbit skeletal actomyosin, measured using a novel fluorescent probe for phosphate. Biochemistry 36 (1997) 11828-36.

Whittaker, M., Wilson-Kubalek, E.M., Smith, J.E., Faust, L., Milligan, R.A. and Sweeney, H.L.: A 35-A movement of smooth muscle myosin on ADP release. Nature 378 (1995) 748-51.

Wirth, J.A., Jensen, K.A., Post, P.L., Bement, W.M. and Mooseker, M.S.: Human myosin-IXb, an unconventional myosin with a chimerin-like rho/rac GTPase-activating protein domain in its tail. J Cell Sci 109 (Pt 3) (1996) 653-61.

Xu, J.Q., Harder, B.A., Uman, P. and Craig, R.: Myosin filament structure in vertebrate smooth muscle. J Cell Biol 134 (1996) 53-66.

Yamamoto, M., Marui, N., Sakai, T., Morii, N., Kozaki, S., Ikai, K., Imamura, S. and Narumiya, S.: ADP-ribosylation of the rhoA gene product by botulinum C3 exoenzyme causes Swiss 3T3 cells to accumulate in the G1 phase of the cell cycle. Oncogene 8 (1993) 1449-55.

Yanagida, T., Kitamura, K., Tanaka, H., Hikikoshi Iwane, A. and Esaki, S.: Single molecule analysis of the actomyosin motor. Curr Opin Cell Biol 12 (2000) 20-5.

Yengo, C.M., Chrin, L., Rovner, A.S. and Berger, C.L.: Intrinsic tryptophan fluorescence identifies specific conformational changes at the actomyosin interface upon actin binding and ADP release. Biochemistry 38 (1999) 14515-23.

Yengo, C.M., Chrin, L.R., Rovner, A.S. and Berger, C.L.: Tryptophan 512 is sensitive to conformational changes in the rigid relay loop of smooth muscle myosin during the

MgATPase cycle. J Biol Chem 275 (2000) 25481-7.

Yengo, C.M., De La Cruz, E.M., Chrin, L.R., Gaffney, D.P., 2nd and Berger, C.L.: Actin-induced closure of the actin-binding cleft of smooth muscle myosin. J Biol Chem 277 (2002a) 24114-9.

Yengo, C.M., De la Cruz, E.M., Safer, D., Ostap, E.M. and Sweeney, H.L.: Kinetic characterization of the weak binding states of myosin V. Biochemistry 41 (2002b) 8508-17.

Yengo, C.M., Fagnant, P.M., Chrin, L., Rovner, A.S. and Berger, C.L.: Smooth muscle myosin mutants containing a single tryptophan reveal molecular interactions at the actin-binding interface. Proc Natl Acad Sci U S A 95 (1998) 12944-9.

Yildiz, A., Forkey, J.N., McKinney, S.A., Ha, T., Goldman, Y.E. and Selvin, P.R.: Myosin V walks hand-over-hand: single fluorophore imaging with 1.5-nm localization. Science 300 (2003) 2061-5.

Yoshimura, M., Homma, K., Saito, J., Inoue, A., Ikebe, R. and Ikebe, M.: Dual regulation of mammalian myosin VI motor function. J Biol Chem 276 (2001) 39600-7.